ERDC/CERL CR-16-5

US Army Corps
of Engineers®
Engineer Research and
Development Center

ERDC
INNOVATIVE SOLUTIONS
for a safer, better world

DoD Corrosion Prevention and Control Program

Field Testing and Load Rating Report for Bridge No. 4, Hybrid Composite Beam Span, at Fort Knox, Kentucky

Contractor's Supplemental Report for Project F12-AR15

Brett Commander and Brice Carpenter

September 2016

Construction Engineering
Research Laboratory

The U.S. Army Engineer Research and Development Center (ERDC) solves the nation's toughest engineering and environmental challenges. ERDC develops innovative solutions in civil and military engineering, geospatial sciences, water resources, and environmental sciences for the Army, the Department of Defense, civilian agencies, and our nation's public good. Find out more at www.erdc.usace.army.mil.

To search for other technical reports published by ERDC, visit the ERDC online library at http://acwc.sdp.sirsi.net/client/default.

ERDC/CERL CR-16-5
September 2016

Field Testing and Load Rating Report for Bridge No. 4, Hybrid Composite Beam Span, at Fort Knox, Kentucky

Contractor's Supplemental Report for Project F12–AR15

Brett Commander and Brice Carpenter

Bridge Diagnostics, Inc. (BDI)
1965 57th Court North
Suite 106
Boulder, CO 80301

Final report

Prepared for Office of the Secretary of Defense (OUSD(AT&L))
3090 Defense Pentagon
Washington, DC 20301-3090

Under Contract W9132T-07-D-0007, Delivery Order 0022, "Demonstration and Validation of 3-D Gridform and Hybrid Composite Beams for Bridges for Project F12-AR15, "Corrosion-Resistant Hybrid Composite Bridge Beams for Structural Applications"

Monitored by Construction Engineering Research Laboratory
U.S. Army Engineer Research and Development Center
2902 Newmark Drive
Champaign, IL 61822

Abstract

The Army has 1,500 vehicular bridges on its installations, with many experiencing high maintenance or replacement costs due to corrosion of the steel structure or of the reinforcing bar in the concrete deck. Under the Department of Defense Corrosion Prevention and Control Program (Project F12-AR15), a span of Bridge No. 4 at Fort Knox, Kentucky, was selected to demonstrate and validate a new corrosion-resistant hybrid composite bridge beam. The results of that project were published as ERDC/CERL TR-16-22 (September 2016). Bridge Diagnostics, Inc. (BDI) of Boulder, Colorado, was subcontracted to perform load testing and rating for the new bridge beam project to confirm that the replacement bridge span met its required load rating (HL-93) and performance criteria for deflection and strain. Results showed the bridge met all design specifications and load ratings.

Foreword

Bridge Diagnostics, Inc. (BDI) of Boulder, Colorado, was subcontracted by Mandaree Enterprise Corporation (MEC), of Warner Robins, Georgia, to perform load testing on Bridge 4 at Fort Knox, Kentucky. MEC was the prime contractor retained by the Construction Engineering Research Laboratory–Engineer Research and Development Center (ERDC-CERL) to supervise the installation and testing of two novel technologies on two different spans of Bridge 4.

One of the demonstrated technologies is a new corrosion-resistant hybrid composite bridge beam. The technology was selected for demonstration and validation under Project F12-AR15 of the Department of Defense Corrosion Prevention and Control (CPC) Program. The final technical report on that project was published as ERDC/CERL TR-16-22 (September 2016). This contract report, which is incorporated into TR-16-22 by reference, provides complete details on the subcontractor's execution of the load-testing program.

The primary goal of BDI's live load testing was to determine whether the composite beams met design specifications and could deliver safe crossing of Heavy Equipment Transport System (HETS-115) vehicles. Their report (reproduced in its entirety here) outlines the testing procedures used, provides a detailed discussion of the data collected, and summarizes the findings.

Richard G. Lampo
Project Manager and Materials Engineer
ERDC-CERL
Champaign, Illinois

Preface

Load testing was conducted by Bridge Diagnostics, Inc. as a subcontractor under Mandaree Enterprise Corporation's Contract W9132T-07-D-0007, Delivery Order 0022, "Demonstration And Validation Of 3-D Gridform And Hybrid Composite Beams For Bridges" for Project F12-AR15, "Corrosion-Resistant Hybrid Composite Bridge Beams for Structural Applications." The work was conducted for the Office of the Secretary of Defense (OSD) under the Department of Defense (DoD) Corrosion Control and Prevention Program. The project monitor was Mr. Steven C. Sweeney, CEERD-CFM.

The work was monitored by the Engineering and Materials Branch of the Facilities Division (CEERD-CFM), U.S. Army Engineer Research and Development Center, Construction Engineering Research Laboratory (ERDC-CERL), Champaign, IL. At the time of publication, Ms. Vicki L. Van Blaricum was Chief, CEERD-CFM; Mr. Donald K. Hicks was Chief, CEERD-CF; and Mr. Kurt Kinnevan was the Technical Director for Adaptive and Resilient Installations, CEERD-CZT. The Deputy Director of ERDC-CERL was Dr. Kirankumar Topudurti, and the Director was Dr. Ilker Adiguzel.

The Commander of ERDC was COL Bryan S. Green, and the Director was Dr. Jeffery P. Holland.

FIELD TESTING AND LOAD RATING REPORT: BRIDGE NO. 4 - HCB SPAN – FORT KNOX, KY

SUBMITTED TO:

Mandaree Enterprise Corporation

Madaree Enterprise Corporation
812 Park Drive
Warner Robbins, GA 31088-5182
www.mandaree.com

SUBMITTED BY:

BDI

BRIDGE DIAGNOSTICS, INC.
1995 57th Court North, Suite 100
Boulder, CO 80301-2810
303.494.3230
www.bridgetest.com

Original Submission: January 2013 (Load Test I)

Final Submission: March 2014 (Load Test II)

EXECUTIVE SUMMARY

In September of 2012, Bridge Diagnostics, Inc. (BDI) was contracted by the Mandaree Enterprise Corporation (MEC) to load test and load rate Bridge No. 4 on Fort Knox Military Reservation, KY. Load tests were performed as a means of performance verification because the bridge was built with innovative structural materials and construction procedures. An initial diagnostic load test was performed on December 18, 2012. Load test, analysis and rating results indicated the bridge had the desired load capacity and a report was submitted in January 2013. Per the project specifications, a repeat load test was performed one year later on December 18, 2013.

Bridge No.4 consists of two simply supported spans. One span is comprised of five rolled steel girders supporting a non-composite reinforced concrete slab. The other span consists of five Hybrid Composite Beams (referred to hereafter as HCBs). This report focuses on the testing, analysis, and load rating of the HCB span. Ratings were calculated for the HCBs to determine whether or not the span, in its current state, could independently support the live load of the standard AASHTO HL-93 load configuration, the combined military M1070/M1000 load configuration, and the combined military M1070/M747 load configuration. Additionally, a controlling MLC vehicle classification was determined for the bridge for both tracked and wheeled configurations.

During both field test phases, the superstructure was instrumented with a combination of strain, displacement and rotation sensors. Once the structure was instrumented, controlled load tests were performed with a variety of test vehicles. The initial 2012 tests were performed with a pair of 3-axle dump trucks in both single and double truck configurations; while the final 2013 load tests were performed using the HETS/M1A1 military logistics vehicle and the M1A1 Abrams tank.

The response data obtained from the first round of load tests in 2012 was first evaluated for quality and subsequently used to verify and calibrate a finite-element model of the structure. In general, the response data recorded during the load tests was found to be of good quality, however inconsistencies in recorded strain magnitudes were observed on the GFRP shells. Surface strain measurements were very reproducible and the response shapes were very consistent among similar locations but the strain magnitudes varied considerably. There was no evidence of any equipment malfunction so the strain magnitude issue was likely due to local sectional changes such as: changes in the material thickness due to stiffeners or spacers; and/or local flexural responses resulting from imperfections in the thin flexible shell GFRP shell. Model calibration was therefore based on the measured displacements and beam-end rotations as well as the shapes of the strain history results.

Two different model geometries were examined to determine the best method for simulating the measured responses. A planar model with quasi-3D beam-lines was found to perform reasonably well with midspan behavior but didn't accurately simulate rotations or strains near the beam-ends. A full 3-D representation of the beams, including the concrete arch and deck, the GFRP shell and prestress tendons, did a much better job of simulating behavior throughout the structure. The conclusion from this exercise was that the recorded beam behavior was a combination of what is expected from a normal flexural beam and that of a tied-arch. This complex behavior was likely caused by some independent deformation between the shell and the arch, due to the flexibility of the GFRP shell. Therefore the full 3-D model was used for all subsequent simulations and load rating calculations. The resulting calibrated model was then

used to analyze the effects of the specified rating vehicles. All load rating factors were obtained using the guidelines specified in the AASHTO *Manual for Bridge Evaluation – 2011 Edition* and the KYDOT TM08-01 LRFR guidelines.

Strength limit state ratings were performed by BDI and compared with calculations provided in the structure's design documents. Slight variations in the controlling failure criteria were noted with respect to the HCB's flexural and shear capacity, which were examined for all load conditions. In addition, service limit state ratings were examined to determine if the concrete arch was likely to crack under normal service conditions. All component capacity calculations have been described in Section 4 of this report, and have been provided in Appendix A.

All strength load ratings were controlled by the shear capacity of the FRP webs and were above 1.0. The controlling rating was the HL93 Design Shear Rating with an Inventory Level of 1.76. Flexural load ratings obtained from the calibrated model were slightly more conservative than those provided in design document but were still well above 1.0 for all load configurations. Service checks to determine if the concrete arch would crack under the HETS loadings (which were considered the realistic design loads) resulted in a service rating factor of 1.09 indicating that the arch should not crack under normal operation.

All load ratings and Military Load Classifications (MLC) for Bridge No. 4 were controlled by the HCB span and not the steel girder span. The MLC values for tracked and wheeled vehicles were based on AASHTO Operating Load Factors. A tracked MLC of 139 tons was obtained from an M1A1 Abrams tank with an operating rating factor of 1.94. The wheeled MLC of 212 tons was calculated from the Hypothetical MLC-70 wheeled vehicle, which had an operating load factor of 3.04. The wheeled vehicle load configuration was longer than the individual bridge spans and therefore had significantly greater MLC values than the tracked configuration. Rating factors and MLC load limits are provided in the following table. All results indicate the structure can safely carry the examined load configurations with no speed restrictions.

After the second round of tests, data comparisons were made through the 2012 bridge model since direct measurement comparisons were not applicable due to different load conditions. It was found that the HCB span's behavior did not significantly change over the years' time. The inconsistency in recorded strain magnitudes on the GFRP shells was found to still occur but to a lesser magnitude with the heavier military vehicles. This observation supported the conclusion that variations in strain magnitudes were likely due to local flexural responses of the thin flexible GFRP shell. Any imperfections in the fiberglass such as warps in the thin walls straightened out with an increase in tension and influenced the local surface strain measurements. The improved strain measurement consistency was due to the heavier loads straightening out the shell imperfections to a larger degree; at which point the in-plane membrane stresses were a larger component of the measured strains compared to the local out-of-plane flexural stresses. A general conclusion therefore was that future load tests on this type of superstructure should be based primarily on global responses (midspan displacements and end rotations) as surface strains were influenced by minor fabrication imperfections.

The only other notable difference in performance between the two load tests was the degree of beam end-restraint induced by friction in the elastomeric bearing pads. The heavier loads applied in 2013 generated a larger friction resistance and therefore more end-restraint. However, since this behavior was non-linear and considered unreliable for load rating, simple supports were assumed for all load rating analyses. Therefore the load rating model generated in 2012 was found to still be valid along with all load rating results.

Table 1 – Controlling load rating factors and applicable rating weights/classifications.

Loading Condition	Inventory RF	Inventory Weight, Tons	Operating RF	Operating Weight, Tons
HL-93 (Strength)	1.76	---	2.28	---
HL-93 (Service)	---	---	1.00	---
HETS M1070/ M1000	2.22	255	2.88	331
HETS M1070/ M747	1.80	189	2.34	245
M1A1 Tracked	---	---	1.94	MLCT 139
MLC70 Wheeled	---	---	3.04	MLCW 212

This report contains details regarding the instrumentation and load testing procedures, a qualitative review of the load test data, a brief explanation of the modeling steps, a summary of the load rating methods and results, and the overall conclusions of this project.

Submittal Notes:

This submittal includes the following files on CD:

1. BDI-FortKnox_Testing_Documents_Round-1.pdf
   This file provides pertinent details about the instrumentation plan and testing scenarios/procedures for Bridge No. 4 performed in the first round of testing (December 18, 2012).

2. BDI-FortKnox_Testing_Documents_Round-2.pdf
   This file provides pertinent details about the instrumentation plan and testing scenarios/procedures for Bridge No. 4 performed in the first round of testing (December 18, 2013).

3. BDI_FortKnox_ HCB _Submittal_V2_DRAFT.pdf
   This is the BDI report in "pdf" format. It contains details regarding the testing procedures, provides a qualitative data evaluation, describes the modeling procedures and results, and provides the procedure and results of the field-calibrate rating performed on the HCB span.

4. BDI_FortKnox_ HCB _Rating_Output_and_Summary_Files
   The output files contain detailed information regarding the applied load and resistance factors, capacities, unfactored structural responses, and critical load rating results for each of the rated vehicles. The summary files contain the critical load rating results along with the controlling factored responses.

5. BDI_FortKnox_Selected_Data-Round-1.xlsx
   This spreadsheet contains selected data from the 2012 Round 1 testing that has been extracted and formatted as a function of vehicle position for each truck path. Additionally, envelope data (minimum and maximum responses) for every gage location at each of the three lateral truck positions, including the two lanes and tandem tests, is provided in this file. It also gives the vehicle location for each min/max response as related to the test truck's front axle.

6. BDI_FortKnox_Selected_Data-Round-2.xlsx
   This spreadsheet contains selected data from the 2013 Round 1 testing that has been extracted and formatted as a function of vehicle position for each truck path. Additionally, envelope data (minimum and maximum responses) for every gage location at each of the three lateral truck positions, including the two lanes and tandem tests, is provided in this file. It also gives the vehicle location for each min/max response as related to the test truck's front axle.

TABLE OF CONTENTS

1. STRUCTURAL TESTING PROCEDURES

Bridge No. 4 is a two-span simply supported structure that carries Main Range Road over a stream in Fort Knox Military Reservation, KY. The structure's hybrid composite beam (HCB) span (Span 2 in the provided bridge drawings) consists of five HCBs spaced at ~5'-11" that are each comprised of the following: a reinforced concrete arch that is tied with low relaxation prestressing steel; which are both encased in a glass fiber reinforced polymer (GFRP) shell; and were made composite with a reinforced concrete deck through the use of a concrete fin and mild steel stirrups aligned at a 45° angle. Note that the deck was supported by a SAFPLANK stay-in-place form system. According to the structure's plans, the HCB span has an overall width of 27'-8"and a span length of approximately 39' (center-to-center of bearing). It should be noted that BDI did not perform an in-depth visual inspection of the structure during the load testing.

To evaluate the HCB span's response to live-load, the superstructure was instrumented during the ROUND 1 load test (2012) with the following sensors:

- 22 reusable, surface-mounted strain transducers (Figure 1.1, Figure 1.2, and Figure 1.3)
- 3 cantilevered displacement sensors (Figure 1.1 and Figure 1.2)
- 4 surface-mounted tiltmeter rotation sensors (Figure 1.4 and Figure 1.5).

Instrumentation during Round 2 was nearly identical to what was installed during Round 1 except additional sensors were applied to areas that were not accessible during the initial test. The following sensors were applied during the 2013 load test:

- 29 reusable, surface-mounted strain transducers (Figure 1.1, Figure 1.2, and Figure 1.3)
- 5 cantilevered displacement sensors (Figure 1.1 and Figure 1.2)
- 4 surface-mounted tiltmeter rotation sensors (Figure 1.4 and Figure 1.5).

The instrumentation plans for both rounds of tests, including sensor locations and IDs, have been provided in the attached drawings labeled "*BDI-FortKnox_Testing_Documents_Round-1.pdf*" & "*BDI-FortKnox_Testing_Documents_Round-2.pdf*". The instrumentation plan view, sections/elevations, and test vehicle paths are also shown in Figure 1.11 through Figure 1.18. Note that the instrumentation of the HCB span during the first round of load tests was reduced from the original plan due to access issues.

Once the instrumentation was installed, a series of controlled load tests were completed with the test vehicles traveling across the structure at crawl speed (3 to 5 mph). Data was recorded from all sensors at a sample rate of 40 Hz as each test vehicle crossed the structure along three different lateral positions, referred to as Paths Y1, Y2, and Y3 in the southbound direction (further described in Figure 1.18).

During the Round 1 load tests a 3-axle 71 kip dump was used for single lane loaded tests along all three paths. Next, a two lane test was also performed with a 3-axle 72 kip dump truck traveling next to the 3-axle 71 kip dump truck along Paths Y1 and Y3 respectively (Figure 1.7). Lastly, a tandem load test was conducted where the 72 kip truck pulled the 71 kip truck backwards along the center truck path as shown in Figure 1.8. This tandem test was performed to simulate a loading closer to that of the Military HETS vehicle load configuration. The 71 kip truck will be referred to as Truck 1 and the 72 kip truck will be referred to as Truck 2 for the remainder of this report. The Round 1 test vehicles' gross weights, axle weights, and wheel rollout distance (required for tracking its position along the structure) are provided in Table 1.2.

Vehicle "footprints" used in Round 1 are also shown in Figure 1.19 and Figure 1.20. The vehicle weights were obtained from certified scales and all vehicle dimensions were measured in the field at the time of testing.

During the second round of load tests, both a HETS/M1A1 military logistics vehicle and the M1A1 Abrams tank crossed the structure, separately, along all three test paths (Y1, Y2, & Y3). Recorded weights and axle spacing for these vehicles have been provided in Table 1.3 and Table 1.4

The test vehicles' longitudinal position was wirelessly tracked during each crossing so that the response data could later be viewed as a function of vehicle position rather than just an arbitrary point in time. The only live loads applied to the structure while data was being recorded were the wheel loads of the test vehicles.

BDI would like to thank Mandaree Enterprise Corporation for their help in scheduling, planning, organizing, and implementing the testing project.

Table 1.1 – Structure description & testing info.

ITEM	DESCRIPTION
STRUCTURE NAME	Bridge No. 4
MANDAREE PROJECT NUMBER	120246
BDI REFERENCE NUMBER	120901-KY
TESTING DATES	Round 1 - December 18th, 2012 Round 2 - December 18th, 2013
LOCATION/ROUTE	Main Range Road, Fort Knox Military Reservation, KY
STRUCTURE TYPE	Span 2: Composite Hybrid Girder
TOTAL NUMBER OF SPANS	2
SPAN LENGTHS	Span 2: 39'-0" (center-to-center of support)
STRUCTURE/ROADWAY WIDTHS	Structure: 27'-8"
WEARING SURFACE	N/A
SPANS TESTED	2
TEST REFERENCE LOCATION (BOW) (X=0,Y=0)	North-west corner of the structure at the expansion joint and outside edge of the slab
TEST VEHICLE DIRECTION	Southbound
TEST BEGINNING POINT	Front axle 20 ft. north of Span 2 from test reference location (BOW)
LOAD POSITIONS	Truck Path Y1 – Passenger's side wheel 3'-0" from BOW Truck Path Y2 – Passenger's side wheel 10'-3" from BOW Truck Path Y3 – Driver's side wheel 24'-8" from BOW
NUMBER/TYPE OF SENSORS	Round 1 load tests: - 22 Strain Transducers - 3 Cantilevered Displacement Sensors - 4 Tiltmeter Rotation Sensors Round 2 load tests: - 29 Strain Transducers - 5 Cantilevered Displacement Sensors - 4 Tiltmeter Rotation Sensors
SAMPLE RATE	40 Hz
NUMBER OF TEST VEHICLES	2
STRUCTURE ACCESS PROVIDED BY	BDI
VEHICLES PROVIDED BY	Mandaree Enterprise Corporation
TOTAL FIELD TESTING TIME	1 day

TEST FILE INFORMATION:	*FILE NAME*	*LATERAL POSITION*	*FIELD COMMENTS*
ROUND 1 TESTS SINGLE TRUCK TEST: TRUCK 1	FTK_1	Y1	Two missed clicks
	FTK_2	Y1	Missed click at 65 sec.
	FTK_3	Y1	Good test
	FTK_4	Y2	Good test.
	FTK_5	Y2	Clicker malfunction.
	FTK_6	Y2	Dropped node.
	FTK_7	Y2	Good test.
	FTK_8	Y3	Missed click at 41 sec.
	FTK_9	Y3	Good test
ROUND 1 TESTS TWO LANE TRUCK TEST	FTK_10	Y3 & Y1	Missed click at 10 sec.
ROUND 1 TESTS TANDEM TRUCK TEST	FTK_11	Y2	Bad Test.
	FTK_12	Y2	Good test
ROUND 2 TESTS M1A1 TANK	FtKnoxM1_1	Y1	Good Test. Popping in guardrail and offset in responses noted.
	FtKnoxM1_2	Y1	Good test. Less offset, still guardrail popping
	FtKnoxM1_3	Y2	Good Test.
	FtKnoxM1_4	Y2	Good Test.
	FtKnoxM1_5	Y3	Good Test. Popping in guardrail and offset in responses noted.
	FtKnoxM1_6	Y3	Good test. Less offset, still guardrail popping
ROUND 2 TESTS HETS/M1A1 VEHICLE	FtKnoxHETS_1	Y1	Moved vehicle 18" laterally to avoid guardrail. Good Test. Popping in guardrail
	FtKnoxHETS_2	Y1	Good test. Less offset, guardrail popping
	FtKnoxHETS_3	Y2	Good Test.
	FtKnoxHETS_4	Y2	Good Test.
	FtKnoxHETS_5	Y3	Moved vehicle 18" laterally to avoid guardrail. Good Test. Popping in guardrail and offset in responses noted.
	FtKnoxHETS_6	Y3	Good test. Less offset, guardrail popping
WEATHER:	Rain during instrumentation~40°F, sunny during test ~50°F		

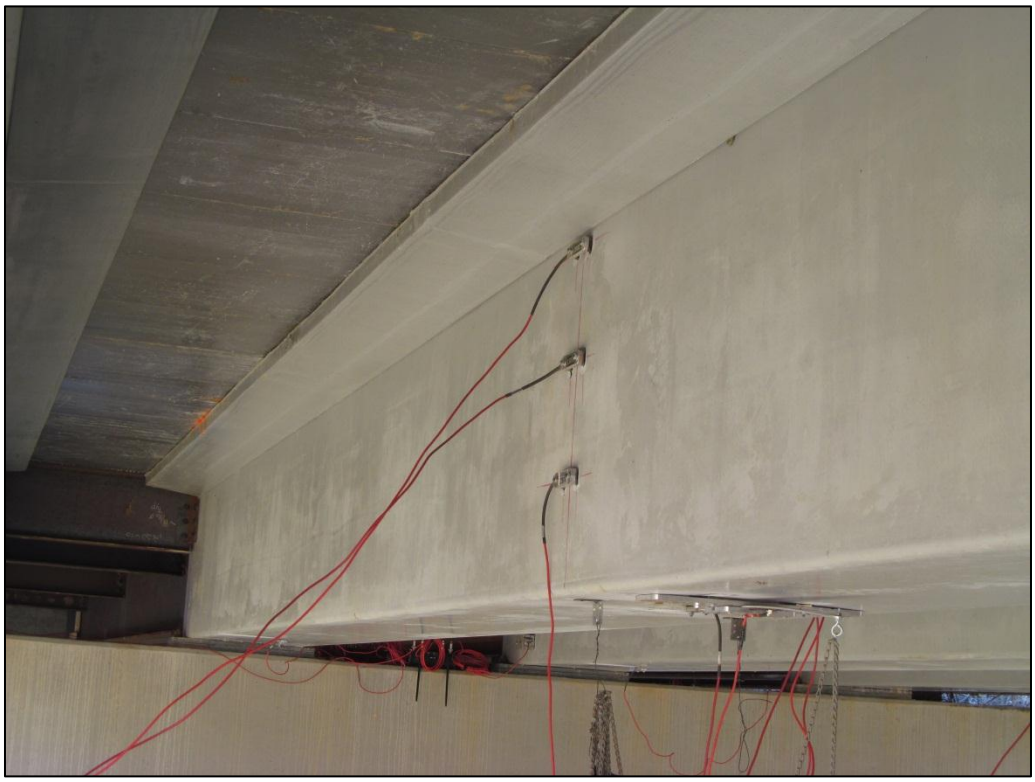

Figure 1.1 – Midspan instrumentation with strain, displacement and rotation sensors (typical of both test phases).

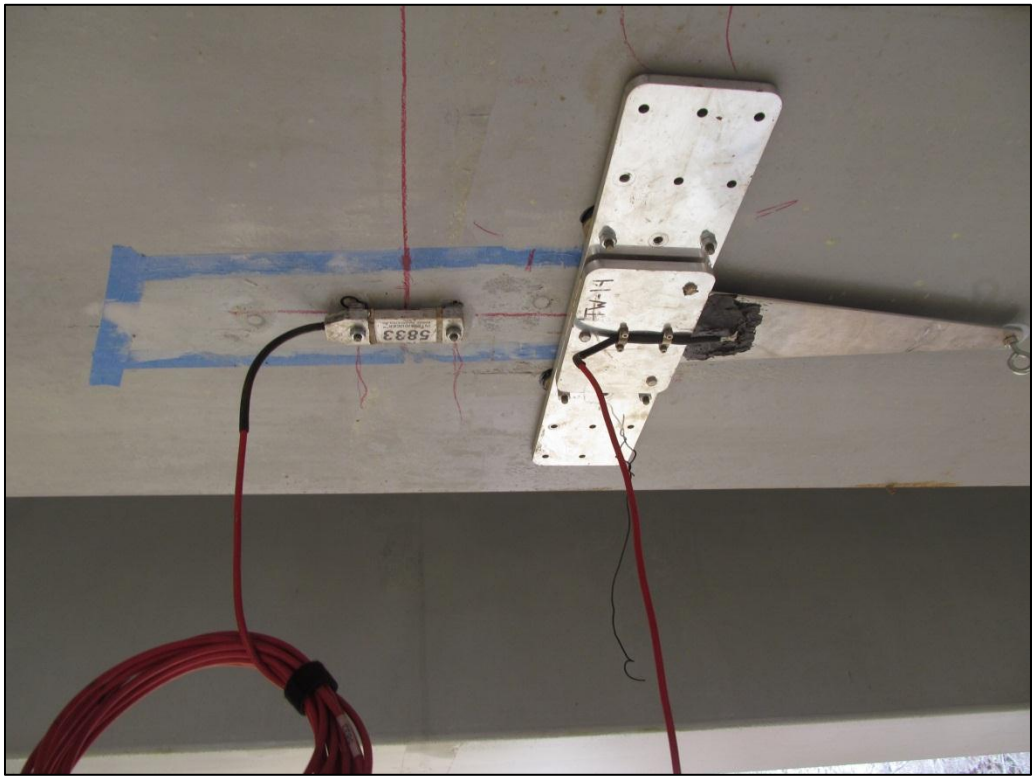

Figure 1.2 - Strain transducer and displacement sensor near midspan of HCB (typical of both test phases).

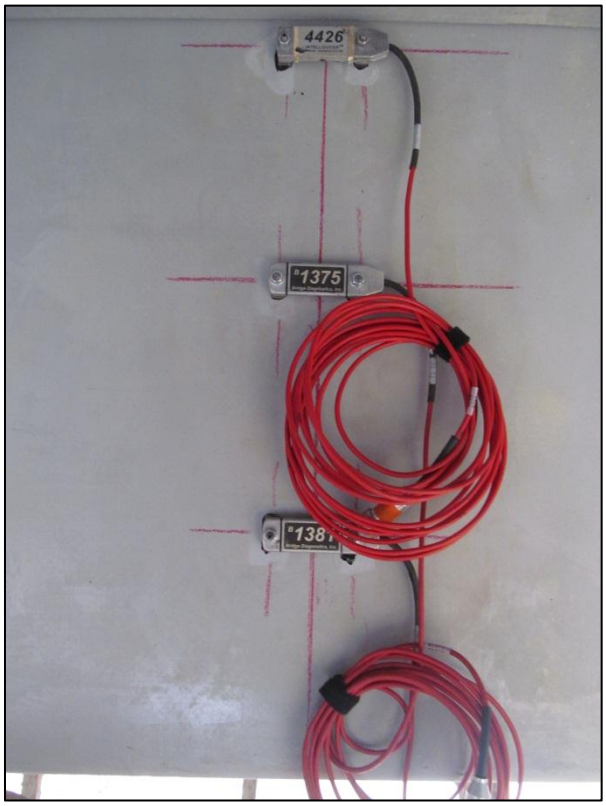

Figure 1.3 – Strain transducers installed on HCB web at midspan (typical of both test phases).

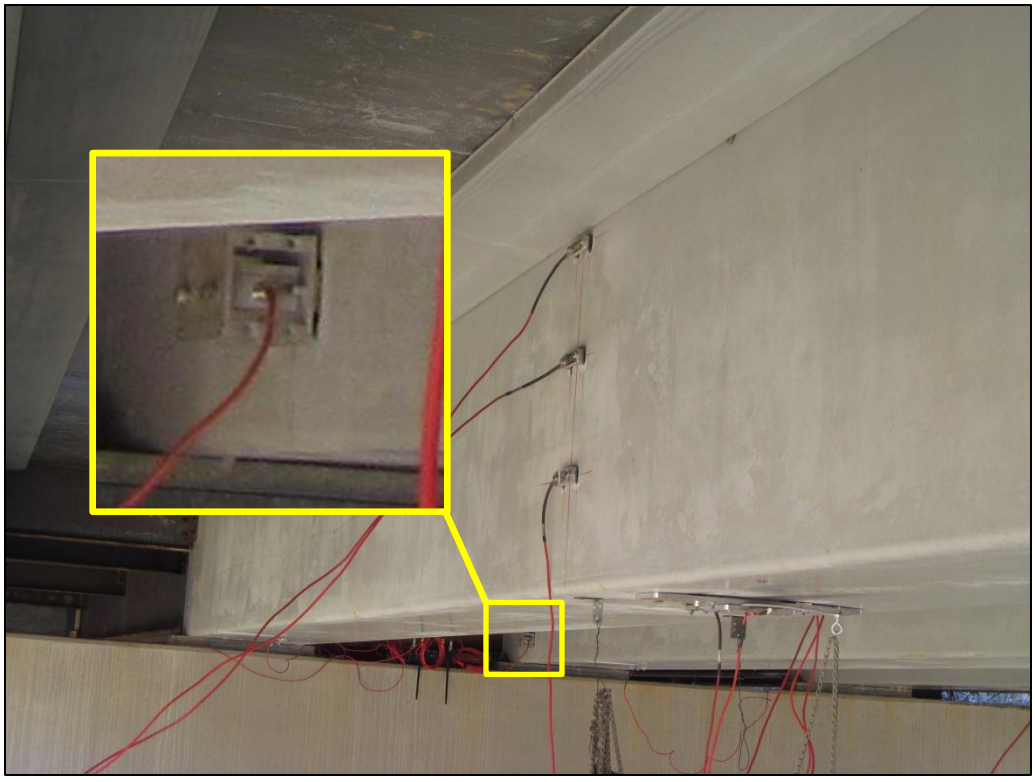

Figure 1.4 –Tiltmeter rotation sensor on HCB near pier beam bearing (typical of both test phases).

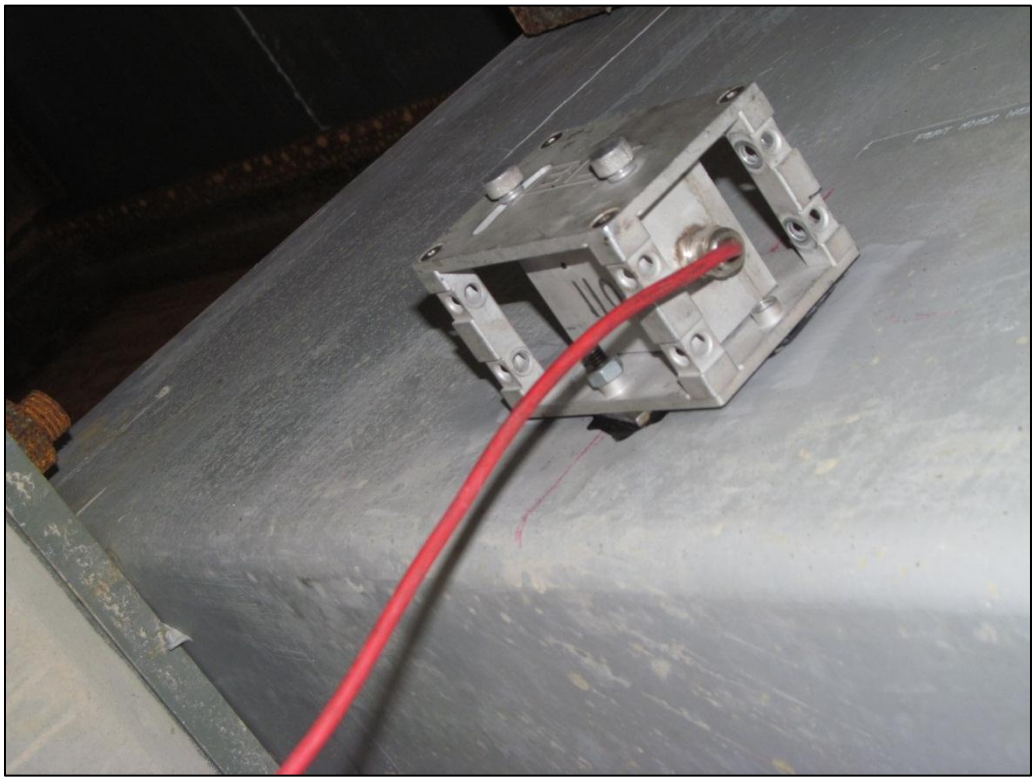

Figure 1.5 –Close up of tiltmeter rotation sensor on HCB (typical of both test phases).

Figure 1.6 – Round 1 Tests - Truck 1 crossing bridge along Path Y3.

Figure 1.7 – Round 1 Tests - Two lane truck test: Truck 1 @ Y3 & Truck 2 @ Y1.

Figure 1.8 – Round 1 Tests - Tandem truck test: Truck 2 pulling Truck 1 @ Y2.

Figure 1.9 – Round 2 Tests – M1A1 Abrams Tank crossing along @ Y1.

Figure 1.10 – Round 1 Tests – HETS vehicle with M1A1 crossing @ Path Y1.

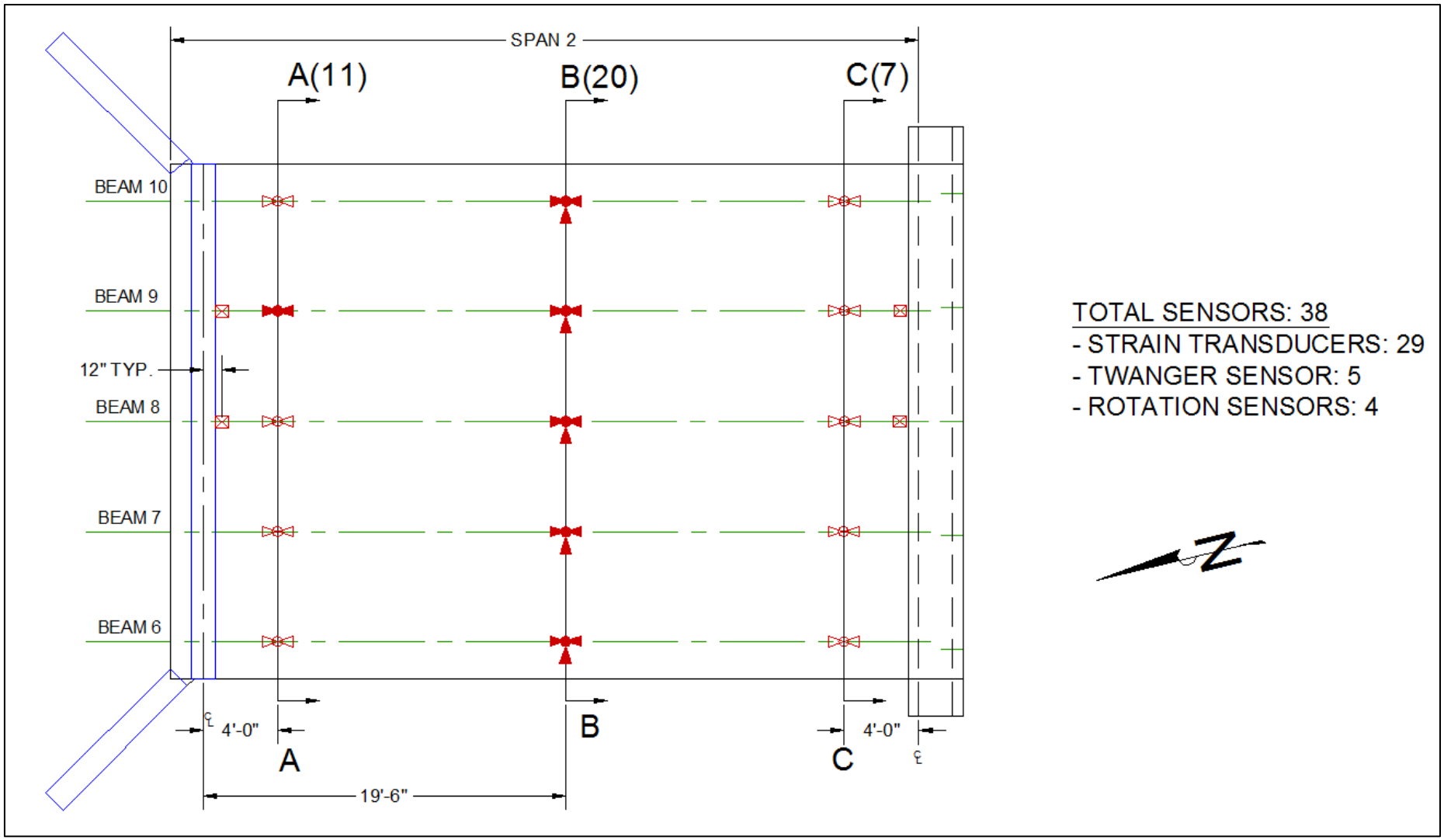

Figure 1.11 - Plan view of Bridge No. 4 – HCB Span - Instrumentation plan including gage types and locations. (Both Rounds of Testing).

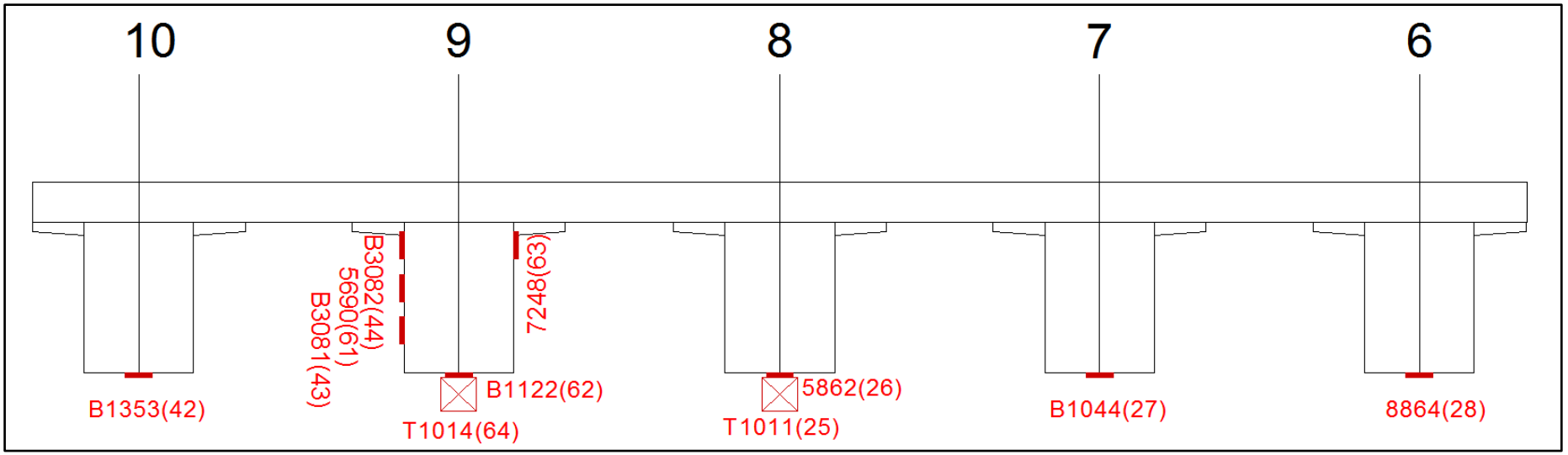

Figure 1.12 - Round 1 Tests - Section A-A instrumentation plan showing sensor IDs, Channel IDs, & sensor locations.

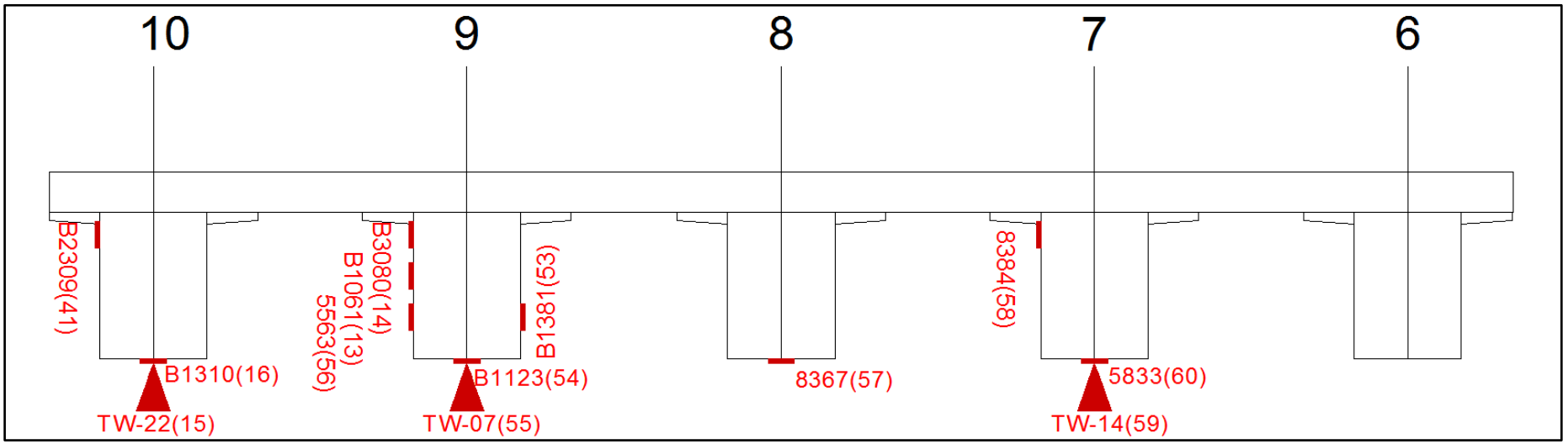

Figure 1.13 - Round 1 Tests - Section B-B instrumentation plan showing sensor IDs, Channel IDs, & sensor locations.

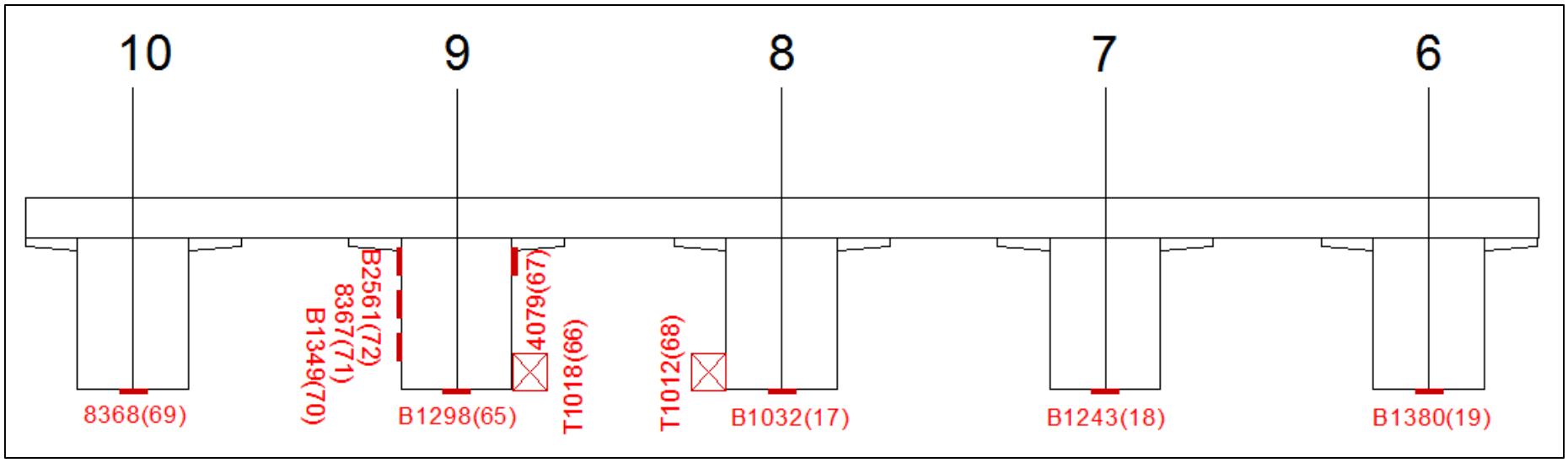

Figure 1.14 - Round 1 Tests - Section C-C instrumentation plan showing sensor IDs, Channel IDs, & sensor locations.

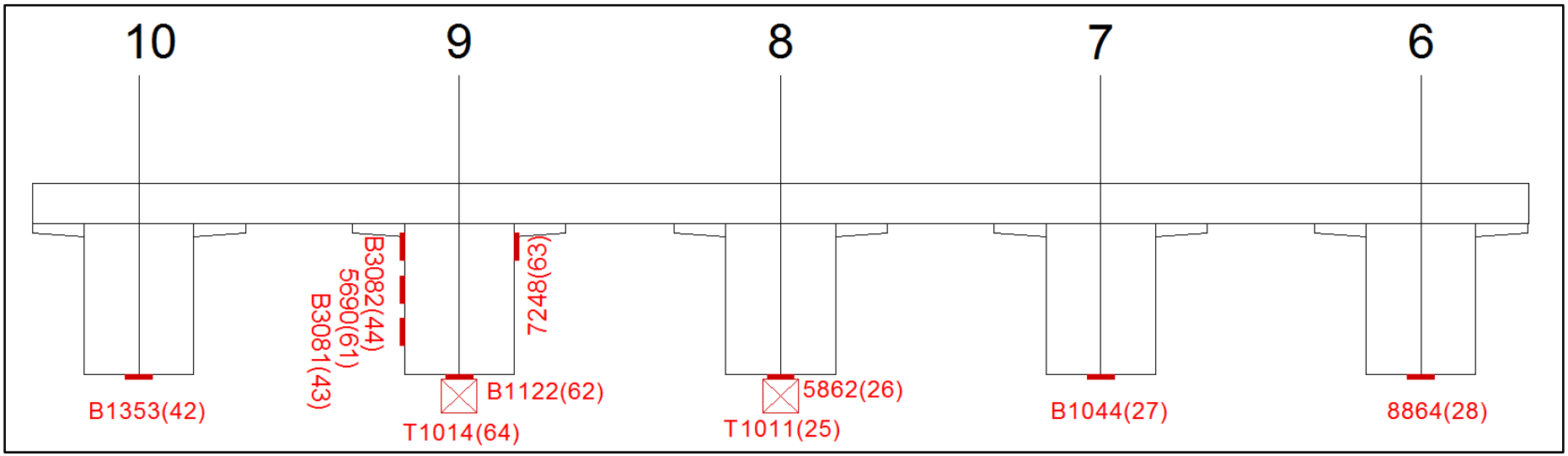

Figure 1.15 - Round 2 Tests - Section A-A instrumentation plan showing sensor IDs, Channel IDs, & sensor locations.

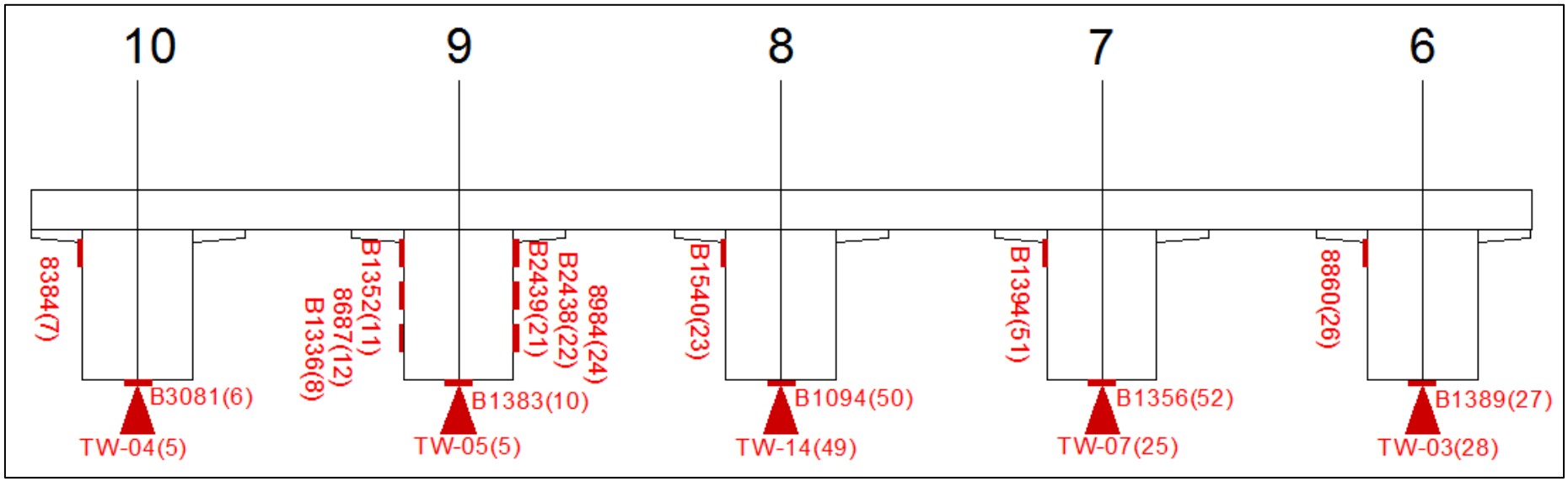

Figure 1.16 - Round 2 Tests - Section B-B instrumentation plan showing sensor IDs, Channel IDs, & sensor locations.

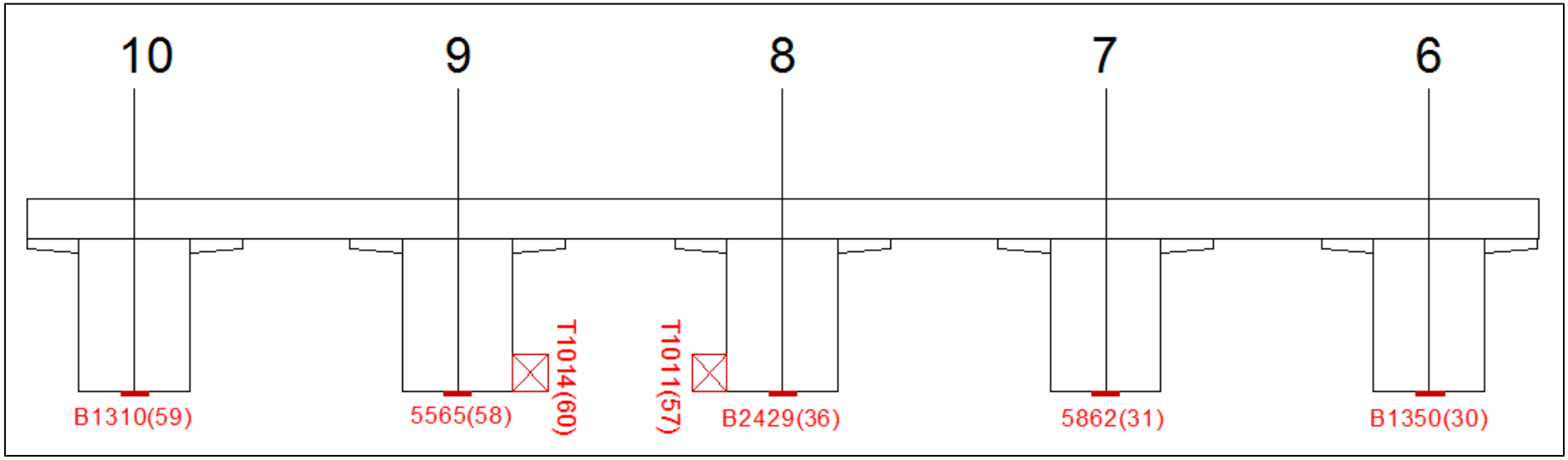

Figure 1.17 - Round 2 Tests - Section C-C instrumentation plan showing sensor IDs, Channel IDs, & sensor locations.

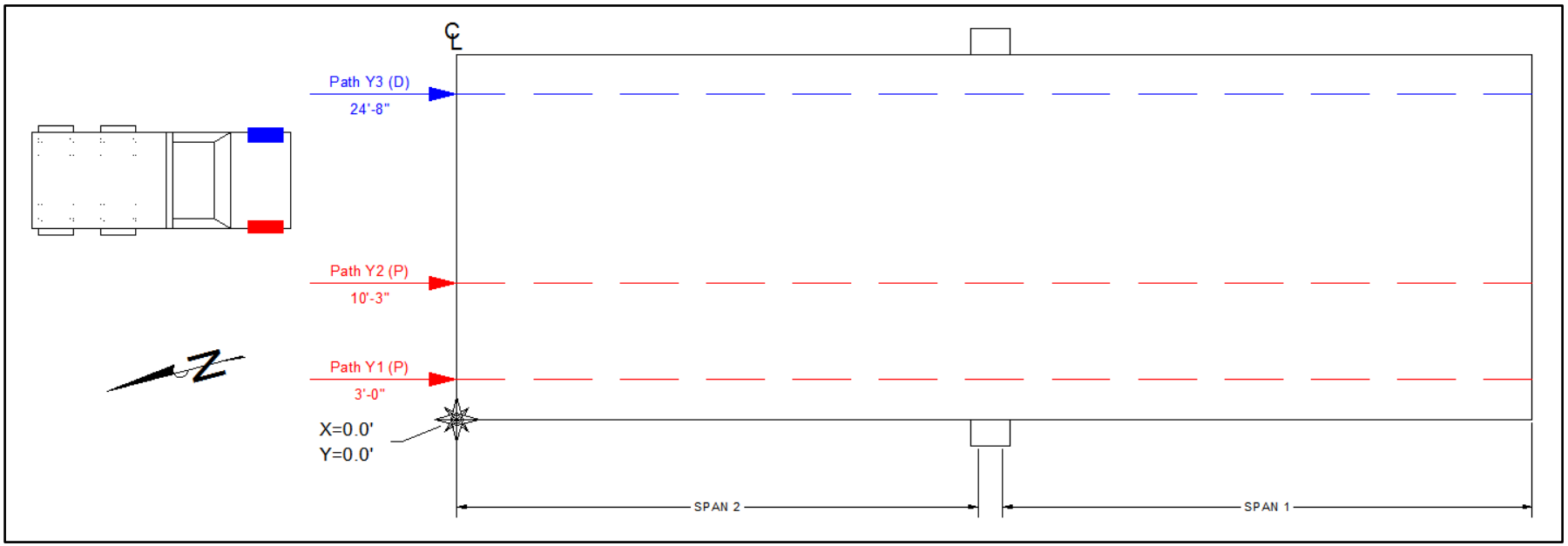

Figure 1.18 - Test vehicle path locations for Bridge #4.

Table 1.2 – Test vehicle information – Round 1 Tests.

VEHICLE TYPE	**TRUCK 1 TEST VEHICLE 3-AXLE DUMP TRUCK**	
GROSS VEHICLE WEIGHT (GVW)	70,920 lbs	
WEIGHT/WIDTH - AXLE 1: FRONT	20,430 lbs	6'-11"
WEIGHT/WIDTH - AXLE 2: REAR TANDEM PAIR 1	25,490 lbs	7'-2"
WEIGHT/WIDTH - AXLE 3: REAR TANDEM PAIR 2	25,000 lbs	7'-2"
SPACING: AXLE 1 - AXLE 2	16'-0"	
SPACING: AXLE 2 – AXLE 3	4'-5"	
WEIGHTS PROVIDED BY	BDI	
WHEEL ROLLOUT DISTANCE	11.08' per wheel revolution	
VEHICLE TYPE	**TRUCK 2 TEST VEHICLE 3-AXLE DUMP TRUCK**	
GROSS VEHICLE WEIGHT (GVW)	71,940 lbs	
WEIGHT/WIDTH - AXLE 1: FRONT	18,720 lbs	7'-0"
WEIGHT/WIDTH - AXLE 2: REAR TANDEM PAIR 1	26,720 lbs	7'-1"
WEIGHT/WIDTH - AXLE 3: REAR TANDEM PAIR 2	26,500 lbs	7'-1"
SPACING: AXLE 1 - AXLE 2	16'-6"	
SPACING: AXLE 2 – AXLE 3	4'-5"	
WEIGHTS PROVIDED BY	BDI	

Table 1.3 – Test vehicle information – Round 2 Tests – HETS/M1A1.

VEHICLE TYPE	HETS/M1A1 VEHICLE	
GROSS VEHICLE WEIGHT (GVW)	216,730 lbs	
WEIGHT/WIDTH - AXLE 1	20,150 lbs	7'-0"
WEIGHT/WIDTH - AXLE 2	21,050 lbs	7'-0"
WEIGHT/WIDTH - AXLE 3	19,440 lbs	7'-0"
WEIGHT/WIDTH - AXLE 4	18,750 lbs	7'-0"
WEIGHT/WIDTH - AXLE 5	24,940 lbs	11'-3"
WEIGHT/WIDTH - AXLE 6	25,030 lbs	11'-3"
WEIGHT/WIDTH - AXLE 7	24,320 lbs	11'-3"
WEIGHT/WIDTH - AXLE 8	30,810 lbs	11'-3"
WEIGHT/WIDTH - AXLE 9	32,240 lbs	11'-3"
SPACING: AXLE 1 - AXLE 2	13'-0"	
SPACING: AXLE 2 – AXLE 3	5'-0"	
SPACING: AXLE 3 – AXLE 4	5'-0"	
SPACING: AXLE 4 – AXLE 5	15'-0"	
SPACING: AXLE 5 – AXLE 6	6'-0"	
SPACING: AXLE 6 – AXLE 7	6'-0"	
SPACING: AXLE 7 – AXLE 8	6'-0"	
SPACING: AXLE 9 – AXLE 10	6'-0"	
WEIGHTS PROVIDED BY	BDI	
WHEEL ROLLOUT DISTANCE	13.78' per wheel revolution	

Table 1.4 – Test vehicle information – Round 2 Tests – M1A1 Abrams.

VEHICLE TYPE	M1A1 ABRAMS TANK	
GROSS VEHICLE WEIGHT (GVW)	70,920 lbs	
WEIGHT/WIDTH - AXLE 1	20,220 lbs	9'-4"
WEIGHT/WIDTH - AXLE 2	23,360 lbs	9'-4"
WEIGHT/WIDTH - AXLE 3	23,030 lbs	9'-4"
WEIGHT/WIDTH - AXLE 4	22,430 lbs	9'-4"
WEIGHT/WIDTH - AXLE 5	17,720 lbs	9'-4""
WEIGHT/WIDTH - AXLE 6	16,060 lbs	9'-4""
WEIGHT/WIDTH - AXLE 7	12,290 lbs	9'-4""
SPACING: AXLE 1 - AXLE 2	2'-5"	
SPACING: AXLE 2 – AXLE 3	2'-5"	
SPACING: AXLE 3 – AXLE 4	2'-5"	
SPACING: AXLE 4 – AXLE 5	2'-5"	
SPACING: AXLE 5 – AXLE 6	2'-6"	
SPACING: AXLE 6 – AXLE 7	3'-6"	
WEIGHTS PROVIDED BY	BDI	
WHEEL ROLLOUT DISTANCE	7.05' per wheel revolution	

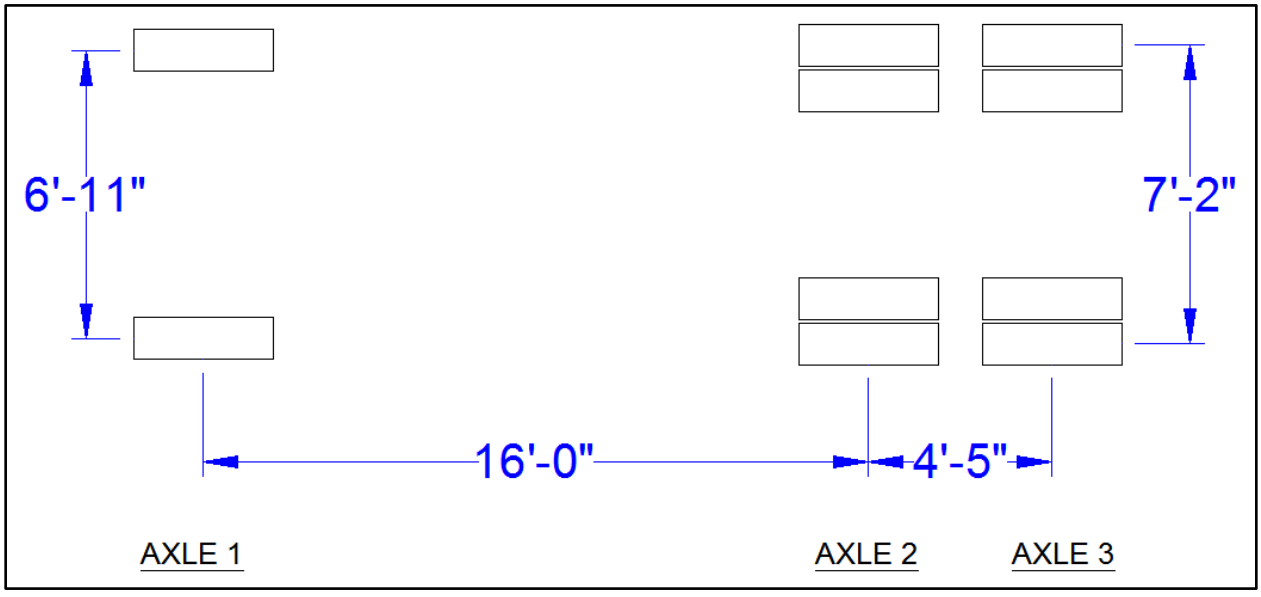

Figure 1.19 - Test vehicle footprint – Round 1 Tests- Truck 1.

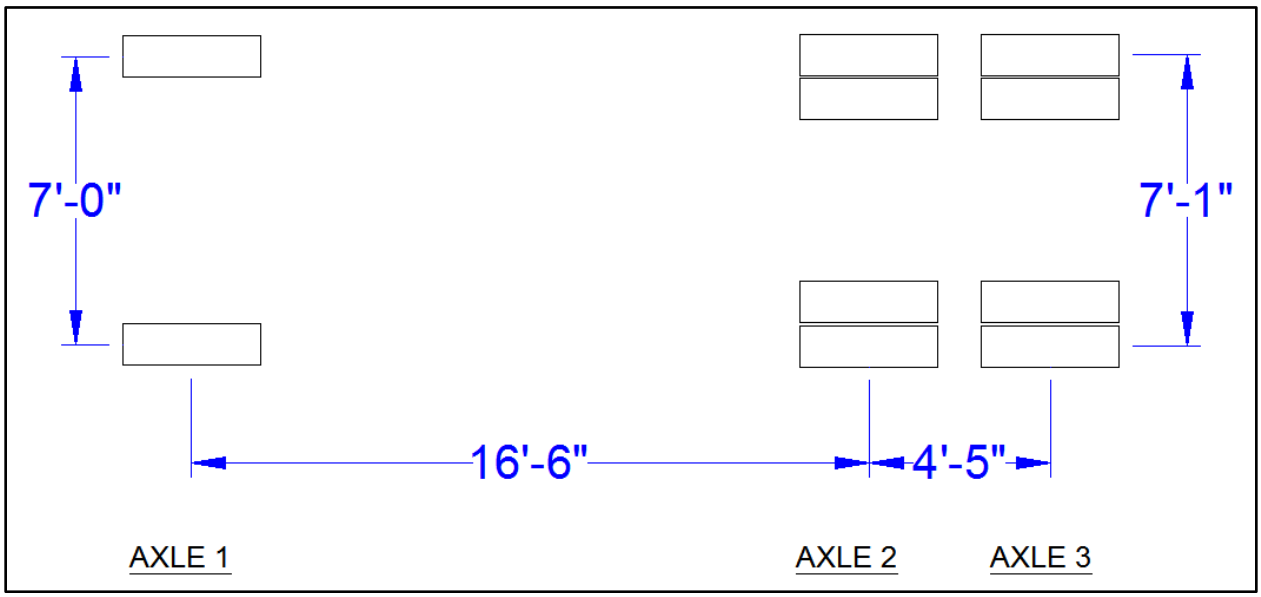

Figure 1.20 - Test vehicle footprint – Round 1 Tests – Truck 2.

2. PRELIMINARY INVESTIGATION OF TEST RESULTS

All of the field data was examined graphically to provide a *qualitative* assessment of the structure's live-load response. Some indicators of data quality include reproducibility between tests along identical truck paths, elastic behavior (strains returning to zero after truck crossing), and any unusual-shaped responses that might indicate nonlinear behavior or possible gage malfunctions. This process can provide a significant insight into a structure's response due to live-load, and is extremely helpful in performing an efficient and accurate structural analysis.

- *RESPONSES AS A FUNCTION OF LOAD POSITION:* Data recorded from the wireless truck position indicator (BDI AutoClicker) was processed so that the corresponding response data could be presented as a function of vehicle position. This step was crucial during the model calibration process since it allowed the engineer to easily compare the measured and computed responses as the truck loads moved across the structure. Please note that the test reference location (denoted at "Beginning of World" or "BOW) was located at the bridge's north expansion joint and corresponds to the 0 ft load position in provided figures.

  Once all data was processed as a function of load position, one file from each of the test types was selected as having the best apparent quality. Table 2.1 and Table 2.2 provide a list of the selected data for all test types for both rounds of load tests. Please note that the selected data was used to determine the response envelopes for all gages.

- *REPRODUCIBILITY AND LINEARITY OF RESPONSES:* Responses from identical truck passes were found to be very reproducible as shown in Figure 2.1 through Figure 2.6. In addition, all response data appeared to be linear with respect to load magnitude and truck position. Note that the majority of responses returned to zero indicating elastic behavior, with the exception of residual responses that occurred when each girder was loaded with a heavier loading than it had previously resisted. This response mechanism occurred during both rounds of testing and is discussed further in the next bullet point. Despite the initial loading offset observed in a few test files, all of the response histories had a similar degree of reproducibility and linearity, indicating that the data collected was of good quality.

- *MOVEMENT AT BEARINGS & BRIDGE RAILS OBSERVED UNDER HEAVY LOADINGS:* Residual readings or "response offsets" were observed after each heavier test load crossed the structure. These offsets were primarily seen on directly loaded girders during the load tests in which a heavier loading crossed the structure for the first time. This phenomenon occurred first with the single Round 1 dump trucks crossings; next with the Round 1 double dump truck configuration crossings; then with the Round 2 M1A1 tank crossings; and finally with the Round 2 HETS crossing. Note: each test load was heavier than the previous vehicle configuration that had crossed the structure. However, all of the structural responses were found to essentially return to zero in duplicate load tests, indicating that the girders returned to their original state once the initial movement had occurred. Figure 2.7 through Figure 2.10 provide strain and displacement histories from initial and duplicate tests that illustrate this observed behavior.

  After reviewing the Round 1 test data, it was found that the initial residual responses under the dump truck configurations were most likely caused by movement at the bearing locations. This bearing movement simply occurred in the girders that had never been loaded to such a large magnitude before that given load test. This behavior is common for simply supported

structures with bearing conditions that can develop friction between the bearing plates and the bottom of the beams.

After reviewing the Round 2 test data, it was found that not only was there evidence of movement at the bearings, but there was also evidence of movement at the connection between the bridge rail and the deck edge. This additional movement was observed as much larger offsets along the exterior beams when compared to the interior beams. This data observation was supported by loud popping noises coming from the metal guardrail as the military vehicles crossed the structure; especially during the first tests run near the structure's edges (Test Paths Y1 & Y3). This behavior was likely due to the fact that the bridge rails were not installed during the first round of tests, and the M1A1 and HETS crossings were the first time these details were heavily loaded.

In general, this type of behavior is common for newer structures and does not affect the structural capacity of the bridge.

- *LATERAL LOAD DISTRIBUTION OBSERVED IN THE HCB DISPLACEMENTS:* When evaluating a bridge for the purpose of developing a load rating, the bridge's ability to laterally distribute load is an essential characteristic to quantify. The Round 1 displacement responses were found to be very consistent and symmetrical as shown in Figure 2.11. This plot shows midspan displacements of an exterior beam, interior beam, and center beam under the symmetrical loading of Truck Paths Y1, Y2, and Y3. Note that due to access issues, a full line of displacement sensors could not be installed at midspan of the HCBs.

  Lateral distribution is most easily observed by plotting the response values from an entire gage line cross-section as shown in Figure 2.12. The Round 2 response values shown in this figures correspond to the longitudinal load positions producing the maximum displacement responses for each truck path at a midspan gage line (Sections B-B). It can be observed from this figure that a substantial amount of lateral load distribution was observed and that the displacement distribution was symmetrical. This symmetric behavior is important to note when looking at the inconsistent strain magnitudes (discussed in the following bullet point).

- *INCONSISTENT STRAIN MAGNITUDES RECORDED ON GFRP:* Although strain responses from a given location were found to be reproducible, it was found that the strain magnitudes measured in similar locations varied significantly. For example, even though the midspan displacement responses were found to be very consistent and symmetrical (as shown in Figure 2.11 and Figure 2.12), the maximum strain magnitudes from similarly loaded beams varied by up to 50% as shown in Figure 2.13. This inconsistency in the recorded strain magnitude was observed throughout the HCB span (both at midspan and near the beam ends), as shown in Figure 2.14 through Figure 2.15. Conversely to the strain magnitudes being highly variable, the strain history shapes were very consistent among similar transducer locations.

  The strain discrepancies did not appear to be a function of the transducers and it was determined that the strain magnitudes were heavily influenced by local conditions at the transducer locations. The two most likely possibilities include: discrete changes in shell thickness due to stiffeners or spacers near some of the gage locations or flexural induced strains due to imperfections in the thin GRFP plate. Small cups or warps in the GRFP shell could have a significant effect on surface strains because those curved surfaces would tend to flatten out as a result of in-plane tension. It should be noted at under the heavier load configurations (M1A1 tank and HETS vehicle loaded with M1A1 tank) the variation in strain

magnitude between similar locations was reduced, especially near the abutments. This observation likely provides evidence that these variations were due to small imperfections in the GFRP shell (i.e., slight warps along the GFRP shell surface). These warps would eventually straighten out under loading and have a lesser effect on the measurements.

Due to this observation, only the shapes of the strain responses were used during modeling since the strain shapes were found to be consistent and could provide valuable information on the structural behavior under live-load.

- *CONTINUITY AT SUPPORTS:* It was noted that both spans were acting somewhat continuous across the pier, as shown in Figure 2.17. The observed level of continuity was not expected since each span was designed to be simply supported. The continuity was most likely due to the pier wall's ability to transfer load axially between the each span's bearing-seat. This type of continuity and end-restraint can be considered inconsequential when performing load rating calculations, but must be considered during model calibration procedures because it influences the measured responses.

  As previously stated, all test data was initially processed and assessed for quality. Then, one set of test data for each truck path was selected for having the best apparent quality. This selected data was then used to verify and calibrate the finite-element (FE) model of the structure, which was in turn used to load rate the HCB span. Table 2.1 and Table 2.2 provide a list of the data files that were used in the FE analysis for both rounds of load tests.

Table 2.1 – Round 1 Tests - Bridge No. 4 Selected Truck Path File Information.

TEST TYPE	TRUCK PATH	SELECTED DATA FILE
Single Truck Crossing – Truck 1	Y1	FTK_3.dat
	Y2	FTK_7.dat
	Y3	FTK_9.dat
Side-by-Side Truck Crossing	Truck 1(Y3), Truck 2 (Y1)	FTK_10.dat
Tandem Truck Crossing	Truck 2 towing backwards Truck 1	FTK_12.dat

Table 2.2 – Round 2 Tests - Bridge No. 4 Selected Truck Path File Information.

TEST TYPE	TRUCK PATH	SELECTED DATA FILE
M1A1 Abrams Tank	Y1	FtKnoxM1_2.dat
	Y2	FtKnoxM1_4.dat
	Y3	FtKnoxM1_6.dat
HETS/M1A1 Vehicle	Y1	FtKnoxHETS_2.dat
	Y2	FtKnoxHETS_4.dat
	Y3	FtKnoxHETS_6.dat

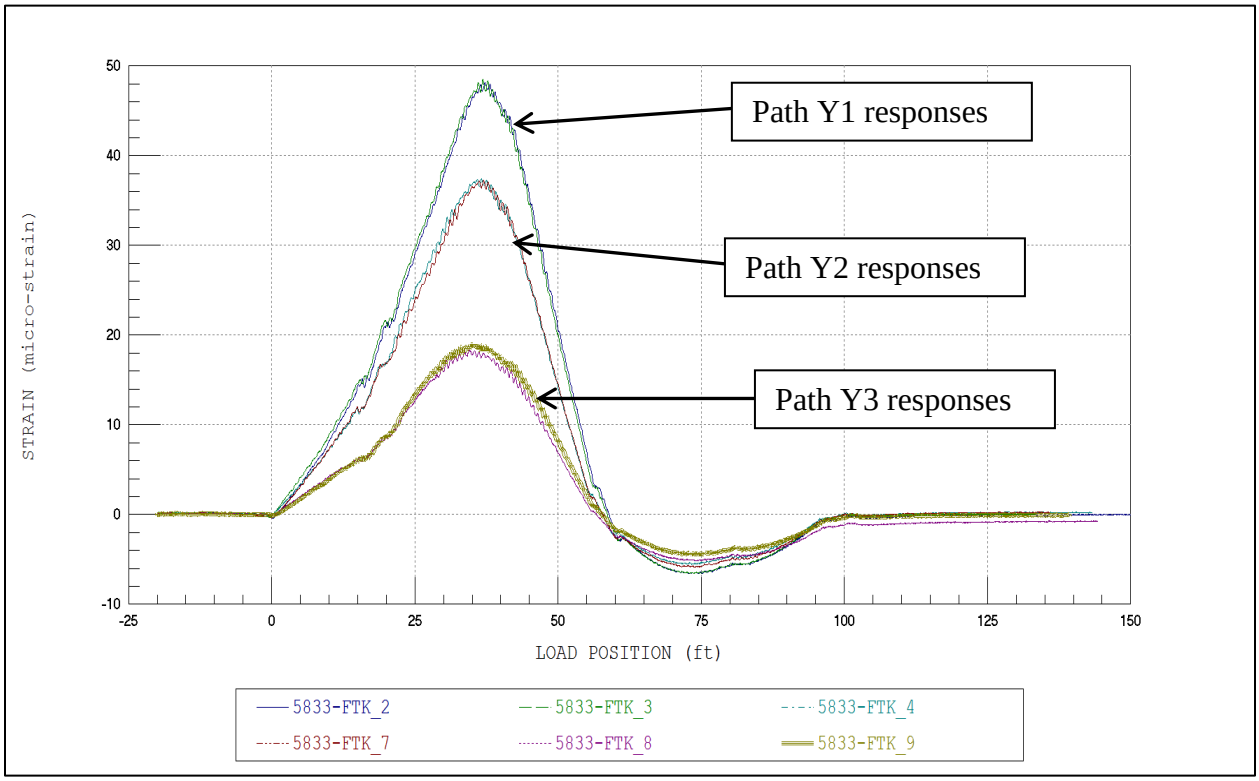

Figure 2.1 - Round 1 Tests - Example of Strain Reproducibility – Near Midspan (Typical).

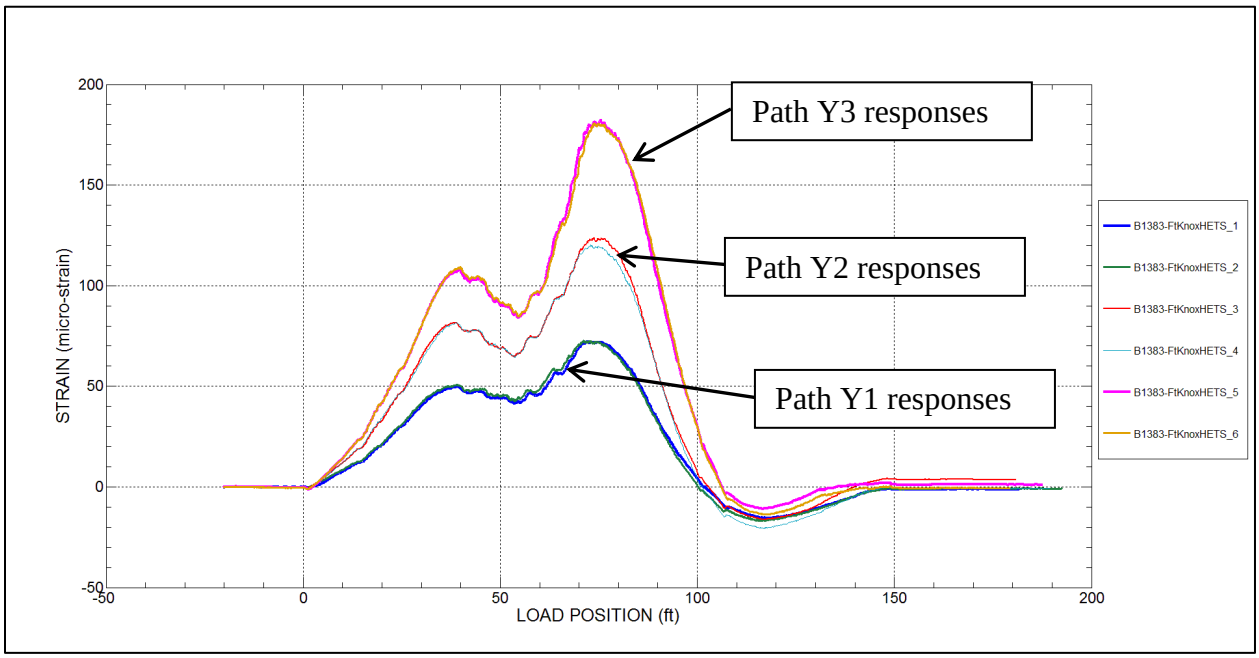

Figure 2.2 - Round 2 Tests - Example of Strain Reproducibility – Near Midspan (Typical).

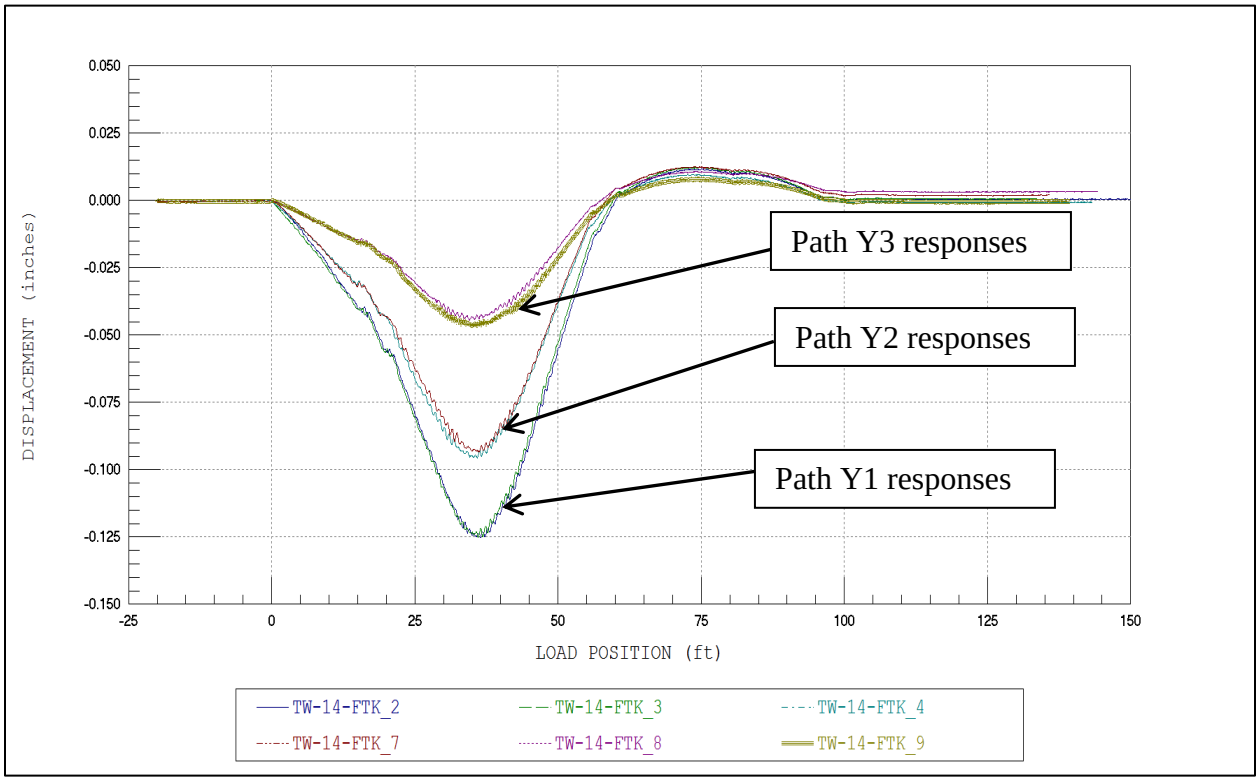

Figure 2.3 – Round 1 Tests - Example of Displacement Reproducibility – Near Midspan (Typical).

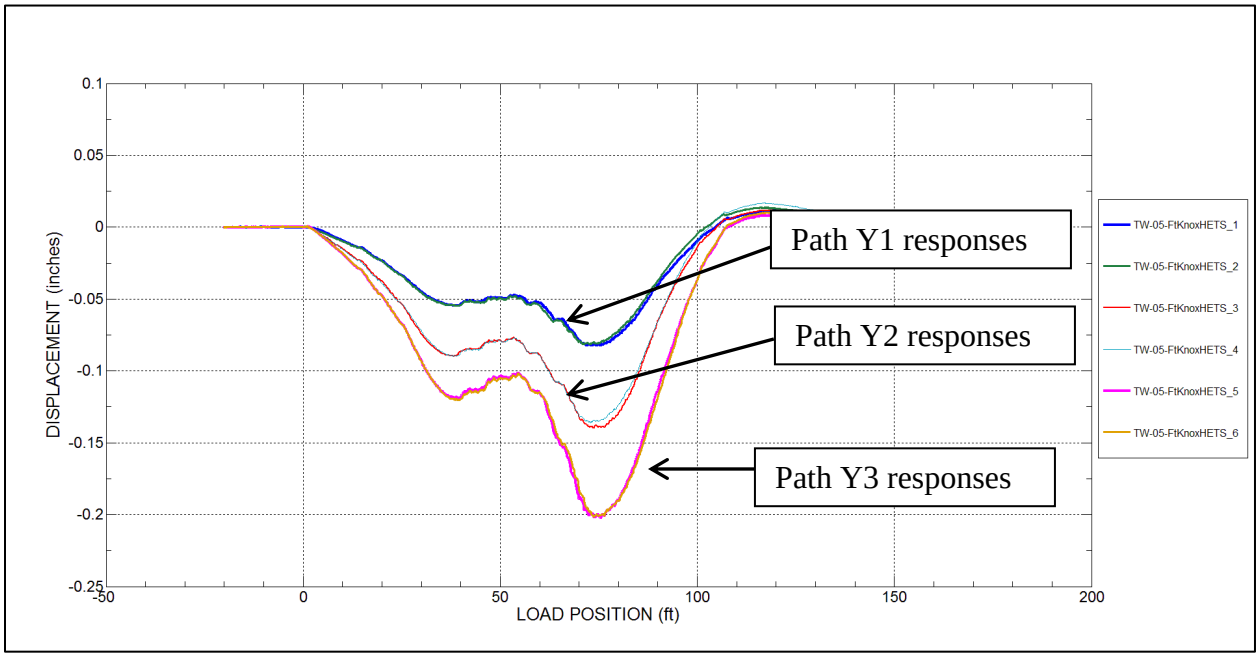

Figure 2.4 – Round 2 Tests - Example of Displacement Reproducibility – Near Midspan (Typical).

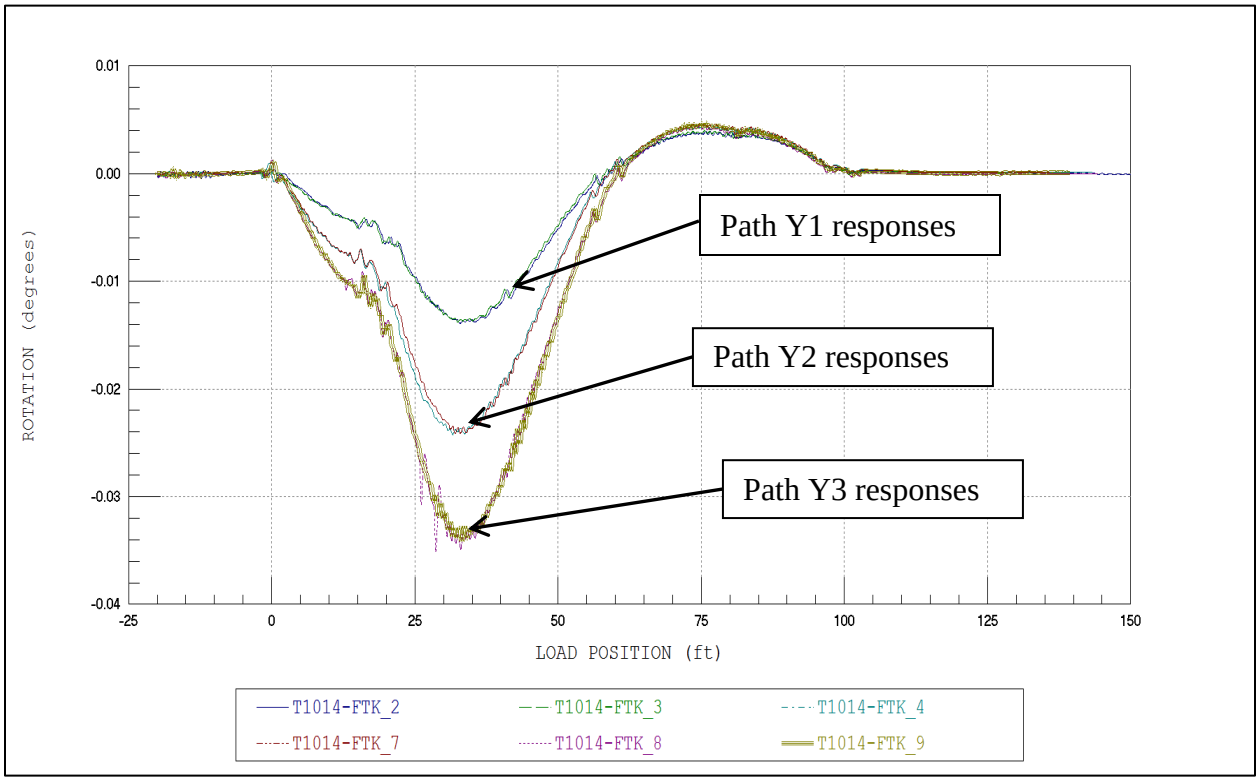

Figure 2.5 – Round 1 Tests - Example of Rotation Reproducibility – Near Abutment (Typical).

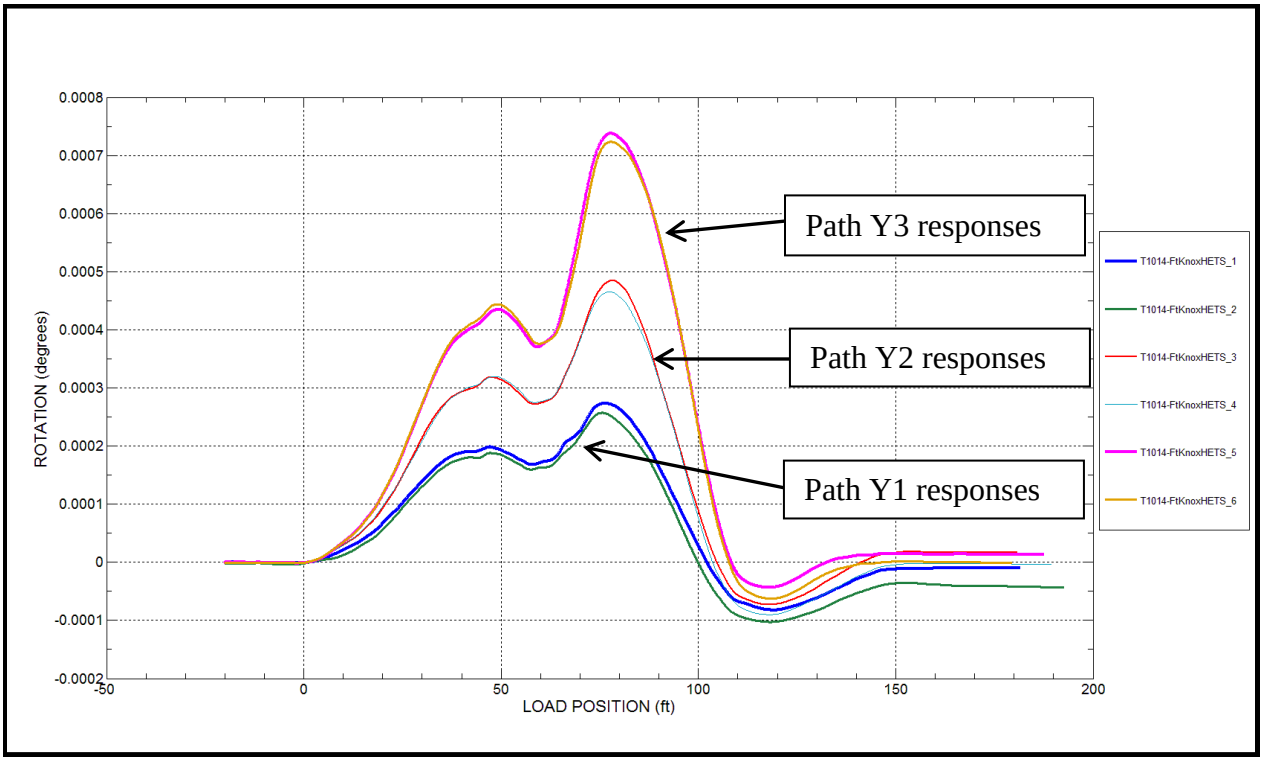

Figure 2.6 – Round 2 Tests - Example of Rotation Reproducibility – Near Abutment (Typical).

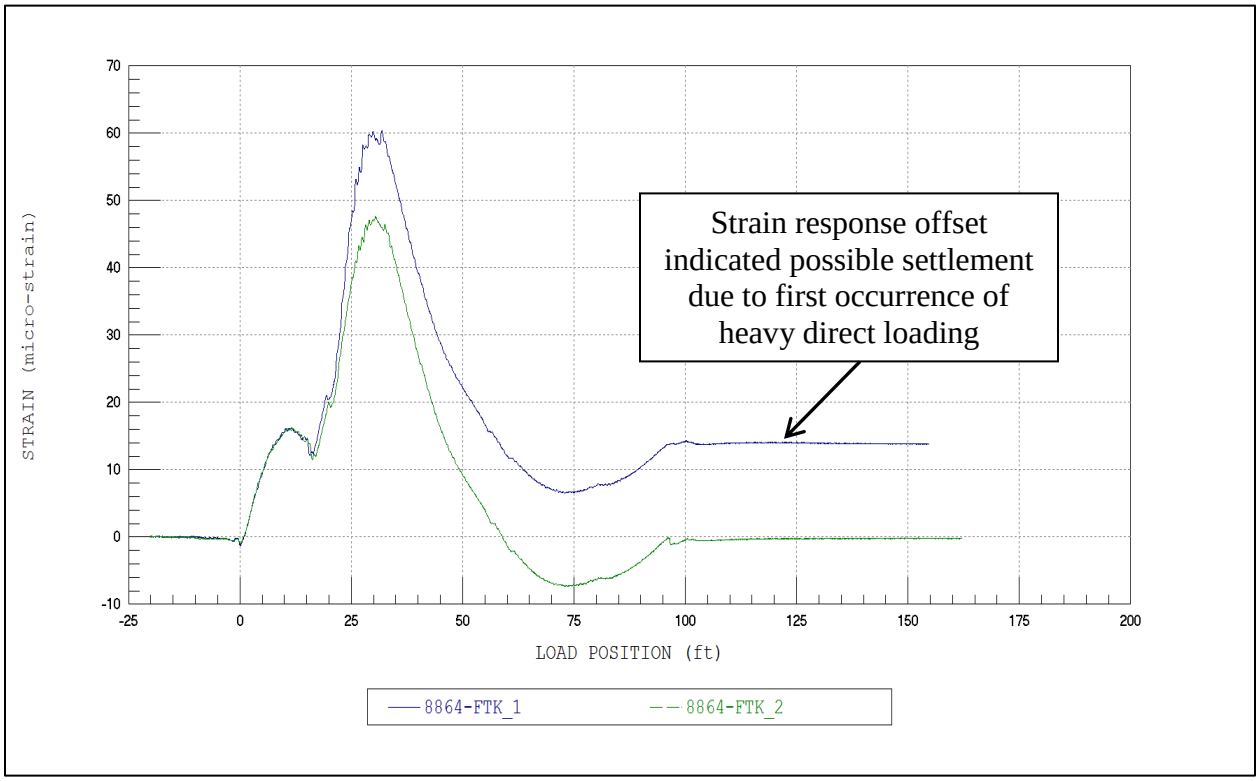

Figure 2.7 - Round 1 Tests - Strain Response History – Near Abutment – Directly Loaded by Truck Path Y1 – Highlighting movement at Bearings under First Heavy Loading.

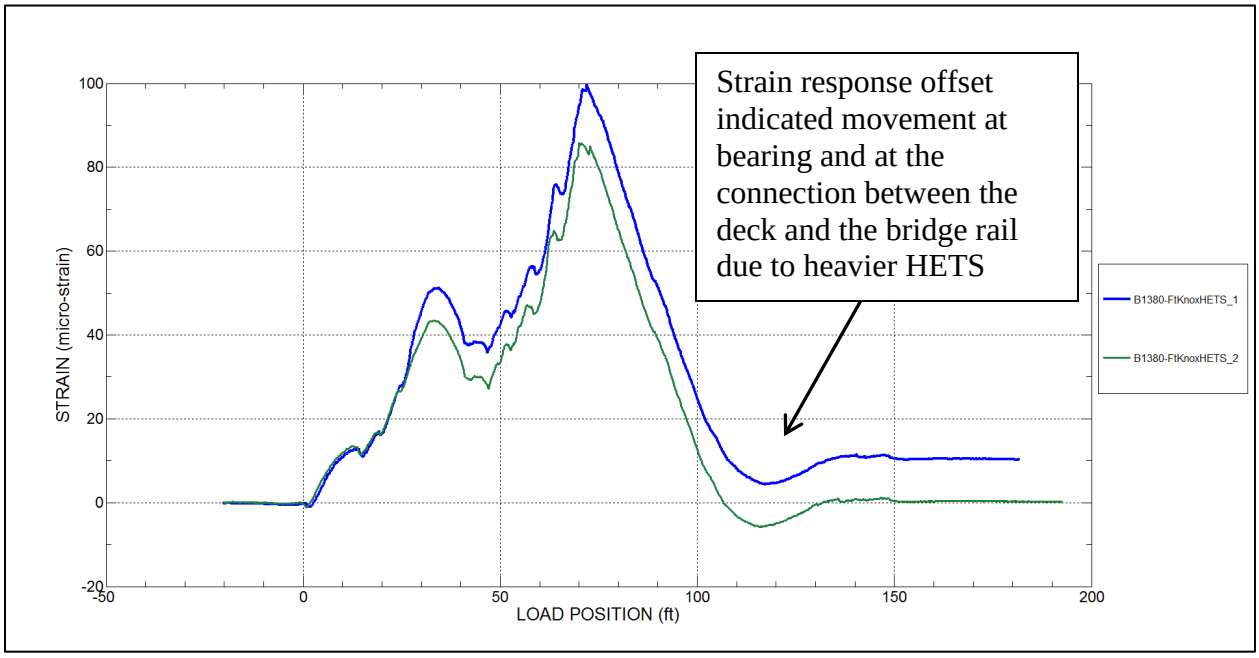

Figure 2.8 - Round 2 Tests - Strain Response History – On HCB near pier – Directly loaded by truck path Y3 – HETS vehicle caused offsets.

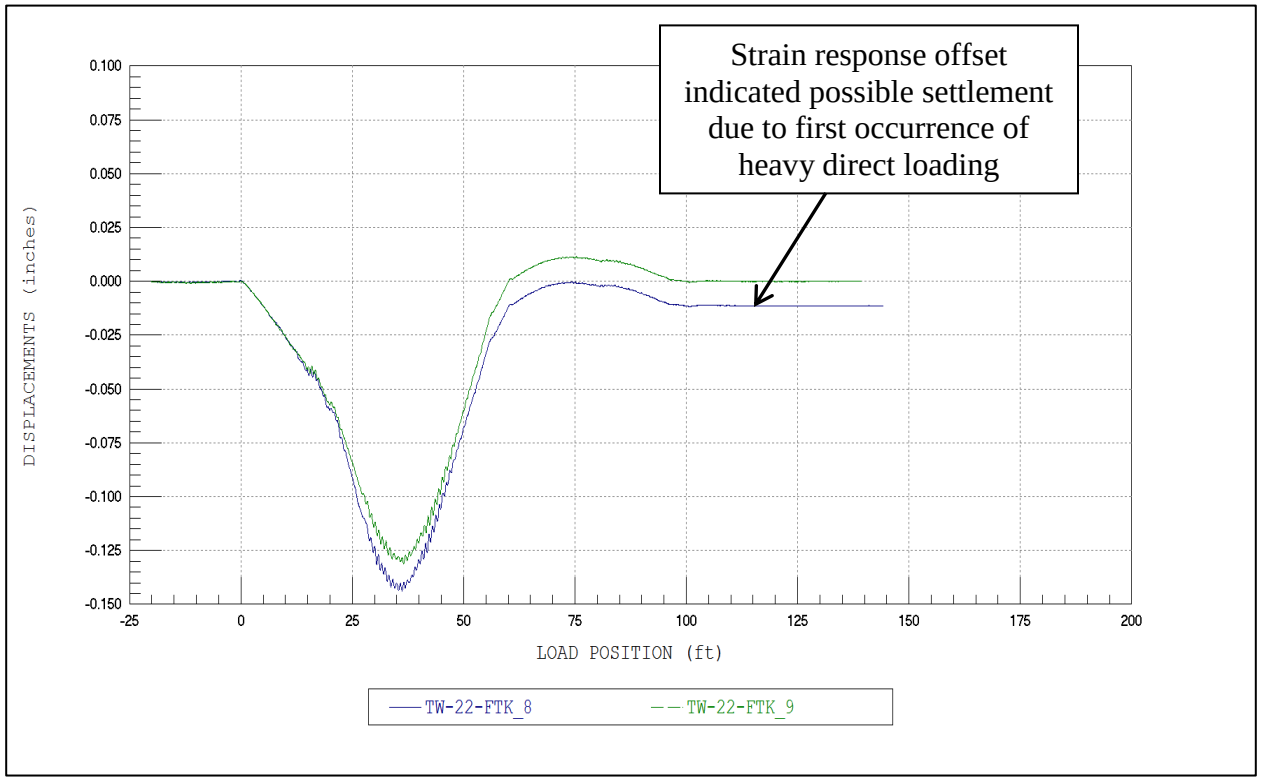

Figure 2.9 – Round 1 Tests - Midspan Displacement Response History – Directly Loaded by Truck Path Y3 – Highlighting movement at Bearings under First Heavy Loading.

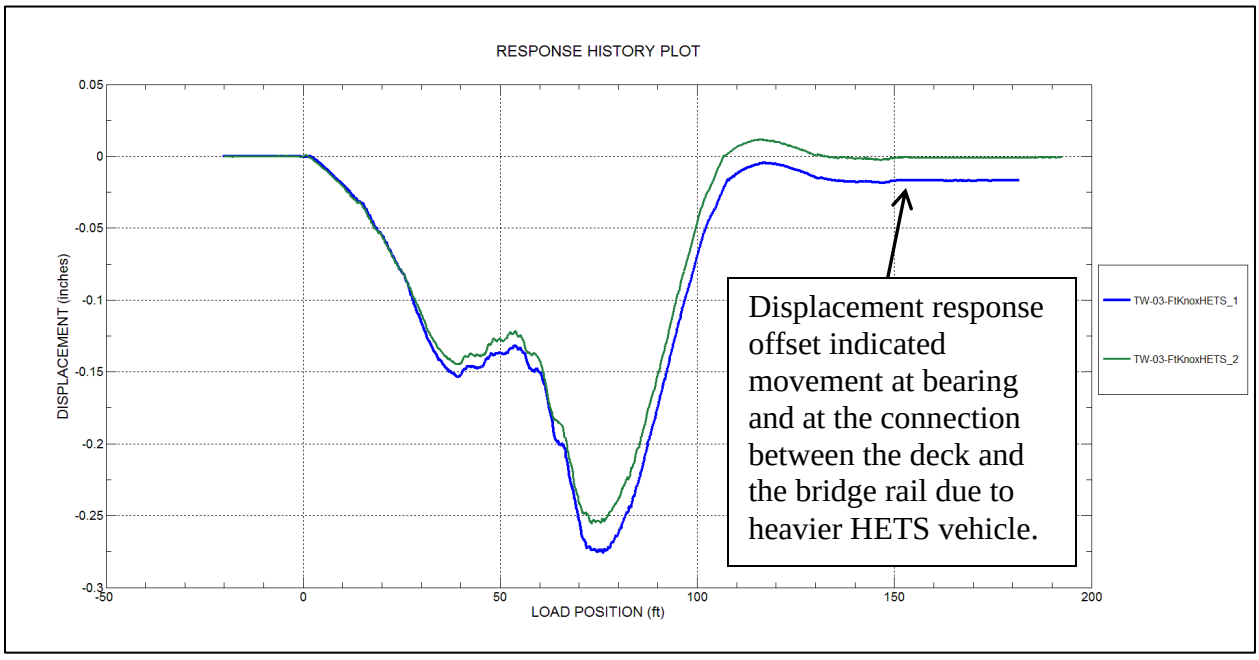

Figure 2.10 – Round 2 Tests - Displacement Response History – On HCB near midspan – Directly loaded by truck path Y3 - HETS vehicle caused offsets.

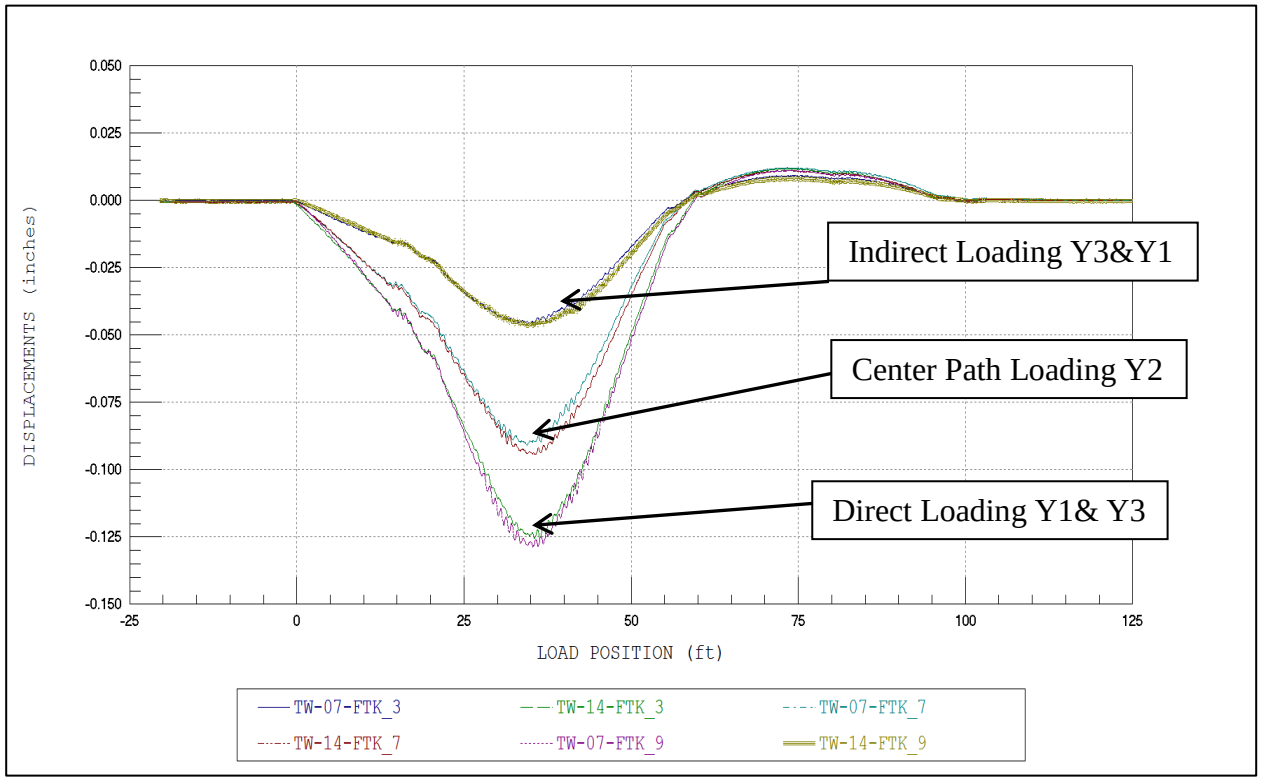

Figure 2.11 – Round 1 Tests - Displacement Response Histories – Interior Beams 7 & 9 – All Truck Paths - Highlighting very symmetrical loading and behavior.

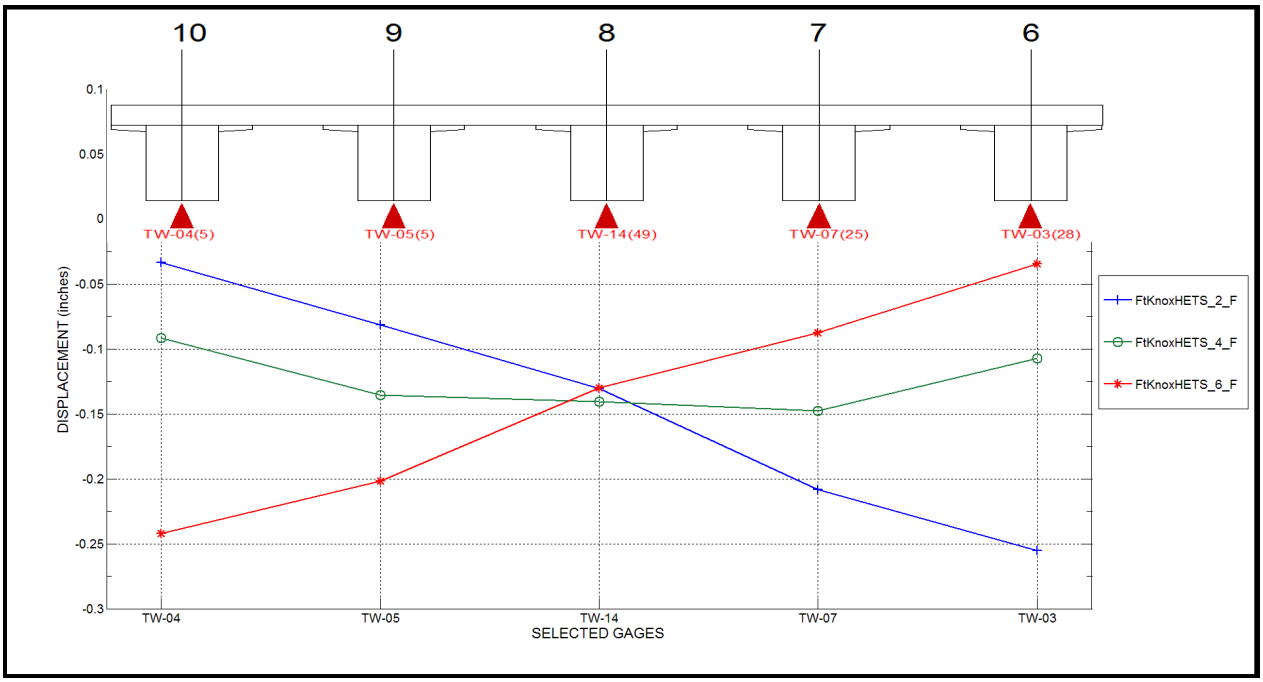

Figure 2.12 – Round 2 Tests - Lateral Load Distribution – Peak midspan strain values – Paths Y1-Y3 – HETS Vehicle.

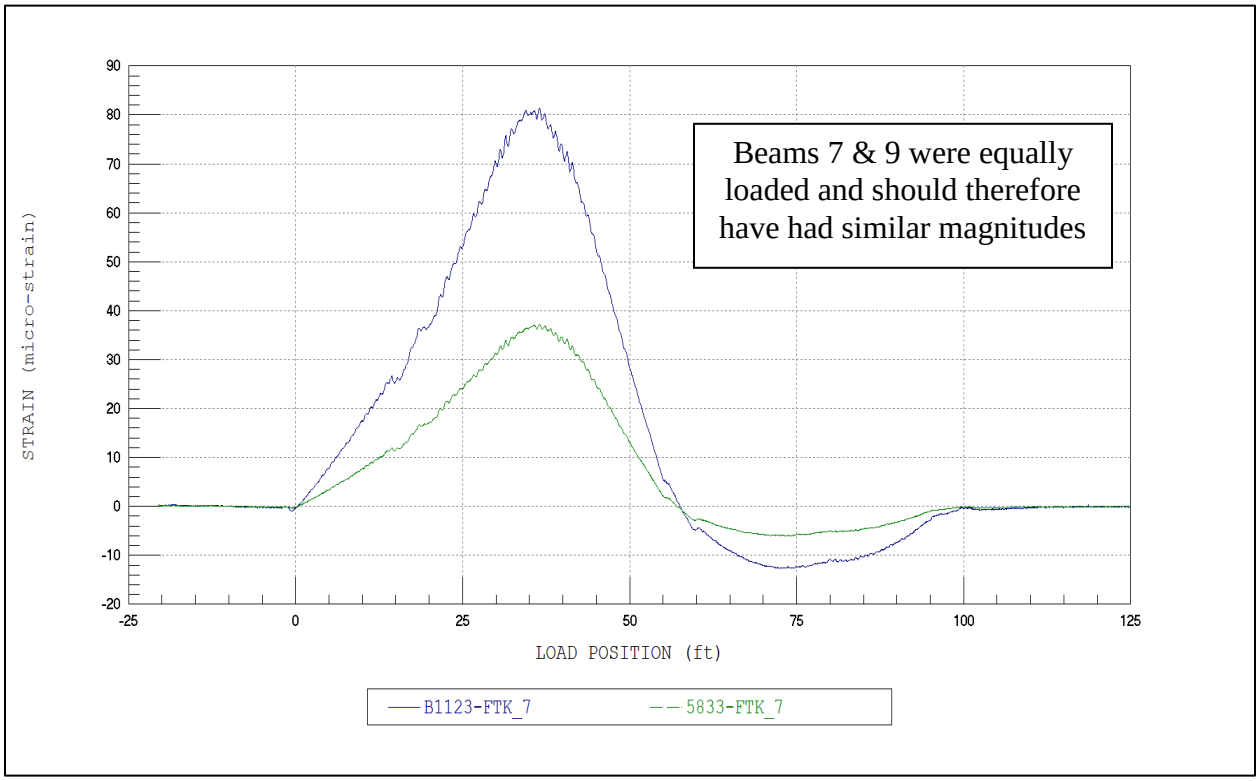

Figure 2.13 – Round 1 Tests - Strain Response Histories – Interior Beams 7 & 9 near Midspan – Center Truck Path Y2 - Highlighting inconsistent strain magnitudes.

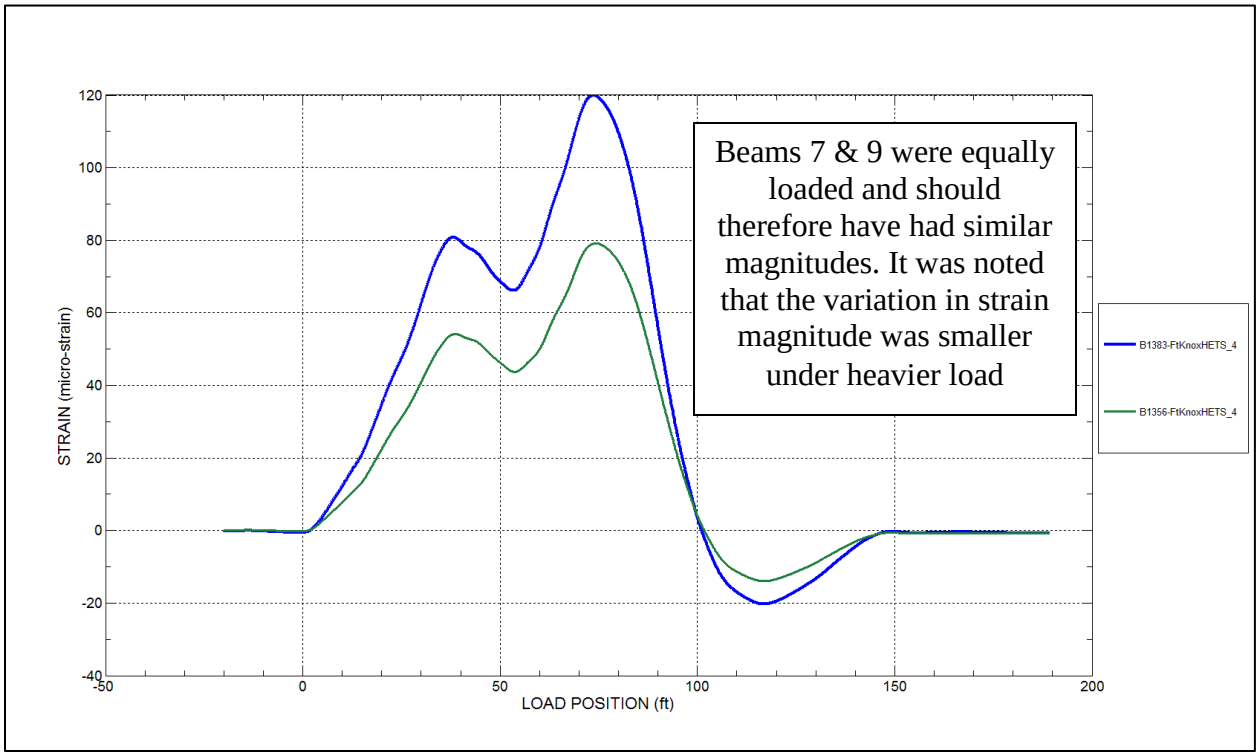

Figure 2.14 – Round 2 Tests - Strain Response Histories – Interior Beams 7 & 9 near Midspan – Center Truck Path Y2 - Highlighting slightly more consistent strain magnitudes under heavier loads.

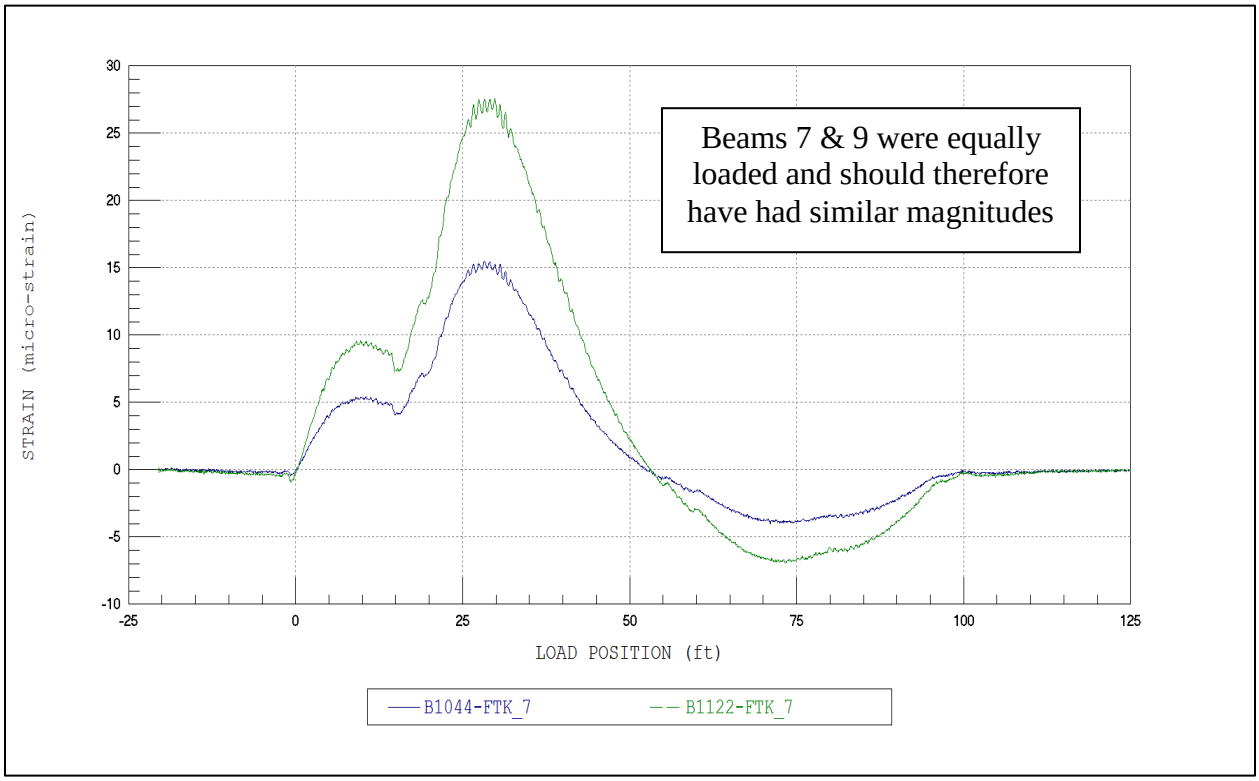

Figure 2.15 – Round 1 Tests - Strain Response Histories – Interior Beams 7 & 9 near Abutment – Center Truck Path Y2 - Highlighting inconsistent strain magnitudes.

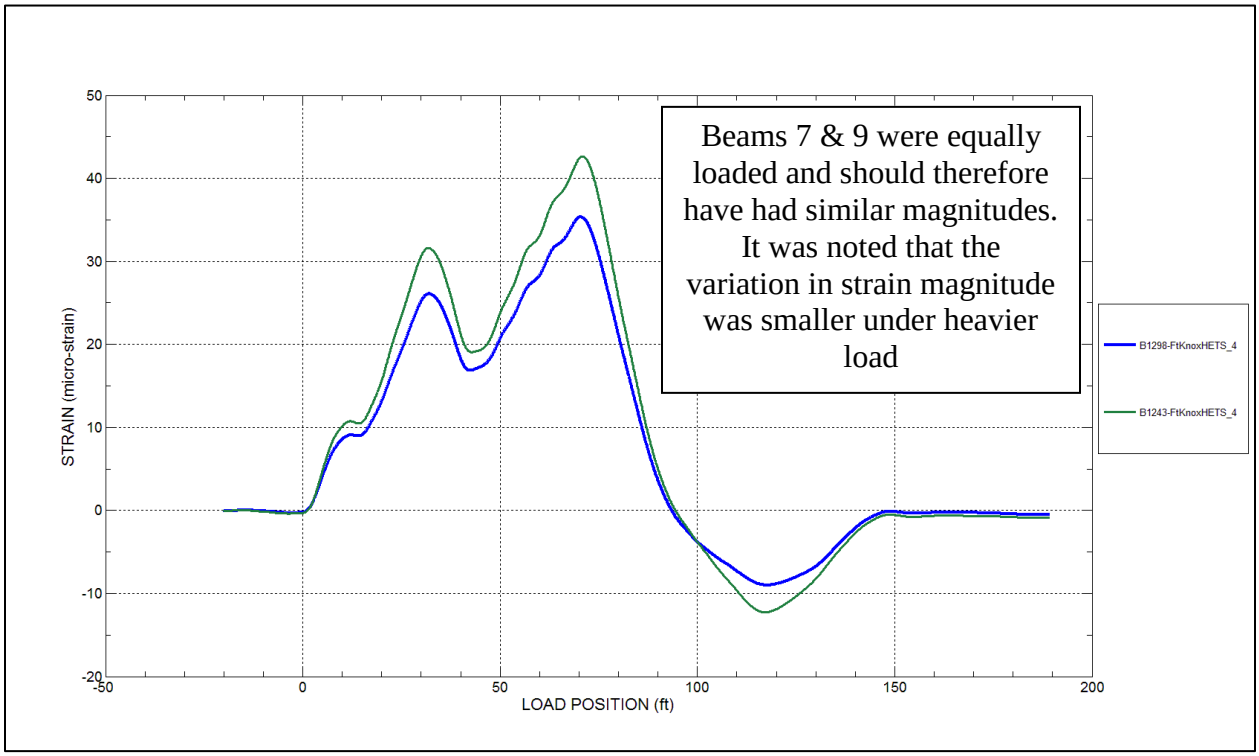

Figure 2.16 – Round 2 Tests - Strain Response Histories – Interior Beams 7 & 9 near Abutment – Center Truck Path Y2 - Highlighting slightly more consistent strain magnitudes under heavier loads.

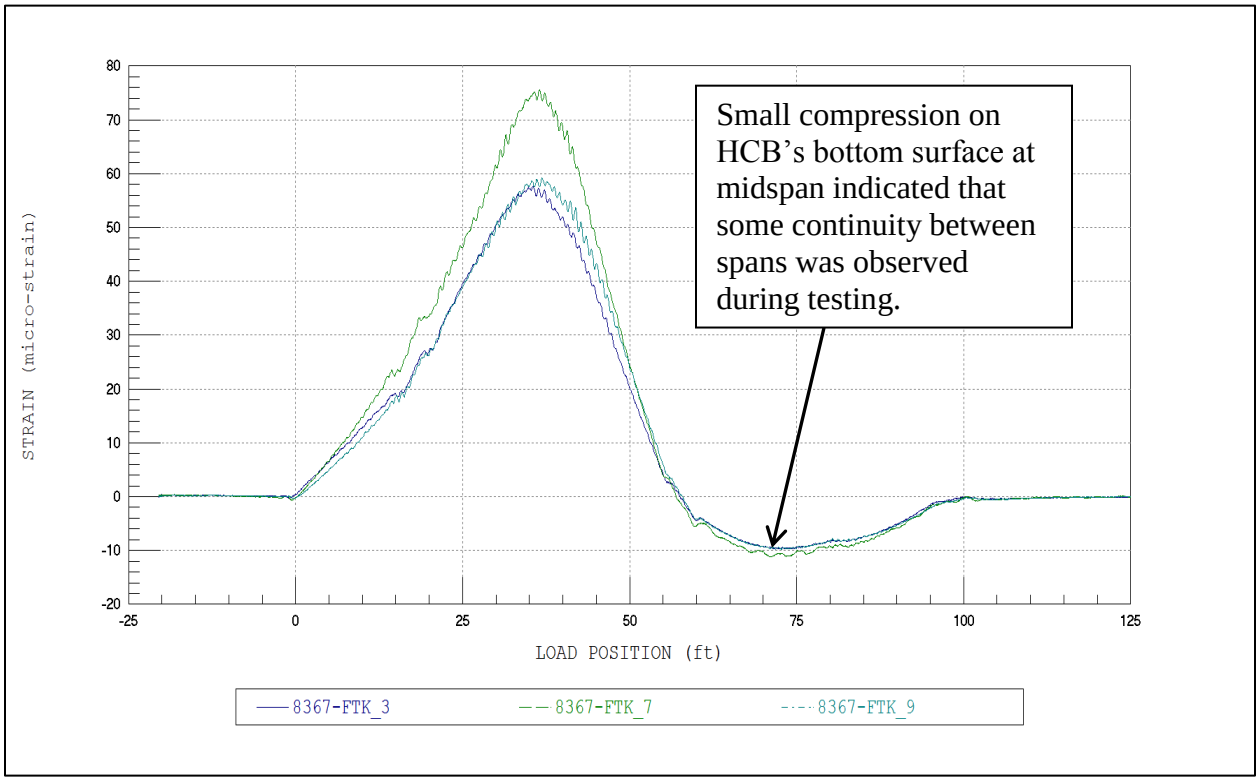

Figure 2.17 – Round 1 Tests - Strain Response History – Near midspan of HCB span – Highlighting continuity between spans.

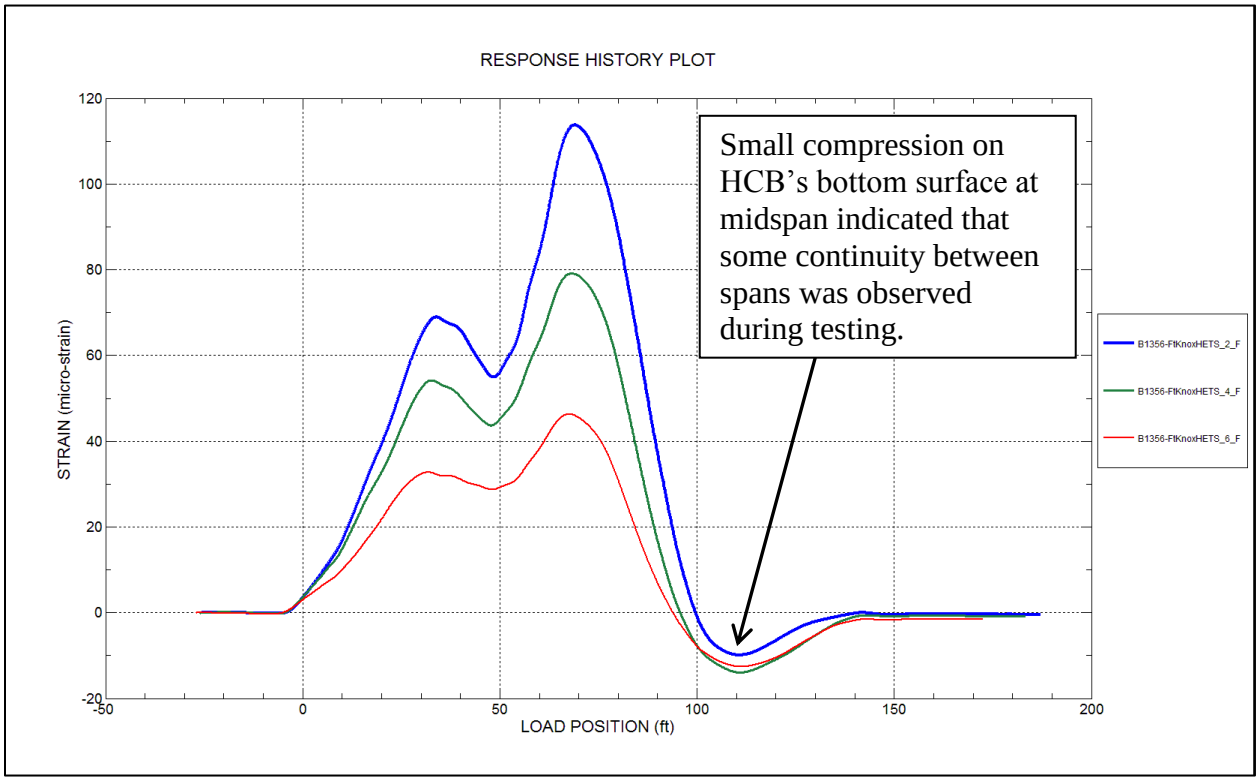

Figure 2.18 – Round 2 Tests - Strain Response History – Near midspan of HCB span – Highlighting continuity between spans.

3. MODELING, ANALYSIS, AND DATA CORRELATION OF SPAN 1

The key objectives of calibrating a finite-element bridge model were to accurately simulate the behaviors recorded during the load test, and in turn utilize this model to accurately predict the structure's response under standard and site-specific rating loads. The HCB span was evaluated independently from the adjacent steel girder span due to the variation in required modeling and analysis techniques. This section briefly describes the methods and findings of the HCB span modeling procedures. A list of modeling and analysis parameters specific to this bridge is provided in Table 3.1.

MODEL CALIBRATION PROCEDURES

First, geometric data collected in the field and insight gained from the qualitative data investigation were used to create an initial, finite-element model of the HCB span using BDI's WinGEN modeling software, which is illustrated in Figure 3.1. While the analysis focused on only the HCB Span, a second steel girder span was included in the model to account for the continuity effects noted in the data review. This initial model used a quasi-three-dimensional modeling approach in which the deck was modeled using shell elements and the beams were represented by frame elements with varying eccentricities and cross-sections, as shown in Figure 3.2 and Figure 3.3. This eccentric beam-deck model simulated the changing composite cross-sectional properties due to the concrete arch. It should be noted that this approach assumed perfect composite action and deformation consistent with flexural beam theory throughout the entire HCB section.

Once the initial model was created, the load test procedures were reproduced using BDI's WinSAC structural analysis and data correlation software. This was done by moving a two-dimensional "footprint" of the test truck across the model in consecutive load cases that simulated the designated truck paths used in the field, as depicted in Figure 3.1. The analytical responses of this simulation were then compared to the field responses to validate the model's basic structure and to identify any gross modeling deficiencies.

After this initial model had been calibrated (process further described below), the quasi-3-D modeling approach was found to accurately match many of the responses (e.g., displacements and strain history shapes at midspan); however the shapes of the strain histories and rotation plots responses near the supports could not be accurately reproduced using this approach, as shown in Figure 3.4. In all cases, the truck positions inducing the peak measured strains were shifted towards midspan rather than directly over the gage locations. The measured responses were therefore a combination of beam-theory behavior and that of a tied-arch. This indicated that the GFRP shell deformed with the concrete arch but not with perfect continuity. The relative flexibility of the shell allowed some independent deformations to take place. Therefore if shell deformations were to be accurately represented by an analysis, a more realistic geometry was required.

A refined model was then developed in which the beam cross-section geometry was represented in full 3-D. The individual beam components were located in their true location as separate model elements using either shell or frame type elements: deck (shell); concrete arch (frame); PS Strands (frame); concrete fin (shell); GFRP shell (shell); and concrete at the beam ends (shell). Renderings of the full 3-D model and a 3-D HCB cut have been provided in Figure 3.5 and Figure 3.6 as further reference.

Once the full 3-D model geometry and general properties were validated, this model was then calibrated until an acceptable match between the measured and analytical responses was achieved. This calibration involved an iterative process of optimizing material properties and boundary conditions until they were effectively quantified. This iterative process involved using engineering judgment and modeling experience to decide which parameters likely caused the differences between the measured and computed responses. Reasonable lower and upper bounds for each of these parameters were then input into the WinSAC software, which uses a least squares curve fitting approach to minimize the error between the data and the model. Many different phases of this iterative process are typically run to ensure that the assumptions used to calibrate the model were correct.

In the case of this structure, the majority of the calibration effort was spent modeling the effective stiffness of the concrete elements (deck, arches, fins, etc.), the end-restraint at the supports, and the continuity between spans at the pier. This was accomplished by obtaining calibrated values for the following items:

- DECK, ARCH, & FIN STIFFNESS: The concrete stiffness of the deck, arch and fin elements was optimized to accurately simulate the observed lateral load distribution and the composite longitudinal stiffness. This calibration was performed by adjusting the elastic modulus of these elements.
- GIRDER BEARING DETAILS: The bearing details were modeled as a combination of vertical and axial translational springs at the center of the bearing of each girder. The stiffnesses of these springs were adjusted until a realistic boundary conditions were achieved that accurately represented the support behavior observed during testing. Accurate simulation of the support condition behavior was important to capture because it ensured that other properties were not unrealistically adjusted to compensate for their effect on the observed structural behavior.
- CONTINUITY BETWEEN SPANS OVER THE INTERIOR PIER: The observed continuity between spans was modeled using truss elements between the bearing springs at the pier that help simulate the interaction between the girder bearings and the interior pier. These elements were given an effective stiffness (calibrated using an adjusted elastic modulus and cross-sectional area) that best simulated the observed level of span interaction.

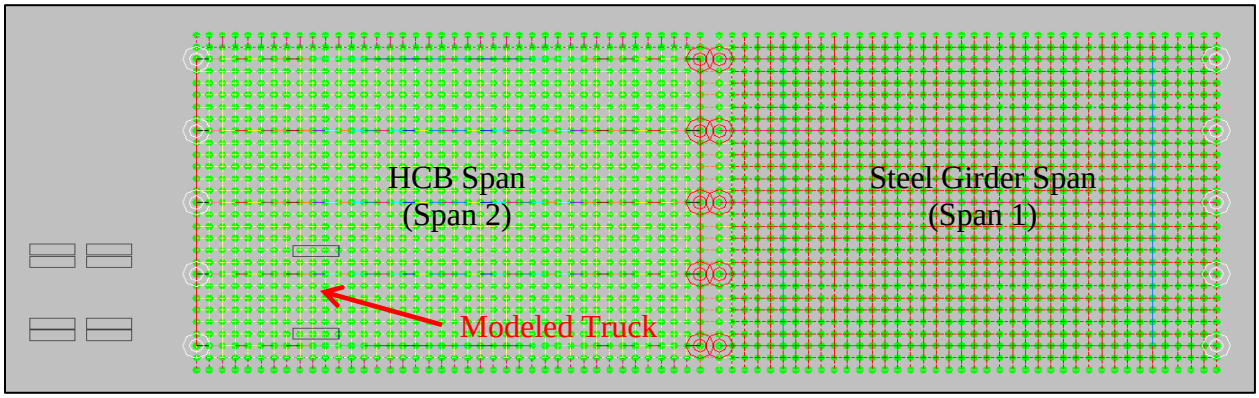

Figure 3.1 - Finite-element model of steel girder span (Span 1) with modeled test truck load.

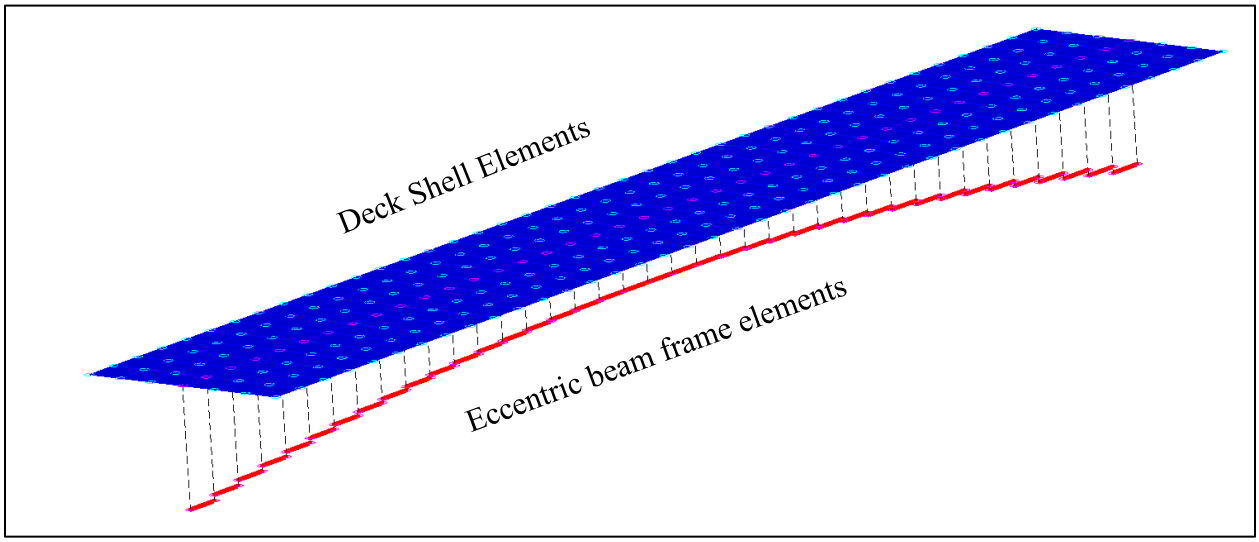

Figure 3.2 – Depiction of initial quasi 3-D finite-element modeling of the Hybrid Composite Beams.

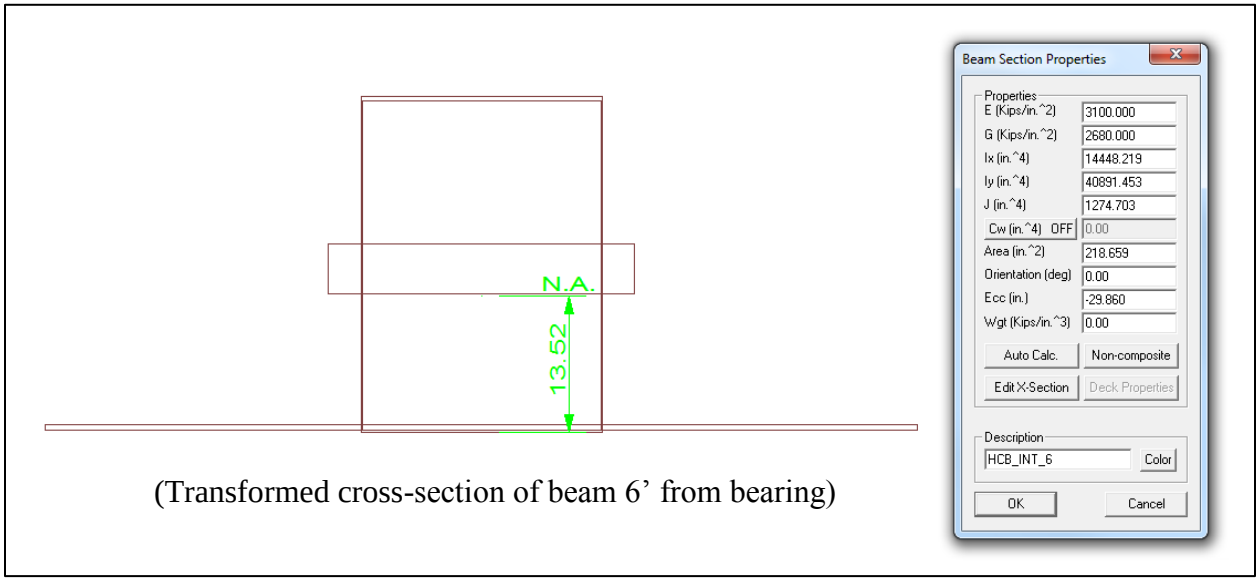

Figure 3.3 – Depiction of a transformed cross-section used in the initial quasi 3-D finite-element modeling of the Hybrid Composite Beams.

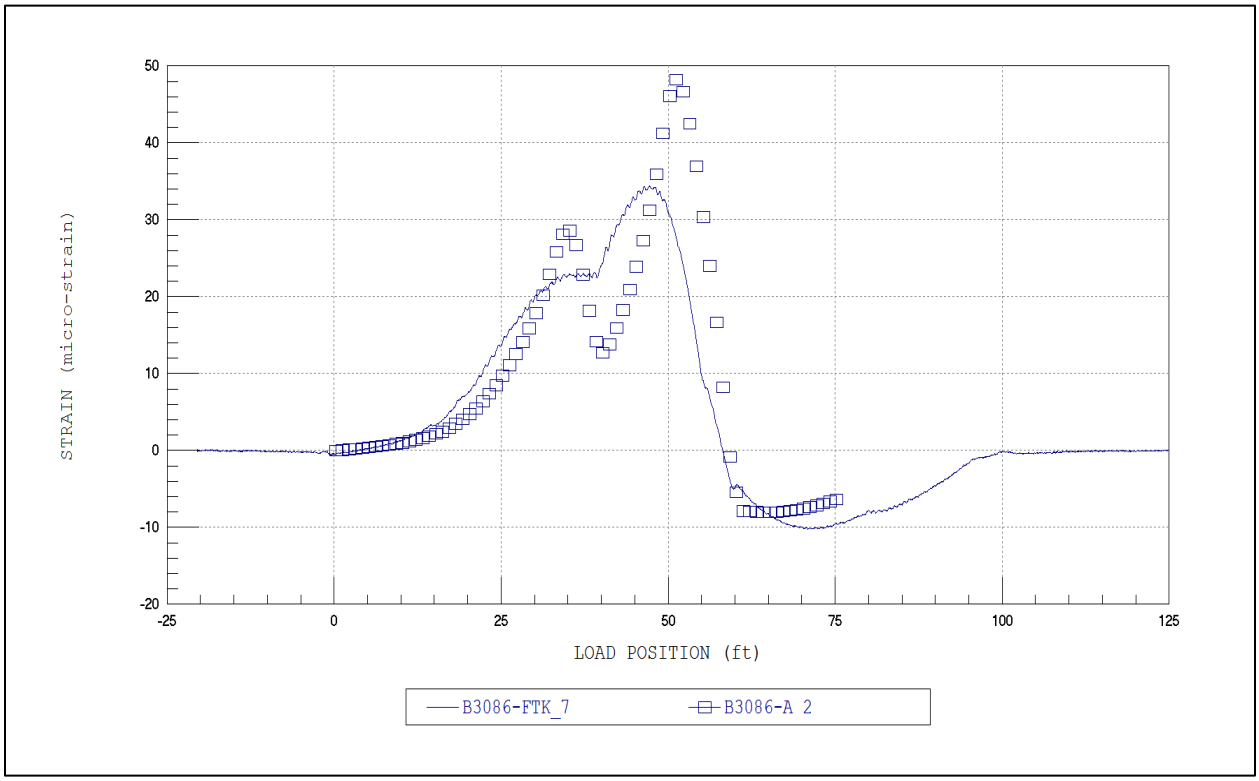

Figure 3.4 – Initial HCB Span model – Example strain comparison plot at Section C-C showing model deficiency.

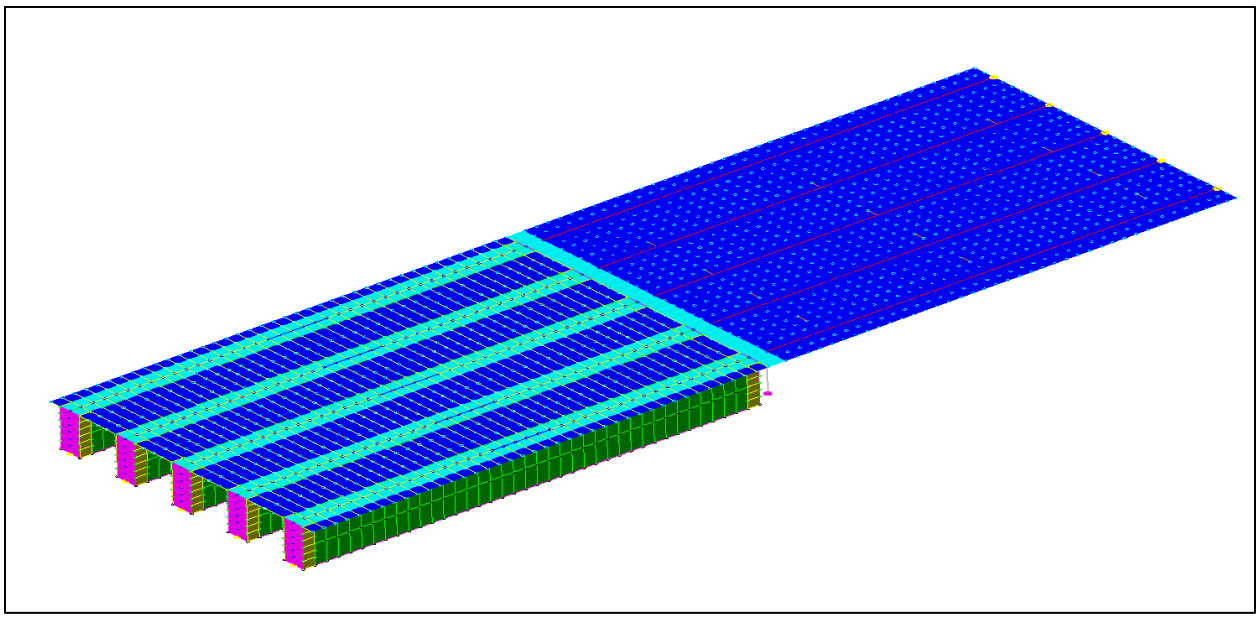

Figure 3.5 – 3-D Rending of Final Full 3-D HCB Span model, including adjacent 2-D steel girder span.

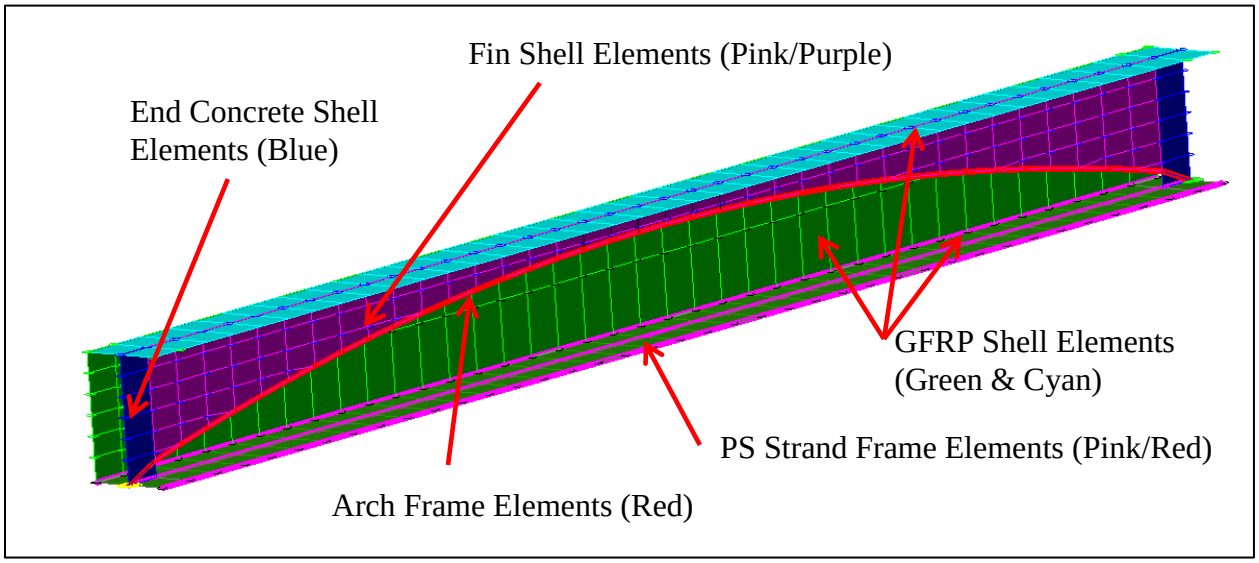

Figure 3.6 – 3-D Rending of HCB, Cut to illustrate beam elements.

Table 3.1 – Bridge No. 4 HCB Span - Analysis and Full 3-D Model Details.

ANALYSIS TYPE	- Linear-elastic finite element - stiffness method.
MODEL GEOMETRY	- 3D model composed of frame elements, shell elements, and springs.
NODAL LOCATIONS	- Nodes placed at all four corners of each shell element. - Nodes placed at both ends of each girder element - Nodes placed at all spring locations.
MODEL COMPONENTS	- Shell elements representing the deck, fin (between deck and arch), and GFRP shell elements. - Frame elements representing the arch, PS strands, and the SAFPlank SIP forms. - Frame elements representing the interaction between the two spans at the pier through the pier cap. - Springs representing the bearing conditions at the abutments and interior pier.
LIVE-LOAD	- 2-D footprint of test truck consisting of vertical point loads for each wheel. Truck paths simulated by series of load cases with truck footprint moving at 1 ft increments along a straight path.
DEAD-LOAD	Applied through a combination of distributed loads and the analysis program's self-weight function
TOTAL NUMBER OF RESPONSE COMPARISONS	Round 1 Tests - 12 strain gage locations x 228 load positions = 2,736 strain comparisons - 3 displacement gage locations x 228 load positions = 684 displacement comparisons - 4 rotation gage locations x 228 load positions = 912 rotation comparisons Round 2 Tests - 12 strain gage locations x 228 load positions = 2,736 strain comparisons - 3 displacement gage locations x 228 load positions = 684 displacement comparisons - 4 rotation gage locations x 228 load positions = 912 rotation comparisons
MODEL STATISTICS	- 4115 Nodes - 7171 Elements - 30 Cross-section/Material types - 228 Load Cases - 19 Round 1 Gage locations

MODEL CALIBRATION RESULTS

Following the optimization procedures, the final Round 1 model produced a 0.98 linear correlation with the global responses (e.g., displacements and rotations) measured along the three single truck paths and a 0.99 linear correlation with the tandem truck global responses. Additionally, linear correlations of approximately 0.95 were produced for both the single and tandem tests when the strain response shapes recorded along the bottom of the HCBs were also considered. This level of accuracy can be considered an excellent match for any structure, and indicates that the model successfully simulated the observed structural behavior under the test loads. Model accuracy values from the final bridge model for the single and tandem truck tests have been provided in Table 3.2

. These measures of accuracy or "error parameters" are based on comparisons between the **measured** responses and analytical model **computed** responses, and each error parameter type has been briefly described in Table 3.4 for clarification.

The following are bulleted observations/conclusions made during the Round 1 optimization process:

- STRAIN RESPONSE COMPARISONS NEAR THE BEAM ENDS: It was found that the full three-dimensional model produced an accurate match to the shapes of the recorded strain responses near the ends of the HCBs. This finding indicated that the more refined modeling approach was able to simulate the observed tied-arch type behavior. Remember that the initial quasi-3-D beam model could not represent the observed strain shape behavior near the beam ends because it was based on basic beam theory in which all components at a cross-section remain in a consistent plane. This would imply that perfect composite behavior between the upper concrete section (deck, fin, and arch) and the bottom HCB layer (GFRP and PS strands) was achieved through the very thin GFRP shell walls. In reality, the shear deformation of the GFRP walls likely occurred slightly independent of the concrete arch and deck. The 3-D model in which the shell and concrete were modeled as individual components did a much better job of simulating this behavior.
- EFFECTIVE CONCRETE STIFFNESS IN THE DECK, ARCH, & FIN: It was found that an average effective modulus of approximately 4500 ksi for the concrete deck, arch and fin best matched the composite behavior and the lateral load distribution observed during testing. While this effective stiffness value is relatively high for the deck, it provided an acceptable match to the observed lateral load distribution in combination with the SAFPLANK SIP form elements (briefly described in the next bullet point).
- MODELING OF THE SAFPLANK STAY-IN-PLACE FORMS: In order to achieve accurate representation of both the lateral and longitudinal load distribution of the structure, it was found necessary to model the SAFPLANK SIP forms. These elements were modeled as lateral grillage type frame elements that helped distribute the live-load in the lateral direction. Since increasing the deck modulus stiffens the model in both the longitudinal and lateral directions, the SAFPLANK elements allowed the lateral load distribution to be improved without over predicting the longitudinal stiffness of the HCBs.
- VARIABLE END-RESTRAINT AT THE EXTERIOR AND INTERIOR SUPPORTS: It was found that a varying level of end-restraint at the support locations was present during testing. This end-restraint was modeled using axial spring stiffnesses at the bearing locations along the bottom of the beams. The end-restraint had a significant effect on the

midspan displacements and beam end-rotation and was a function of the friction between the bottom of the HCBs and the bearing plates. The variability of resistance was influenced by the load magnitude such that directly loaded beams had more effective end-restraint than beams with minimal load. It should be noted that although considering this behavior during modeling was an important part of understanding how the bridge behaved during testing, this end-restraint was not considered to be reliable enough to use during the rating process.

- SPAN CONTINUITY OVER THE INTERIOR PIER: It was found that a relatively low stiffness value in the span interaction elements allowed a much better fit to the measured responses. The presence of this element in the finite-element model simulated the low level of load transfer believed to be caused by slight movement of the pier wall, which induced movement of the beam bearings on the adjacent span. As with the end-restraint, this condition was considered irrelevant with respect to load rating, but needed to be considered during the model calibration process because it influenced the measured responses.

The data from Round 2 was first compared with the final Round 1 model. It was found that in general the behavior was nearly identical, with the exception of slight differences in the boundary conditions (described below). Following a second set of optimization procedures, the Round 2 final model produced a 0.972 correlation with the HETS measured responses and a 0.972 correlation with the M1A1 Tank measured responses. The model accuracy values used in the initial and final bridge models are provided in Table 3.3.

- VARIABLE END-RESTRAINT AT THE EXTERIOR AND INTERIOR SUPPORTS: Using Round 2 data it was still found that a varying level of end-restraint at the support locations was present during testing. This end-restraint was modeled using axial spring stiffnesses at the bearing locations along the bottom of the beams. The end-restraint had a significant effect on the midspan displacements and beam end-rotation. This variation was likely still a function of the friction between the bottom of the HCBs and the bearing plates. In general the end-restraint was found to increase slightly under the heavier loads which support the conclusion that the support behavior was friction based. The variability of resistance was influenced by the load magnitude in such that directly loaded beams had more effective end-restraint than beams with minimal load.

The final model was found to closely match the member responses (with the exception of the strain magnitudes) as shown in the comparison plots provided in Figure 3.7 though Figure 3.18. Note that in these comparison plots the measured responses are represented as solid lines while the computed responses are represented as discrete markers. Additionally, it should be noted that the errors in response magnitude were generally on the conservative side.

Table 3.2 – Bridge No. 4 - Span 1 – Round 1 tests – Final model accuracy values.

FINAL MODEL ERROR PARAMETERS	ABSOLUTE ERROR	PERCENT ERROR	SCALE ERROR	CORRELATION COEFFICIENT
Single Truck Tests – Truck Path Y1, Y2, & Y3 *All Responses Types*	34,469.8	22.5%	12.2%	0.945
Single Truck Tests – Truck Path Y1, Y2, & Y3 *Global Responses Only*	9,654.1	5.6%	3.1%	0.979
Tandem Truck Test – Truck Path Y2 *All Responses Types*	13,203.9	14.7%	20.2%	0.956
Tandem Truck Test – Truck Path Y2 *Global Responses Only*	2,930.6	2.3%	4.6%	0.989

Table 3.3 – Bridge No. 4 - Span 1 – Round 2 tests - Model accuracy values.

FINAL MODEL ERROR PARAMETERS	ABSOLUTE ERROR	PERCENT ERROR	SCALE ERROR	CORRELATION COEFFICIENT
Initial Comparison w/ 2012 Model **Single M1A1 Tests** *All Responses Types*	34954.6	30.9%	14.8%	0.961
Final 2013 Model **Single M1A1 Tests** *All Responses Types*	21,214.2	9.4%	5.4%	0.956
Initial Comparison w/ 2012 Model **Single M1A1 Tests** *Global Responses Only*	10196.4	18.0%	8.5%	0.964
Final 2013 Model **Single M1A1 Tests** *Global Responses Only*	6623.5	4.4%	5.4%	0.979
Initial Comparison w/ 2012 Model **Single HETS Tests** *All Responses Types*	50,823.1	28.6%	11.3%	0.952
Final 2013 Model **Single HETS Tests** *All Responses Types*	32,747.1	7.8%	6.6%	0.961
Initial Comparison w/ 2012 Model **Single HETS Tests** *Global Responses Only*	16,021.0	20.8%	16.0%	0.955
Final 2013 Model **Single HETS Tests** *Global Responses Only*	11,383.6	5.9%	7.5%	0.970

The following table contains the equations used to compute each of the statistical error values:

Table 3.4 - Error Functions

ERROR FUNCTION	EQUATION	BRIEF DESCRIPTION
Absolute Error	$\Sigma \lvert \varepsilon_m - \varepsilon_c \rvert$	Weighted absolute sum of the differences. Used to determine small response changes in accuracy due to parameters.
Percent Error	$\Sigma(\varepsilon_m - \varepsilon_c)^2 / \Sigma(\varepsilon_m)^2$	Sum of the response differences squared divided by the sum of the measured responses squared. Helps provide a better qualitative measure of accuracy
Scale Error	$\frac{\Sigma \max \lvert \varepsilon_m - \varepsilon_c \rvert_{gage}}{\Sigma \max \lvert \varepsilon_m \rvert_{gage}}$	Maximum error from each gage divided by the maximum response value from each gage. Helps determine error with respect to maximum magnitude.
Correlation Coefficient	$\frac{\Sigma(\varepsilon_m - \overline{\varepsilon_m})(\varepsilon_c - \overline{\varepsilon_c})}{\Sigma\sqrt{(\varepsilon_m - \overline{\varepsilon_m})^2(\varepsilon_c - \overline{\varepsilon_c})^2}}$	Measure of the linearity between the measured and computed data. Helps determine the error with respect to response shape and phase.

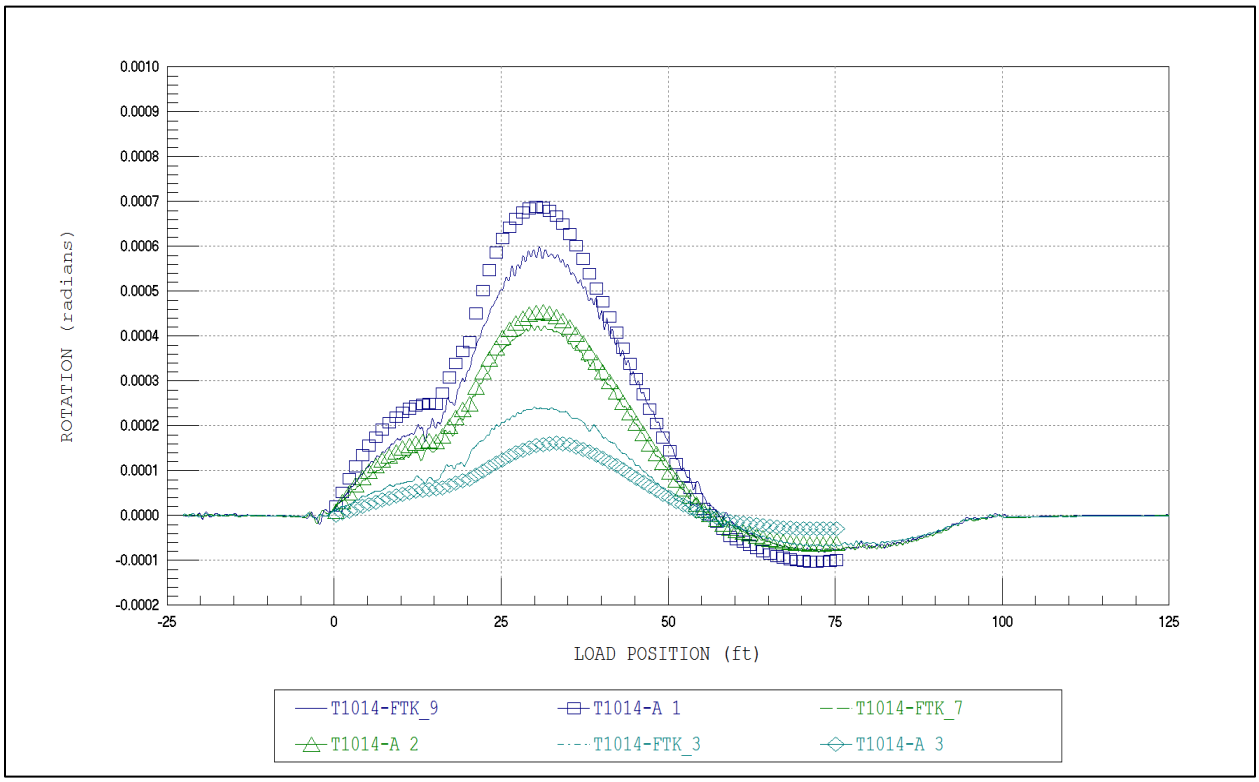

Figure 3.7 - Final Round 1 HCB Span model – Single Truck Tests - Example rotation comparison plot at Section A-A on Beam 9.

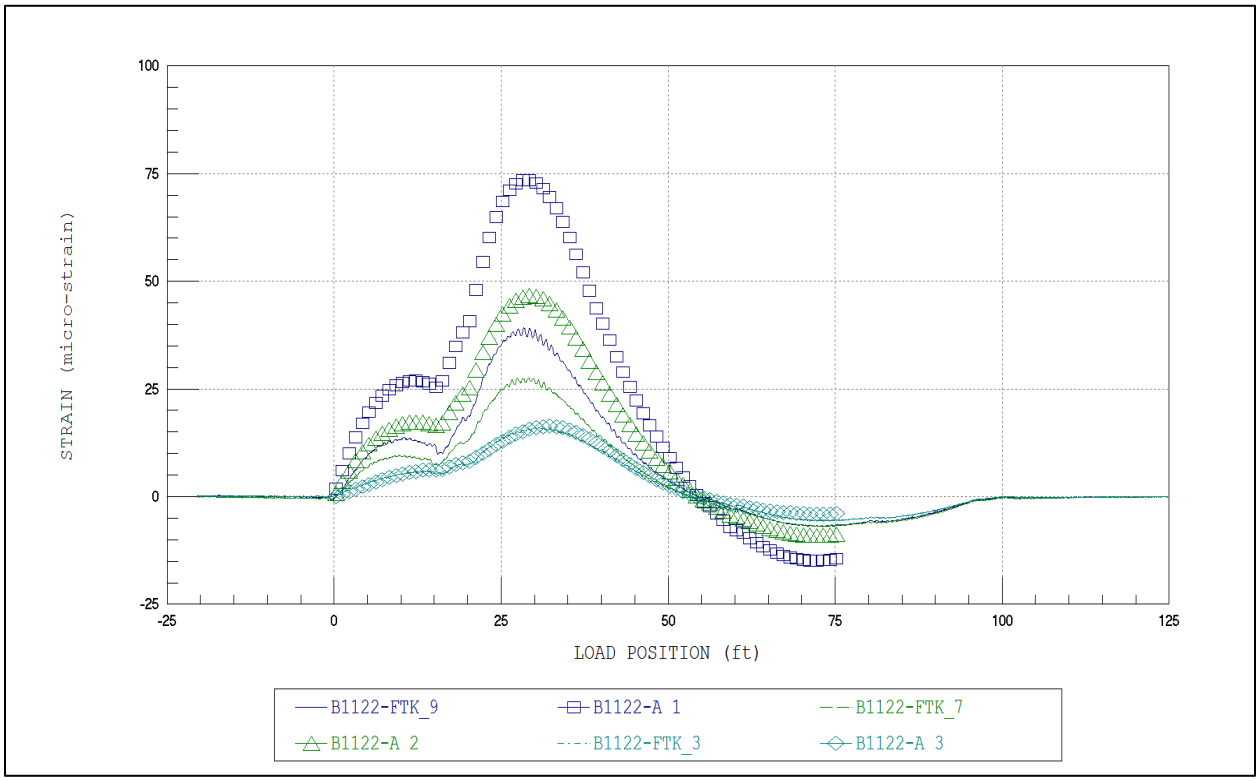

Figure 3.8 - Final Round 1 HCB Span model – Single Truck Tests - Example strain comparison plot at Section A-A on Beam 9.

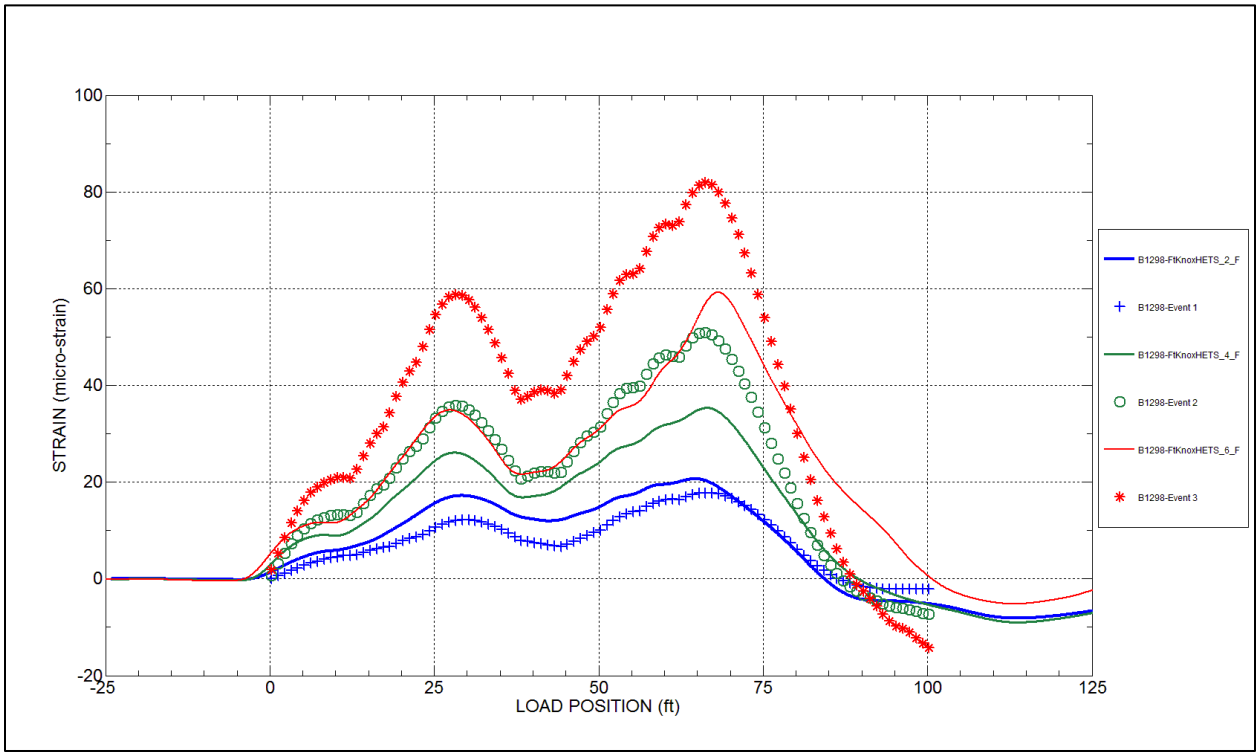

Figure 3.9 - Final Round 2 HCB Span model – HETS Tests - Example strain comparison plot at Section A-A on Beam 9.

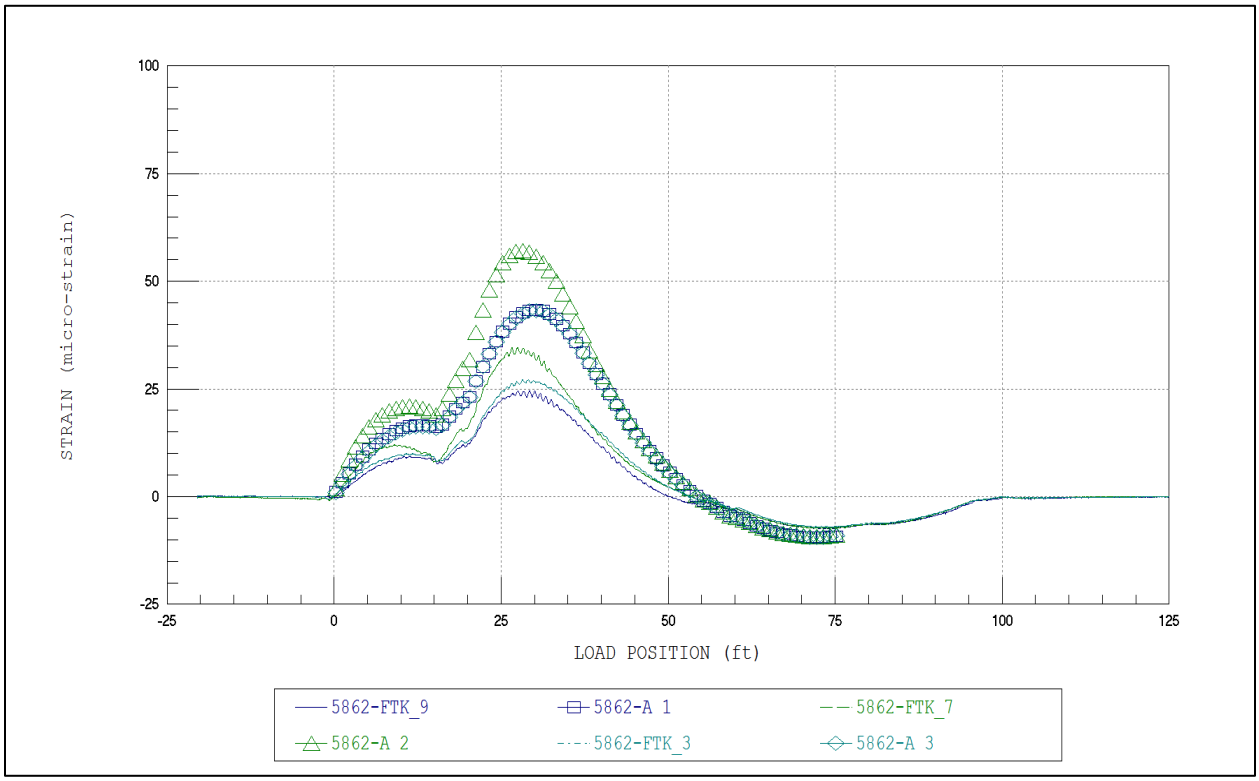

Figure 3.10 - Final Round 1 HCB Span model – Single Truck Tests - Example strain comparison plot at Section A-A on Beam 8.

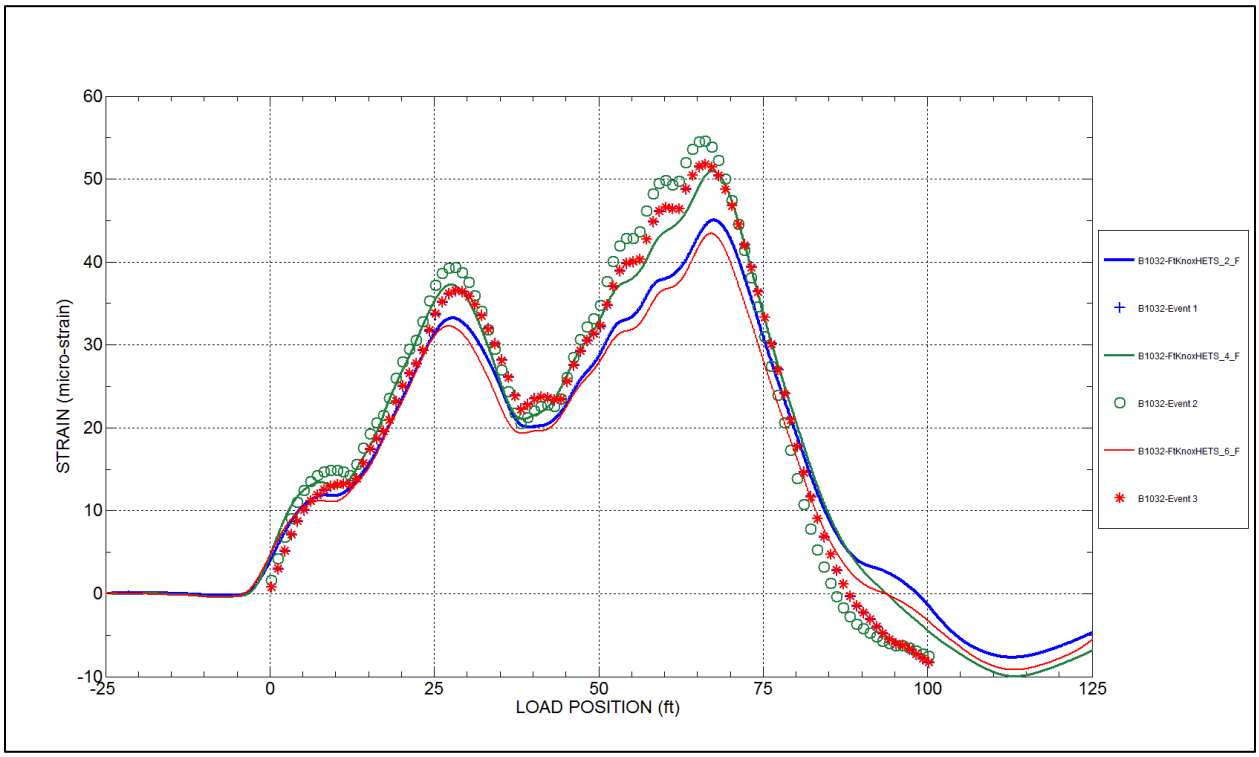

Figure 3.11 - Final Round 2 HCB Span model – HETS Tests - Example strain comparison plot at Section A-A on Beam 8.

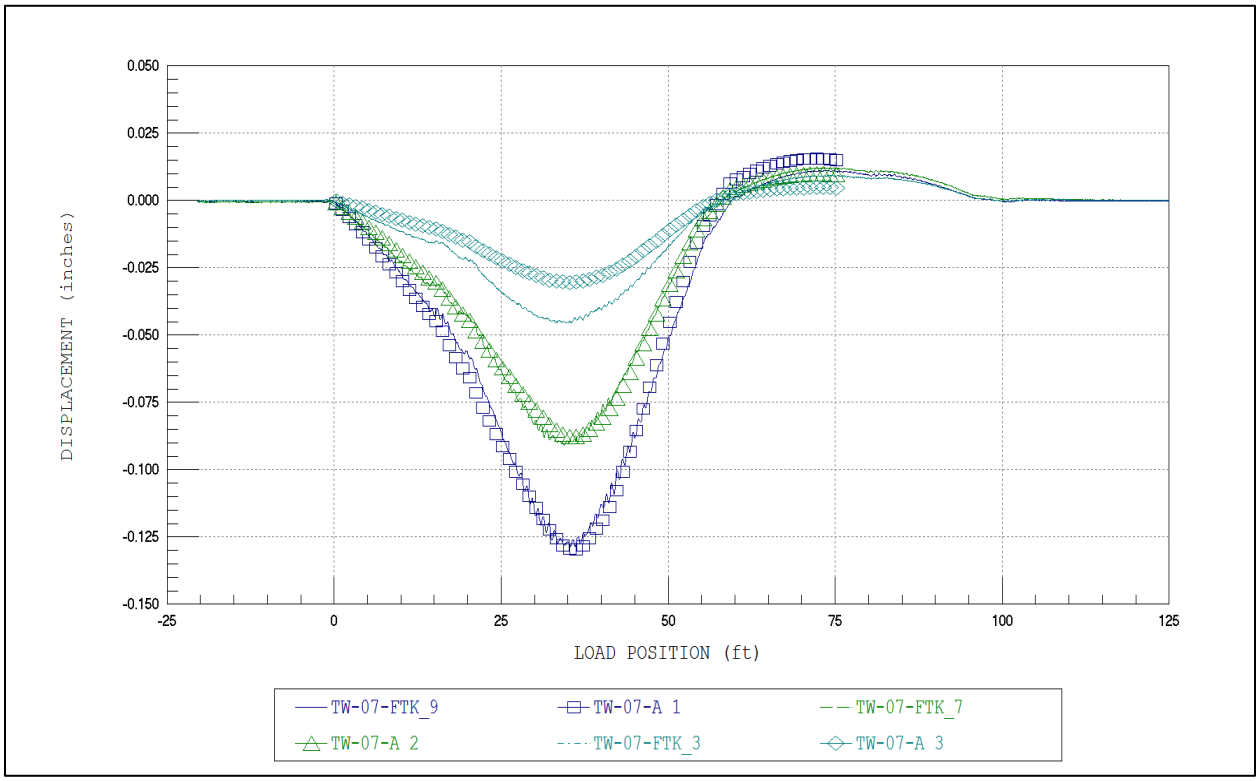

Figure 3.12 - Final Round 1 HCB Span model – Single Truck Tests - Example displacement comparison plot at Section B-B on Beam 9.

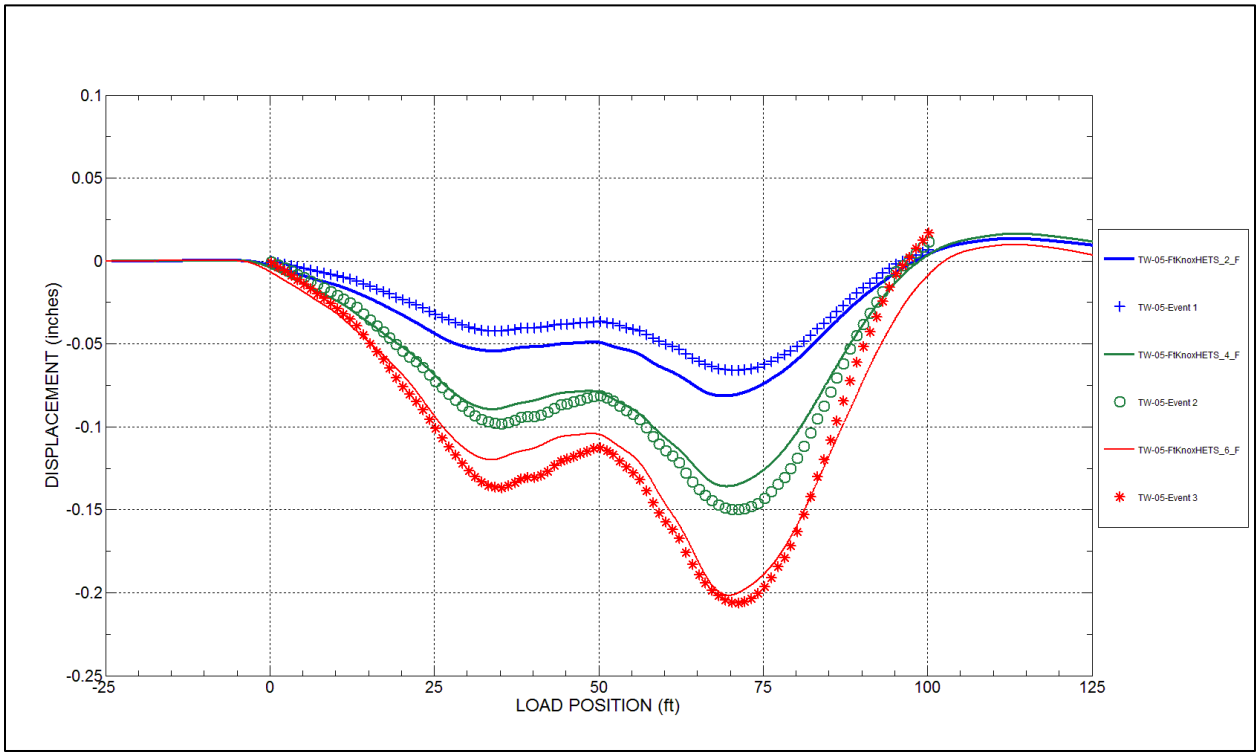

Figure 3.13 - Final Round 2 HCB Span model –HETS Tests - Example displacement comparison plot at Section B-B on Beam 9.

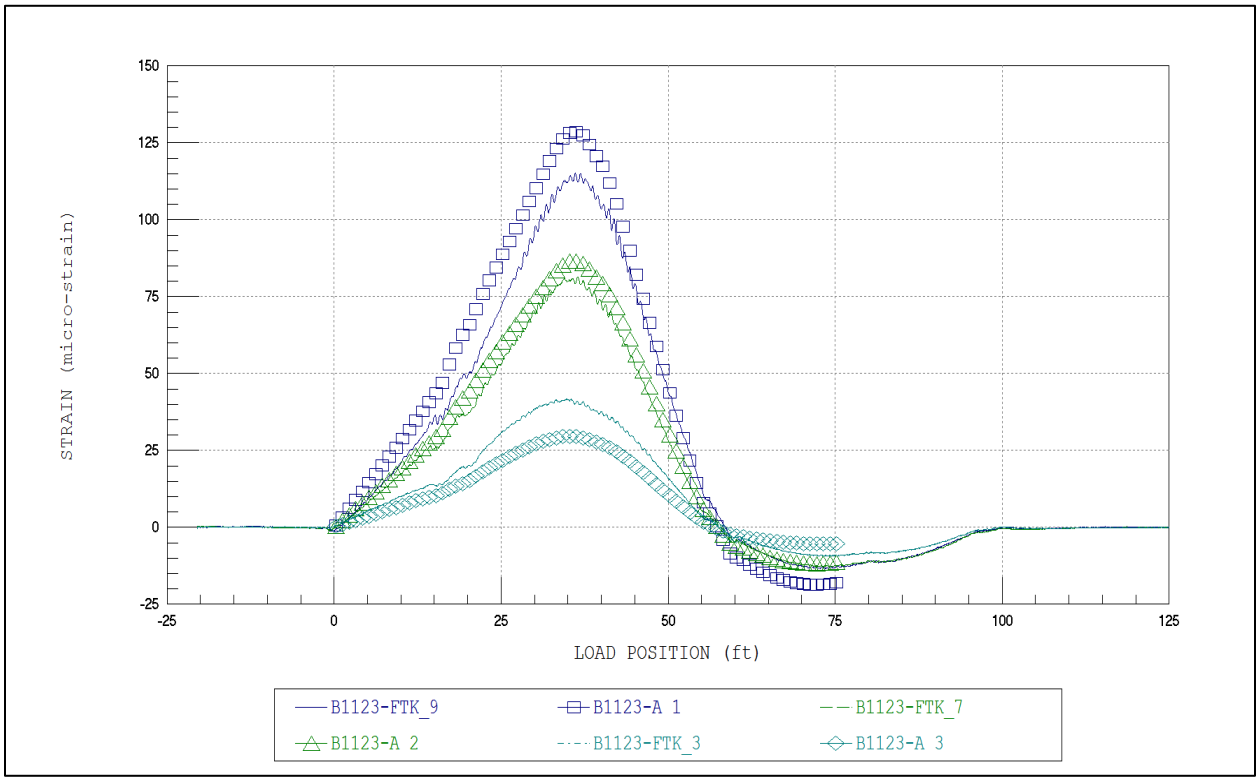

Figure 3.14 - Final Round 1 HCB Span model – Single Truck Tests - Example strain comparison plot at Section B-B on Beam 9.

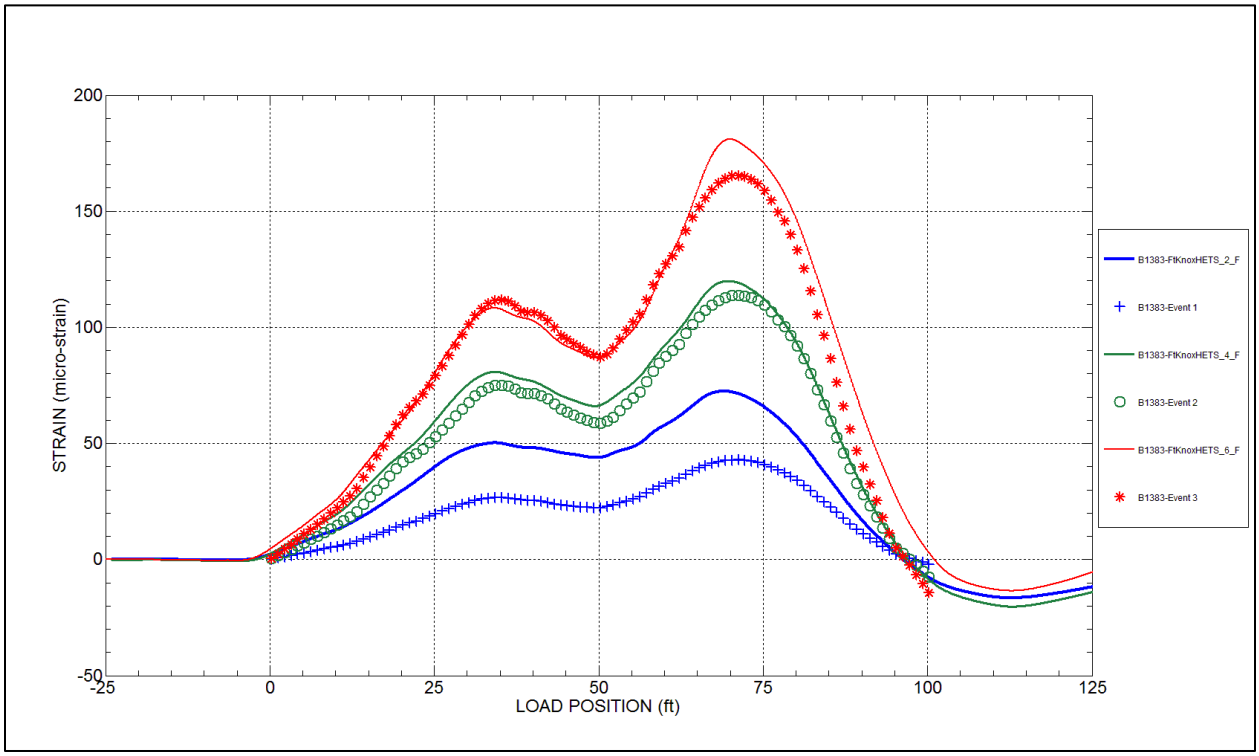

Figure 3.15 - Final Round 2 HCB Span model – HETS Tests - Example strain comparison plot at Section B-B on Beam 9.

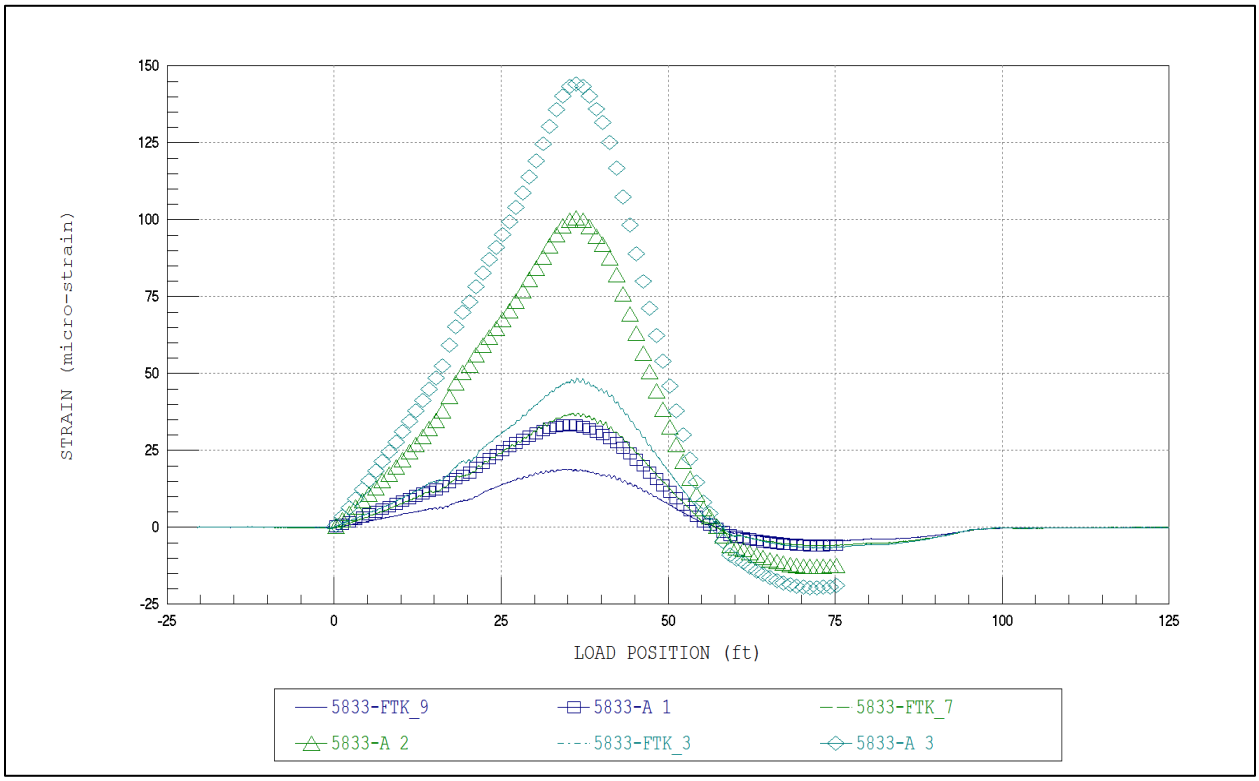

Figure 3.16 - Final Round 1 HCB Span model – Single Truck Tests - Example strain comparison plot at Section B-B on Beam 7.

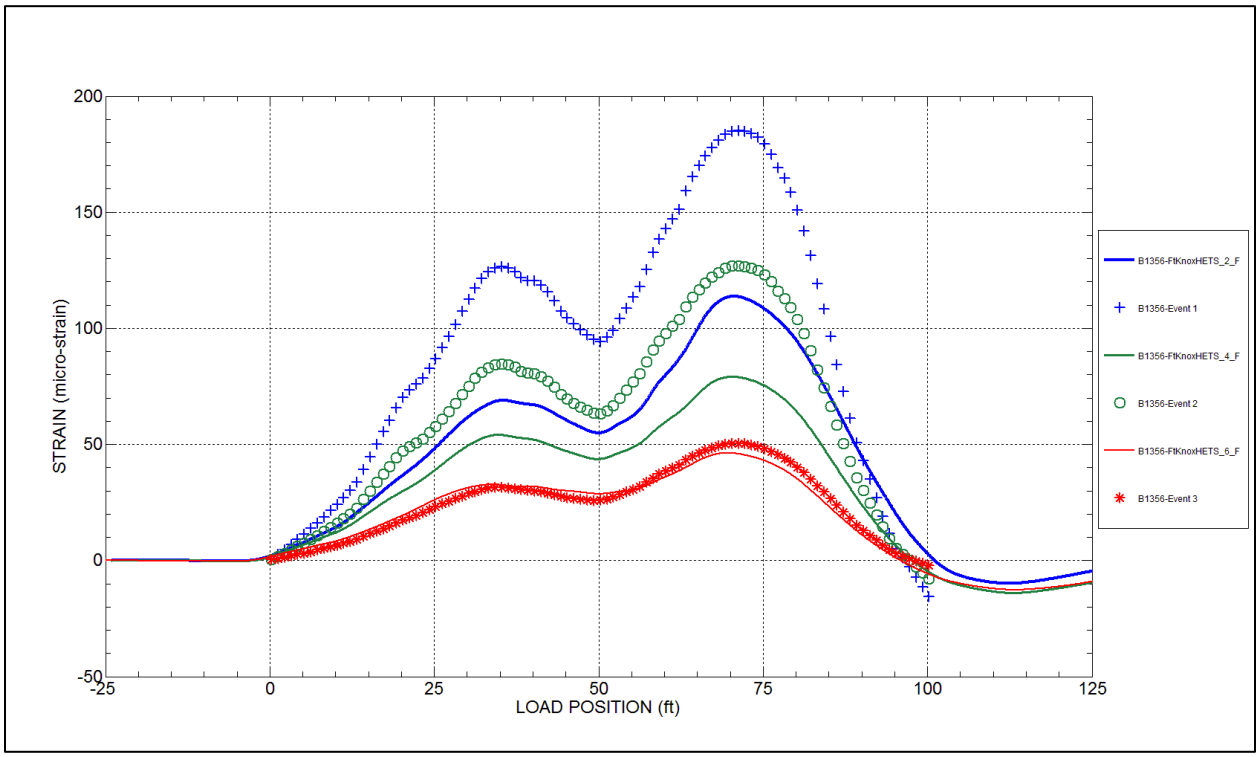

Figure 3.17 - Final Round 2HCB Span model – Single Truck Tests - Example strain comparison plot at Section B-B on Beam 7.

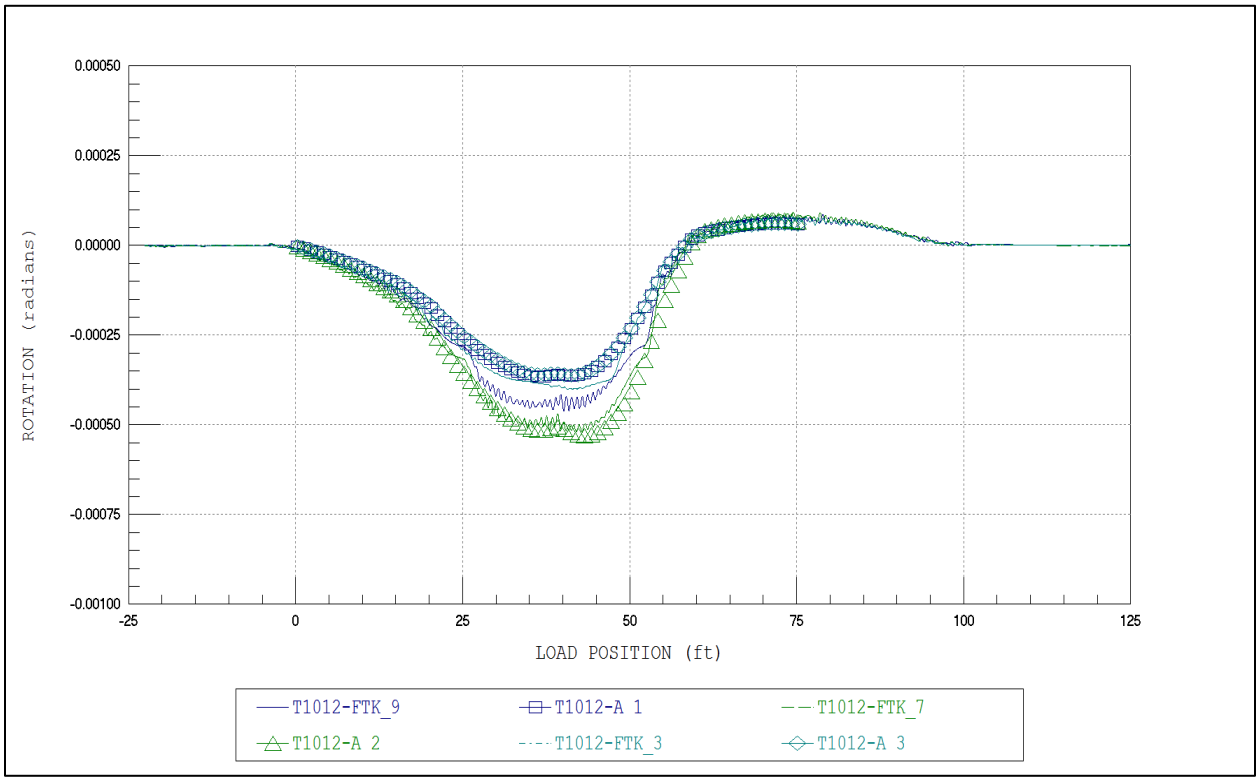

Figure 3.18 - Final Round 1 HCB Span model – Single Truck Tests - Example rotation comparison plot at Section C-C on Beam 8.

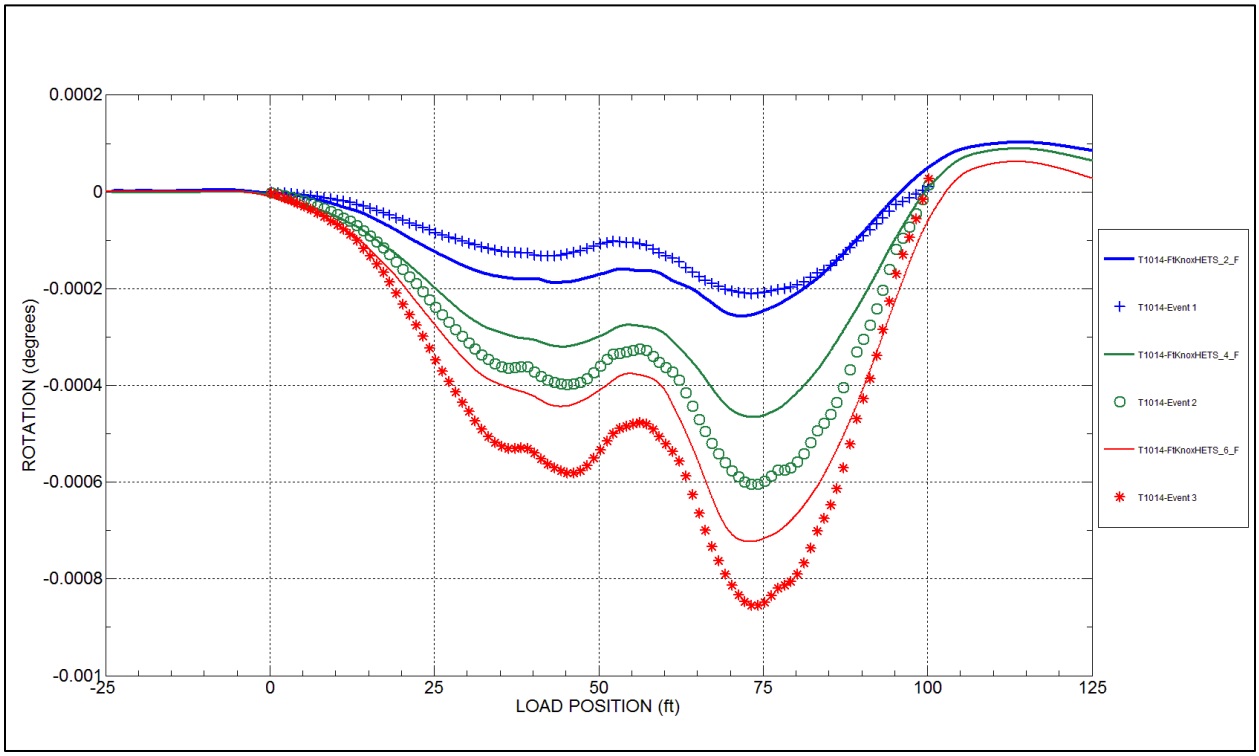

Figure 3.19 - Final Round 2 HCB Span model – Single Truck Tests - Example rotation comparison plot at Section C-C on Beam 9.

4. LOAD RATING PROCEDURES & RESULTS

RATING PROCEDURES

Load rating was performed on the hybrid composite beam (HCB) span in accordance with the AASHTO and KYDOT LRFR guidelines. Structural responses were obtained from slightly modified versions of the final calibrated model. Member capacities were based on procedures similar to those provided in the design calculations (performed by Eriksson Technologies) and AASHTO LRFD specifications. The rating methods used in BDI's approach closely match typical rating procedures, with the exception that a field-verified finite-element model analysis was used rather than a typical AASHTO beam-line/distribution factor approach. This section briefly discusses the methods and findings of the load rating procedures.

Once the analytical model was calibrated to produce an acceptable match to the measured responses, the model was adjusted to ensure the reliability of all optimized model parameters. This adjustment involved the identification of any calibrated parameters that could change over time or could become unreliable under heavy loads.

The following assumptions were made during the load rating of the structure:

- Perfectly simply-supported behavior was assumed for rating by removing the axial end-restraint springs at the bearing locations and the span interaction elements between the HCB span and the adjacent steel girder span. This assumption was made because the friction induced end-restraint would not be reliable for heavy loading conditions or consistent over the life of the structure.
- In the provided design calculations (Eriksson Technologies), the ultimate flexural strength was assumed to be consistent with reinforced concrete principles in which beam failure occurs with a limiting concrete strain and yielding of the reinforcing steel. However, because the reinforcing steel was composed of pre-stressing strands which do not have a large yield plateau in the stress/strain relationship, the strain compatibility assumptions took the steel far beyond rupture. The design moment capacities were limited by the steel strength so the resulting limits were still reasonably accurate but distance between the tension and compression couple was over estimated. BDI produced an independent failure limit for flexure based on a steel strain limitation at the yielding of the strands (assumed to occur at 0.9Fu). This approach produced a moment capacity that was more conservative than the original calculations but was consistent with limits in Table 6A.5.4.2.2b-1 of the AASHTO MBE. This assumption was supported by the fact that the available compression capacity in the effective deck flange was larger than the available tensile capacity of the bottom beam layer, and that the PS strands should not be allowed to be stressed beyond this yield limit.
- Based on the modeling results, it was found that there was local bending likely occurring in the GFRP shell walls near the beam ends, which caused the HCB components to not act perfectly composite in these regions. Therefore, the flexural section at ultimate was conservatively assumed to be made up solely of the concrete deck and the bottom beam layer (containing the bottom GFRP layer and PS strands) acting composite with each other.
- Because the 3-D model was component based rather than full beam cross-sections, the results were primarily in terms of axial force for the deck and bottom layer of the beam.

Therefore moment limits were simulated in the 3-D model as force limits in the primary tension and compression components.

- Based on limitations of using a linear-elastic model to load rate the structure under flexure at the ultimate condition, compression in the deck elements were used as the limiting factor for flexure. This was done because the deck elements were in compression under all loading conditions and the only elements in compression at midspan while the tension was carried by many different element types in the linear-elastic model (e.g., arch, GFRP shell, and PS strands). Therefore even though yielding of the PS strands was found to control the flexural capacity, but it was simpler to apply this steel tension limit as a compression limit in the deck elements. Calculations of the component force limits are provided in Appendix A.
- It was assumed that for ultimate flexural load considerations the dead and live-load could be applied to the same composite model. Since the resulting deck compression was used as the limit state associated to rate the HCBs in flexure, it was conservatively assumed that the non-composite dead load will be shed into the deck at the ultimate loading condition. This behavior was based on the assumption that as the HCB section approaches ultimate and the beams continue to deflect (due to cracking of the arch concrete), an increasing amount of the overall induced load will be carried by the composite section left at ultimate (i.e., the deck and bottom beam layer).
- The 3-D analysis results indicated that the RC fin would be the first HCB component to fail based on AASHTO shear capacity calculations. However, laboratory test results performed at the AEWC Advanced Structures & Composites Center showed that the overall beam shear capacity was not heavily influenced by the fin and was controlled by the shear stress in the GFRP webs. The laboratory test results showed that the HCBs could reach over twice the AASHTO based shear capacity and that shear failure was not limited by the assumed shear capacity of the shear stirrups and concrete fin. This additional shear strength was likely due to the GFRP shell's ability to exhibit post-buckling (tension field) behavior and enhanced load sharing between the HCB's GFRP shell, stirrup steel, and concrete components.
- The HCB shear ratings were limited to the GFRP's allowable shear stress of 7.5 ksi provided in HCB design specifications. It should be noted that based on the lab tests and ASTM D4255 tests performed on the GFRP, this stress limit is likely conservative.
- It was assumed that the beam shear failure would be controlled by failure of the GFRP webs after the RC components had cracked in varying degrees. Therefore a reduction in stiffness of the HCB concrete arch and fin was considered during the shear rating process (described in more detailed on the following page). This assumption allowed the live and dead load shear to be carried primarily by the webs, but allowed some load sharing to occur. This modeling approach of reducing the fin and arch stiffness for shear was primarily an attempt to simulate the non-linear behavior of these concrete elements at ultimate shear failure using the calibrated linear elastic model.
- Railing loads were assumed to be evenly distributed across the structure, which was done to better match the design assumptions and typical AASHTO rating assumptions.
- Standard AASHTO serviceability ratings were not directly applicable to the HCB span. Therefore, the only serviceability ratings performed were based on determining if the arch would likely crack under service loads. This check was performed by using the axial

tension force achieved at cracking (using the arch's modulus of rupture and cross-section area) as the serviceability limit.

- For the serviceability ratings, the calibrated model was used since it should accurately predict response behavior up to the linear-elastic limit of the arch. Single-lane loads with the M1070/M747 and M1070/M1000 versions of the HETS with full impact were applied as the service loads. The 60 psf of future wearing surface (specified by the KYDOT) was not considered since it was determined that this loading was equivalent to over five inches of asphalt and was not appropriate for checking if the arch will crack under normal service loads. Additionally, over-decking the current structure would completely change the structure's behavior and capacity.

Multiple versions of the bridge model were necessary to simulate multi-stage construction and the conditions for the different assumed failure criteria in both shear and flexure (described above). The two versions of the final model were used for simulating the different structural behavior and corresponding load effect types for the shear ratings:

- **Non-Composite Behavior for Shear Ratings** – *Beam Casting & Deck Dead Load* - The model was adjusted so that all the beam casting dead load shear was induced on the GFRP shell during the pouring of the arch and the fin concrete (based on the construction procedures) & the deck dead load was induced on the GFRP shell at ultimate, meaning:
    - The arch and fin element stiffnesses were set near zero (these members were assumed to not contribute during the beam casting or at the ultimate shear failure condition)
    - The deck and SAFPLANK SIP element stiffnesses were set near zero (these members were assumed to not contribute before the deck had cured)
    - The end-restraint springs and span interaction were set to zero (conservative assumption based on the variability of this observed behavior and the bearing details.)
- **Composite Behavior for Shear Ratings** - *Composite Dead Load, & Composite Live-Load* – The model was adjusted to account for the nonlinear stiffness behavior expected from the concrete fin and arch at the ultimate condition, meaning:
    - The arch and fin element stiffnesses near midspan were reduced by ~75%. These members were found to be in tension under factored loads and were therefore assumed be severely cracked at the ultimate condition. The partial stiffness left in these regions represented the steel (strands and stirrups) that are likely holding these sections together at ultimate.
    - The rest of the arch and fin element stiffnesses were reduced by ~30%. These members were assumed to be slightly cracked at ultimate and a smeared reduction in stiffness was used to simulate this cracking. BDI performed many iterations of reduction in these concrete elements and found that this stiffness did not have a huge effect on the rating result. Therefore, these elements were reduced by the ratio of the shear strength provided by the shear stirrups and the total shear strength (~0.70).
    - The end-restraint springs and span interaction were set to zero (conservative assumption based on the variability of this observed behavior and the bearing details.)

Only one model version was used for the moment ratings, as described below:

- **Composite Behavior** - *Construction Dead Load for Moment Ratings, Composite Dead Load, & Composite Live-Load* – This was basically a simply-supported version of the calibrated model described in the previous section, meaning:
    - The end-restraint springs and span interaction were set to zero

This modeling approach simulated the shedding of the load from the uncracked HCB section to the components left resisting the load at the ultimate state (deck, GFRP shell, & the PS strands). This assumption allowed the compression induced by both the dead and live load to be applied the deck elements, which was the member group used for flexural rating.

Member capacities were calculated based on provided design drawings and calculations, the AASHTO specifications, and the results of the laboratory testing performed on this HCB type. A summary of the calculated HCB capacities used in strength and serviceability ratings, as well as important member properties have been provided in Table 4.1 through Table 4.3 while detailed capacity calculations have been provided in Appendix A.

Table 4.1 - Flexural Capacity of HCB, based on limiting steel tension (0.9Fy) but applied as limiting compression in the Deck Elements per Unit Length (ΦFn, kips/in).

Section	Design Deck Depth, inch	Design Deck Width, inch	PS strand area, in^2	GFRP Layer Area, in^2	N.A. Location at Ultimate from Top of Deck, inch	ΦF_N (kip/in)
Composite Section at Ultimate	8	71	4.90	10.32	4.18	**18.52**

Table 4.2 - Shear Capacity of GFRP Shell – FE Elements & Overall (ΦVn, kips/in).

Allowable GFRP shear stress, ksi	Thickness of GFRP Shell Wall, inches	Resistance Factor	ΦV_N of Shell Elements (kip/in)	Area of GFRP Shell Walls, in^2	ΦV_N of Both Webs, kips
7.5	0.11	0.9	1.33	7.331	**49.5**

Table 4.3 – Serviceability Tensile Capacity of Arch based on F_R (Fn, kips/in).

Section	Design Arch Depth, inch	Design Arch Width, inch	Modulus of Rupture, ksi	F_N (kip)
Arch	5	22.5	0.581	**65.4**

Load ratings were performed using the final adjusted rating models according to the AASHTO *Manual for Bridge Evaluation, 2011 Edition* and *KYDOT TM08-01* (see Table 4.4 for

applied rating factors). Given the 27'-8" wide roadway, one-lane and two-lane loading conditions were considered for the HL-93 strength and serviceability ratings. Only the single lane loading condition was considered for the HETS ratings, and the MLC ratings. Please note that for the single lane loaded strength limit states, a multiple presence factor of 1.2 was applied to the loads. It was assumed that multiple lanes of HETS and HLC vehicles were not possible due to inadequate bridge width.

Figure 4.1 shows the load configurations and weights for the AASHTO standard HL-93 design load rating vehicles, the two HETS military design loads from the structure's design document, and the controlling MLC tracked and wheeled load configurations. As specified in KYDOT's TM08-01, the HL-93 truck-loads were increased by 25%. All structural component dead loads were applied through a combination of distributed loads and the analysis program's self-weight function. Note that a uniform weight of 60 psf was applied to the roadway as the future wearing surface as specified in TM08-01 and load of 0.295 klf was used as the applied barrier weight.

According to the AASHTO MBE, the HL-93 load condition was rated for strength at both an inventory and operating level. The HETS M1070/M1000 and HETS M1070/M747 loads were rated for the strength limit state at both an inventory and operating level since the design plans indicated the structure was designed for these loads. Finally, the controlling MLC vehicle classes for the tracked and wheeled load cases for the HCB span was determined by rating the structure for the strength limit state at an Operating level for the M1A1 Abrams tracked load and for the hypothetical MLC70 wheeled load. These loads were used to determine the MLC vehicle classes instead of performing an iterative process through the various MLC load configurations. This was done because of the manner in which the loads are applied to the finite element rating model and a desire to represent realistic load applications. Generally, all MLC loads are applied to a girder line analysis with the use of the same distribution factor for each of the loads. However, when applied to the 3-D finite element model, the size and distribution of the load over the vehicle size causes different load distribution characteristics on the bridge that weren't accounted for in the creation of the standard MLC vehicles. Therefore, the M1A1 Abrams tracked load and MLC70 wheeled load were chosen as baseline vehicles to maintain consistent distribution no matter what load is applied to the vehicle footprints.

Table 4.4 Applied LFR Rating factors.

FACTOR TYPE	DESCRIPTION		FACTOR VALUE
AASHTO Load Factors	Strength Limit State	Dead Load – DC	1.25
		Dead Load – DW	1.50
		Live Load – Inventory	1.75
		Live Load – Operating	1.35
	Service Limit State	Dead Load – DC	1.0
		Dead Load – DW	1.0
		Live Load – Operating	1.0
	Impact Factor (AASHTO Table 3.6.2.1.1)		33%
	HL-93 Truck Load Amplification (TM08-01 3.6.1.2)		25%
AASHTO Strength Reduction Factors	Flexure (Moment) in a Tensile Controlled Reinforced Concrete Section		0.9
	Shear in Reinforced Concrete Section as used in HCB Design		0.9

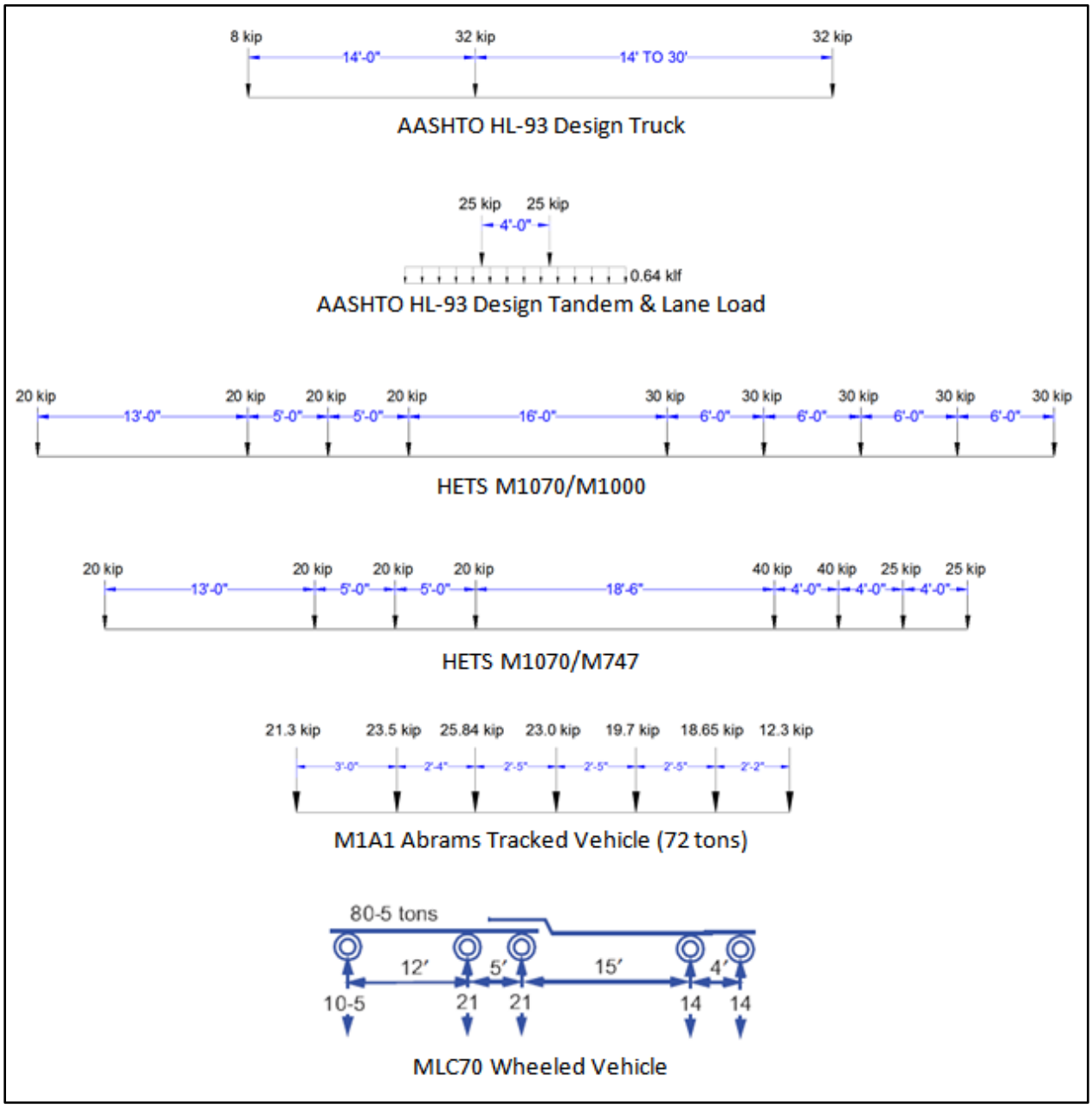

Figure 4.1 Bridge No. 4 load rating vehicle configurations.

RATING RESULTS

Following is a summary of the controlling load rating factors and responses for all rated vehicles on the Bridge No. 4 HCB span, which have been provided in tabular form as shown in Table 4.5 through Table 4.8. Ratings were calculated using a post processor that assembled the responses generated from the WinGEN model from the DC, DW, and LL loading components into the AASHTO LRFR rating equation.

The HCB sections met all of the Inventory and Operating level rating criteria (RF>1.0) for all load configurations. The controlling rating was found to be the HL93 Inventory level shear rating of 1.76 of an exterior girder approximately 12 feet from the bearing location. The structure's ratings were controlled by shear under the single lane loaded condition with the rating load applied close to the exterior girder. This result is likely due to the single-lane multiple presence factor of 1.2 coupled with the fact that the exterior girders had a narrower effective top flange than the interior beams.

The HCB span's controlling MLC tracked rating was a MLC-139 based on an M1A1 Abrams tank load that had an operating rating of 1.94. The controlling MLC wheeled rating was determined to be MLC-212, which was based on the MLC70 Wheeled vehicle that had an operating level rating of 3.04. Lastly, the service level ratings indicated that the HCBs' arches should not crack under the HETS service loads. Although this rating was not a standard AASHTO rating consideration, it verifies that there should not be a serviceability concern with respect to the concrete portion of the HCBs.

Rating output and summary files containing rating results of all rated elements for all loading conditions and applicable limit states have been included in the submittal package. Please note that all "unfactored" live load results in these files included the impact factor, KYDOT HL-93 load amplification, and the multiple presence factors. Therefore, in all rating output files the impact factor applied in the post processor was listed as 0.0.

Table 4.5 - Strength Rating Factors & Responses - HCBs in Positive Flexure.

Loading Condition	Controlling Location	DC Response, kip/in	DW Response, kip/in	LL Response, kip/in	Inventory RF	Operating RF
HL-93 (Strength)	Exterior Girder/ At Midspan	-1.36	-0.61	-3.68	2.47	3.20
HETS M1070/ M1000	Exterior Girder/ At Midspan	-1.36	-0.61	-3.28	2.77	3.60
HETS M1070/ M747	Exterior Girder/ At Midspan	-1.36	-0.61	-3.68	2.47	3.20
M1A1 Tracked	Exterior Girder/ At Midspan	-1.36	-0.61	-4.47	---	2.63
MLC70 Wheeled	Exterior Girder/ At Midspan	-1.36	-0.61	-2.97	---	3.98

Note: Dead Load Responses are unfactored. Live Load Responses have applicable multiple presence & impact factors applied. HL-93 responses also account for 25% load amplification.

Table 4.6 - Serviceability Rating Factors & Responses – Tension Check in HCB's Arch.

Loading Condition	Controlling Location	DC Response, kip	DW Response, kip	LL Response, kip	Service RF
HETS M1070/ M1000	Exterior Girder/ Near Midspan	-17.25	4.48	35.92	1.64
HETS M1070/ M747	Exterior Girder/ Near Midspan	-17.11	4.42	53.65	1.09

Note: Dead Load and Live Load Responses are unfactored.

Table 4.7 - Controlling Strength Rating Factors & Responses - HCBs in shear limited by GFRP shells.

Loading Condition	Controlling Rating Factor	Controlling Location	DC Shear, kips	DW Shear, kips	LL Shear, kips
HL-93 (Inventory)	1.76	Exterior Beam / ~12’ from Bearing	4.25	2.03	13.35
HL-93 (Operating)	2.28				
HETS M1070/M1000 (Inventory)	2.22	Exterior Beam / ~10’ from Bearing	5.28	2.05	10.22
HETS M1070/M1000 (Operating)	2.88				
HETS M1070/M747 (Inventory)	1.80	Exterior Beam / ~12’ from Bearing	4.26	2.02	13.02
HETS M1070/M747 (Operating)	2.34				
M1A1 Tracked	1.94	Exterior Beam / ~11’ from Bearing	4.78	2.06	15.43
MLC70 Wheeled	3.04	Exterior Beam / ~11’ from Bearing	4.78	2.06	9.85

Note: - Provided shear values have been converted from kips/in (related to the GFRP shell elements) into units of kips for clarity
- Dead Load Responses are unfactored. Live Load Responses have applicable multiple presence & impact factors applied. HL-93 responses also account for 25% load amplification.

Table 4.8 Controlling tonnage rating factors for all military loads.

Loading Condition	Controlling Location / Capacity	Inventory RF (Tons)	Operating RF (Tons)
HETS M1070/ M1000	Exterior Beam ~10’ from Bearing / Shear	255	331
HETS M1070/ M747	Exterior Beam ~12’ from Bearing / Shear	189	245
M1A1 Tracked	Exterior Beam ~11’ from Bearing / Shear	-	139
MLC70 Wheeled	Exterior Beam ~11’ from Bearing / Shear	-	212

5. CONCLUSIONS AND RECOMMENDATIONS

During the data review of the hybrid composite beam (HCB) span, the following observations were made:

- In general, the response data recorded during the load tests was found to be of good quality, however inconsistent strain magnitudes were obtained from the GFRP shells.
- It was found that although the responses from each strain transducer were found to be very reproducible, the magnitude of strain recorded in similar locations (i.e., along each transverse gage line) varied significantly. This inconsistency was caused by local variations in material thickness due to stiffeners or spacers or the influence of local flexure in the thin walled shells. The second option was the more likely as it was supported by the fact that the inconsistencies decreased under the heavier military loads. As the load increased these local variations likely straightened out so the out-of-plane flexure had less of an overall effect. Although the strain magnitudes could not be relied on, the strain response shapes proved to be very useful during the modeling process.
- Movement at the beam bearing locations was observed as response offsets after the first occurrences of each heavier loading configuration used for testing. This behavior was not of concern since the structure likely had not yet experienced heavy loads prior to testing. Note that once this initial movement was observed the bridge was found to behave in a linear-elastic manner.
- Friction at the bearing locations was found to likely effect the measurements and cause some interaction between the two adjacent spans, which was verified during the model calibration phase.

Multiple finite-element models were created in order to simulate the structural behavior observed during testing. These models were based on the provided structural drawing and design calculations, and subsequently calibrated until an acceptable match between the measured and analytical responses was achieved. An excellent correlation between the measured and computed response was obtained using the final full 3-D model.

During the modeling process, the following conclusions were made:

- The initial quasi-3-D modeling approach was found to accurately match many of the responses (e.g., displacements, and the shapes of the strain near midspan); however the shapes of the strain and rotation response histories near the supports could not be accurately reproduced. It was determined that the structural response was a combination of that of a theoretical beam and a tied arch. A full 3-D modeling approach was used in order to correctly simulate the interaction between the concrete arches and the GFRP shells.
- It was found that the full 3-D modeling approach succeeded in simulating the overall strain, displacement, and rotation behavior of the structure. This was especially important near the beam ends, where it was found that the GFRP shells had a shear deformation that was different than the concrete arch deformation. As stated above, this behavior approached that of a tied-arch. The maximum bottom fiber strains along the beam were found to be associated with truck positions that were shifted towards midspan rather than centered over the gage locations.

- It was found that the SAFPLANK SIP forms likely increased the lateral load distribution of the structure.
- The friction-based end-restraint and span interaction was verified during modeling. However this behavior was found to be variable and dependent on truck location and weight. Therefore this bearing behavior was not considered to be reliable and in turn was not used during the rating process.
- Overall, the second round of testing using heavier military vehicles verified the conclusions made based on the Round 1 test data. When the two rounds of test data were compared during the modeling process, it was found that very little change in structural behavior occurred throughout the year of 2013.
- Through the comparison of the two rounds of tests it was verified that the unintended support behavior such as end-restraint and continuity between spans was friction based (between bottom of beams and bearing plate) and therefore were dependent on the vehicle location and weight.

In the provided design calculations, the flexural failure was assumed to be controlled by the crushing of the deck in compression and the yielding of the prestressing strands. These calculations were based on standard reinforced concrete beam theory. The HCB tension steel was composed of pre-stress strands, meaning there won't be a large yield plateau before failure. Therefore BDI modified the flexural capacity limits based on a maximum steel strain associated with 0.9Fu of the prestress strand. This resulted in the same force calculations but a slightly different distance between the force couple and a slightly more conservative moment capacity.

Load ratings were performed using the final adjusted rating models according to the AASHTO *Manual for Bridge Evaluation, 2011 Edition* and *KYDOT TM08-01*. In all cases the rating results for the HCBs were controlled by shear in the GFRP webs, under the single lane loaded condition with the rating load close to the exterior girder. The HCB sections met all of the Inventory and Operating level rating criteria (RF>1.0) for all load configurations. The controlling rating was found to be the HL93 Inventory level shear rating of 1.76 of an exterior girder approximately 12 feet from the bearing location.

The HCB span's controlling MLC tracked rating was a MLC-139 based on an M1A1 Abrams tank load that had an operating rating of 1.94. The controlling MLC wheeled rating was determined to be MLC-212, which was based on the MLC70 Wheeled vehicle that had an operating level rating of 3.04. Lastly, the service level rating indicated that the HCBs' arches will not crack under the HETS service level loads. Although this rating was not a standard AASHTO rating consideration, it help verified that there should not be a serviceability concern with respect to the concrete portion of the HCBs.

For additional information about BDI's integrated approach (testing, modeling and rating procedures), supporting documents are available at www.bridgetest.com. The load test, structural investigation, and load rating results presented in this report correspond to the structure at the time of testing. Any structural degradation, damage, and/or retrofits must be taken into account in future ratings.

A. APPENDIX A - CAPACITY CALCULATIONS

Bridge Diagnostics, Inc.

1/18/2013
Project #: 120901-KY
Calc'd By: BAC
Checked By: KNR

HYBRID COMPOSITE BEAM MOMENT CAPACITY CALCULATION

Structure: Fort Knox Bridge Number 4

Location: Midspan Region

Since there is more available compression capacity in the deck than there is tensile capacity in the PS strands and GFRP, this Moment Capacity Calculation is based on the assumption that the failure is controlled by the yielding of the PS strands. The strain profile at the ultimate capacity will be limited by the yielding strain of the PS strands.

Assuming that the ultimate capacity will be only based the deck compression and the tension in both the PS strands and bottom layer of GFRP, the following parameters are given:

Deck Parameters:

Design Compression Strength:	$f'_c := 4.5\text{ksi}$	(Based on Design Calcs)
Elastic Modulus, ksi:	$E_c := 57\cdot\sqrt{\left(\frac{f'_c}{\text{psi}}\right)} = 3823.7$	
Deck Area, in2:	$A_{deck} := 8\cdot 71 = 568$	(Based on beam spacing)
Beta 1:	$\beta_1 := 0.825$	

PS strands Parameters:

Yielding Tensile Strength, ksi:	$f_y := 0.9\cdot 270 = 243$	(Based on Design Code)
Elastic Modulus, ksi:	$E_s := 29000$	
Yielding Strain:	$\varepsilon_y := \frac{f_y}{E_s} = 0.008379$	
Strand Area, in2:	$A_s := 32\cdot 0.153 = 4.896$	
Distance between top of deck and centriod of strands, inches:	$d_s := 40.64$	

1 of 3

GFRP Bottom Layer Parameters:

Elastic Modulus, ksi: $E_f := 3100$

Allowable Strain: $\epsilon_{allow} := 0.013$

Layer Area, in2: $A_f := 0.43 \cdot 24 = 10.32$

Distance between top of deck and centriod of Layer, inches: $d_f := 41.11$

Using Strain Compatibility:

Since the strain in the deck and GFRP Layer will be limited by the PS strands:

$\epsilon_{frp} := \epsilon_y \cdot \frac{(d_f - c_{NA})}{(d_s - c_{NA})}$ (c being equal to the distance from the top of the deck to the neutral axis)

$\epsilon_{deck} := \epsilon_y \cdot \frac{(c_{NA})}{(d_s - c_{NA})}$

Using the Constitutive Law (stress-strain) and Reinforced Concrete Theory:

The resulting stresses in the deck and GFRP at ultimate would be:

$f_{deck} := 0.85 \cdot \beta_1 \cdot \epsilon_{deck} \cdot E_c$

$f_{frp} := \epsilon_{frp} \cdot E_f$

Finally, assuming Equilibrium is satisfied:

The following tension and compression forces must be equal and the location of the neutral axis can be solved:

	TENSION, kips	COMPRESSION, kips
Given	$T := f_{frp} \cdot A_f + f_y \cdot A_s$	$C := f_{deck} \cdot A_{deck}$
Setting:	$T = C$	

$\text{Find}(c_{NA}) \rightarrow 4.1753009221945603525$

$c_{NA} := 4.175 \cdot in$

To check the assumption that the Deck & GFRP strain is limited by yielding of the PS strands:

$$\varepsilon_{frp} := \varepsilon_y \cdot \frac{(d_f \cdot in - c_{NA})}{(d_s \cdot in - c_{NA})} = 0.0085$$ --> the allowable GFRP strain limit of 0.013 was not exceeded

$$\varepsilon_{deck} := \varepsilon_y \cdot \frac{(c_{NA})}{(d_s \cdot in - c_{NA})} = 0.001$$ --> the allowable concrete strain limit of 0.003 was not exceeded

The resulting stresses in the Deck at failure is therefore restricted to:

$$f_{deck} := 0.85\beta_1 \cdot \varepsilon_{deck} \cdot E_c \cdot ksi = 2.57 \cdot ksi$$

The assiociated moment capacity using the Field-Calibrated 3D Linear-Elastic FE model was achieved by limiting the compression force in the deck elements to the following:

$$\phi F_{deck} := 0.9 f_{deck} \cdot 8 \cdot in = 18.52 \cdot \frac{kip}{in}$$

B. APPENDIX B - REFERENCES

For all references to BDI's equipment, services, and analysis/rating methods please go to our website:
www.bridgetest.com

AASHTO, (2010). "AASHTO LRFD Bridge Design Specifications, 5th Edition." Washington, D.C.

AASHTO, (2011). "The Manual for Bridge Evaluation, Second Edition." Washington, D.C.

KYDOT, (2010). "Transmittal Memorandum 08-01"

Snape & Lindyberg, (2009). "Test Results: HC Beam for the Knickerbocker Bridge, AEWC Report 10-15, Project 671", AEWC.

REPORT DOCUMENTATION PAGE

Form Approved
OMB No. 0704-0188

1. REPORT DATE (DD-MM-YYYY)	2. REPORT TYPE	3. DATES COVERED (From - To)
September 2016	Final	

4. TITLE AND SUBTITLE
Field Testing and Load Rating Report for Bridge No. 4, Hybrid Composite Beam Span, at Fort Knox, Kentucky: Contractor's Supplemental Report for Project F12-AR15

5a. CONTRACT NUMBER
W9132T-07-D-0007, DO 0022

5b. GRANT NUMBER

5c. PROGRAM ELEMENT NUMBER
Corrosion Prevention and Control

6. AUTHOR(S)
Brett Commander and Brice Carpenter

5d. PROJECT NUMBER
F12-AR15

5e. TASK NUMBER

5f. WORK UNIT NUMBER

7. PERFORMING ORGANIZATION NAME(S) AND ADDRESS(ES)
Bridge Diagnostics, Inc. (BDI)
1965 57th Court North
Suite 106
Boulder CO 80301

8. PERFORMING ORGANIZATION REPORT NUMBER

9. SPONSORING / MONITORING AGENCY NAME(S) AND ADDRESS(ES)
U.S. Army Engineer Research and Development Center – Construction Engineering Research Laboratory
PO Box 9005
Champaign, IL 61826-9005

10. SPONSOR/MONITOR'S ACRONYM(S)
ERDC-CERL

11. SPONSOR/MONITOR'S REPORT NUMBER(S)
ERDC/CERL CR-16-5

12. DISTRIBUTION / AVAILABILITY STATEMENT
Approved for public release. Distribution is unlimited.

13. SUPPLEMENTARY NOTES

14. ABSTRACT

The Army has 1,500 vehicular bridges on its installations, with many experiencing high maintenance or replacement costs due to corrosion of the steel structure or of the reinforcing bar in the concrete deck. Under the Department of Defense Corrosion Prevention and Control Program (Project F12-AR15), a span of Bridge No. 4 at Fort Knox, Kentucky, was selected to demonstrate and validate a new corrosion-resistant hybrid composite bridge beam. The results of that project were published as ERDC/CERL TR-16-22 (September 2016). Bridge Diagnostics, Inc. (BDI) of Boulder, Colorado, was subcontracted to perform load testing and rating for the new bridge beam project to confirm that the replacement bridge span met its required load rating (HL-93) and performance criteria for deflection and strain. Results showed the bridge met all design specifications and load ratings.

15. SUBJECT TERMS
Structural dynamics, Bridges–Live loads, Bridges–Design and construction, Composite materials–Testing

16. SECURITY CLASSIFICATION OF:			17. LIMITATION OF ABSTRACT	18. NUMBER OF PAGES	19a. NAME OF RESPONSIBLE PERSON
a. REPORT	b. ABSTRACT	c. THIS PAGE			19b. TELEPHONE NUMBER (include area code)
Unclassified	Unclassified	Unclassified	UU	73	